UNLIMITED

UNCLASSIFIED

Approved for Publication

AEEW - R 347



AEEW - R 347




United Kingdom Atomic Energy Authority

REACTOR GROUP





# A REPORT ON THE PLUTONIUM CORES OF ZENITH

F. R. BARCLAY
I. R. CAMERON
A. DRAGESET
R. G. FREEMANTLE
D. J. WILSON



General Reactor Physics Division,

Atomic Energy Establishment,

Winfrith, Dorchester,

Dorset.

1965

INITS : LT

DRIC DEFENCE RESEARCH INFORMATION CENTRE

**DEFENCE RESEARCH INFORMATION CENTRE**
Room2172,KentigernHouse,65BrownStreet,GlasgowG28EX
Telephone (switchboard) 0141 248 7890 Direct dialling 0141 224 2463 Fax 0141 224 2470

DERA

Req 19799

UK ATOMIC ENERGY AUTHORITY
ROOM 473 BLDG A32
WINFRITH
DORCESTER
DORSET
DT2 8DH

**Your reference:** ACQ-0006742
**Our reference:** 16AUG95
**Date:**

## DRIC REQUEST FOR SUPPLY OF REPORTS

Please supply 1, 2 or 3 copies of the following, [If no spare copies are available for retention then would you please forward a loan copy. If a loan copy is forwarded please clearly indicate]

1. Title:
A REPORT ON THE PLUTONIUM CORES OF ZENITH (U).

2. Originator:
ATOMIC ENERGY EST, WINFRITH

Originators Reference No:
AEEW-R-347

4. Authors:
BARCLAY FR, DRAGESET

5. Date of Issue:
1965

Where Quoted:

Hard copy preferred, but microfiche acceptable if not available.

Please forward any acompanying / disks (Video computer)

DCI(GEN)121/91 (being republished) requires that all MoD originated/sponsored Scientific & Technical documents be centrally deposited at DRIC.

If there is any charge for the document please advise us before forwarding. Nevertheless it would be appreciated if you would confirm / complete the details above and SECTION B below before returning this form.

NAME LORRAINE TAYLOR GRADE A.O SIGNATURE L. Taylor

SECTION B. Please complete this section and return one copy of this form with the requested documents.

1. (i) Report prepared under Defence Contract .....
(ii) Name and Address of Defence Release Authority .....
.....

2 (i) Classification of Marking (Tick as appropriate)

| | TITLE | ABSTRACT | REPORT |
|---|---|---|---|
| SECRET | | | |
| CONFIDENTIAL | | | |
| RESTRICTED | | | |
| UNCLASSIFIED LIMITED DISTRIBUTION | | | |
| UNLIMITED | ✓ | ✓ | ✓ |
| COMMERCIAL IN CONFIDENCE | | | |
| OTHER MARKINGS OR CAVEATS | | | |

(ii) Please advise DRIC of any other restrictions. E.g. specific release conditions on a separate letter.

SIGNATURE I.J. Tuhill for and on behalf of .....

DATE 22/08/95 .....

**PLEASE RETURN THIS FORM INTACT**

# A REPORT ON THE PLUTONIUM CORES OF ZENITH

F. R. Barclay
I. R. Cameron
A. Drageset *
R. G. Freemantle
D. J. Wilson

(Including work by: R. P. Brown, D. H. Carter, V. E. Della Loggia*, C. D. Hodgson, H. H. W. Pitcher, Miss M. D. Pittard, B. J. Puckett, J. Reber*, J. C. Stillwell, C. R. Symons and S. J. Wilkinson).

## Abstract

The report describes a series of experiments carried out with plutonium fuel in the heated zero-power reactor ZENITH, with the aim of testing current theoretical methods, with particular reference to excess reactivity, temperature coefficients, differential spectrum and reaction rate distributions. Two cores of widely different fissile/moderator atom ratios were loaded in order to test the theory under significantly varied spectrum conditions. The general agreement is comparable with that found for the U235 cores previously investigated.



*Dragon Project Staff.

A.E.E.,
Winfrith.

March, 1965.

S.C. C20
W.6888

Contents

# CHAPTER 1

## INTRODUCTION

Interest in the utilisation of plutonium in reactor systems arises from its increasing production in the Magnox programme. The most advantageous potential use of this fissile material is in fast reactors where the high eta value allows the possibility of breeding. Until such time as large power-producing fast reactors come into operation, however, interest centres on the use of plutonium in the more advanced thermal systems such as the Advanced Gas Cooled and High Temperature Gas Cooled reactors. Particular physics interest is attached to the examination of the effects of Pu240 which can, in principle, be used to reduce overall changes of reactivity with burn-up, thus easing requirements of control investment.

The theoretical treatment of plutonium-fuelled thermal reactors is more difficult than for reactors fuelled with U235 due largely to the problem of handling the strong low lying resonances in Pu239, Pu240 and Pu241, particularly for a graphite moderated system where additional complication is introduced by the complex scattering law associated with the crystalline structure.

The present paper describes a series of experiments carried out with plutonium fuel in the heated zero-power reactor ZENITH, with the aim of testing current theoretical methods for the treatment of graphite-moderated high-temperature reactors. Two cores of widely different fissile/moderator atom ratio were loaded in order to test the theory under significantly varied spectrum conditions. The first and heavier loading utilised all the available plutonium fuel elements (15 Kg) while the excess reactivity of the more dilute loading (3 Kg) was just sufficient to permit convenient operation of the reactor. A fairly extensive set of measurements was made on the first loading; those on the second were more restricted. The fuel available contained only 2.5% of the Pu240 isotope, though even at this rather low level, the reactivity held in the Pu240 was about 5% in the harder spectrum core. A series of exponential measurements on plutonium-graphite systems, using the same fuel as in the ZENITH experiments and covering a similar range of compositions, has been described elsewhere (Ref. 1.1).

The characteristics of the two cores are summarised in Table 1.1. Steel absorber was added to the more heavily loaded core to adjust the excess reactivity to the desired value. The thermal absorption to scattering cross section ratio of the first plutonium core was similar to that of the earlier U235-fuelled ZENITH Core 5 (C/U235 atomic ratio = 1072); that of the second was similar to that of U235 Core 4 (C/U235 = 7578).

TABLE 1.1

| Plutonium Core | C/Pu239 (atomic ratio) | Steel/Pu239 | $\Sigma_a/\xi\Sigma_s$ (at 2200 m/sec) | Total Pu239 (kgm) |
|---|---|---|---|---|
| 1 | 2666 | 78 | 0.51 | 15.2 |
| 2 | 14555 | - | 0.09 | 3.1 |

The isotopic composition of the plutonium fuel was 97.4% Pu239, 2.5% Pu240 and 0.1% Pu241.

The reactor ZENITH (Ref. 1.2, 1.3) was designed primarily to investigate the reactor physics problems of small, high temperature gas-cooled reactors. It has been used in support of the O.E.C.D. High Temperature Reactor Project (Dragon) (Ref. 1.4, 1.5, 1.6, 1.7) and for more general studies on U235-fuelled graphite moderated systems (Ref. 1.8, 1.9, 1.10, 1.11, 1.12, 1.13, 1.14).

The general features of ZENITH have been described elsewhere (Ref. 1.2, 1.3) and a brief outline will suffice here. Detailed data pertinent to the reactor physics are given in Appendix A. A detailed safety re-appraisal for operation with plutonium fuel was made (Ref. 1.15).

The overall layout of the reactor core and reflector is shown in the vertical section through the reactor vessel (Fig. 1.1) and in the plan view (Fig. 1.2). The plutonium-fuelled core consists of a vertical array of 235 cylindrical graphite sleeves of outer diameter 7.37 cm into each of which a cylindrical graphite box (Fig. 1.3) may be loaded. Running longitudinally inside the box are six parallel grooves which act as locations for the edges of either aluminium-sheathed Pu/Al 'spikes' or graphite wafers of the same external dimensions. Each groove accommodates two spikes end-to-end with a small graphite spacer between to avoid the aluminium welding together when heated. Lateral spacers of graphite or stainless steel fill the five spaces between the six spikes or wafers. The total length of the plutonium-loaded core region is 140 cm, the ends of the element forming graphite reflectors of length 53 cm.

The two fuel loadings investigated had fuel box patterns as shown in Fig. 1.4. The steel content of the heavier loading was varied for certain experiments.

The fuel elements are arranged in a triangular lattice of pitch 7.62 cm to form the reactor core, of diameter 1.23 m, a plan view of which is shown in Fig. 1.5, including the identification code, consisting of a letter and a number, the central element being K10. The interstices between the channels form the measuring channels into which counters and foils may be inserted. These interstices also form the channels through which the nitrogen, used for heating the system, flows up through the core. For reference purposes the interstitial channel to the right of an element, is given the number of the element (e.g. K10), while the channel to the upper right is given the number with an asterisk (e.g. K10*).

A radial graphite reflector of approximately 1 metre thickness surrounds the core region of the reactor. It is separated from it by an annular lamp-black thermal barrier contained within graphite tiles. This barrier reduces heat flow from the core to the radial reflector. Gaps are left in the stacking of the reflector blocks to form channels for the flow of nitrogen down through the reflector.

The control rods move in vertical channels near the inner edge of the radial reflector. Thirty of these channels are provided, twenty of which are occupied by motorised rods. Since the delayed neutron fraction for Pu239 is about one third that of U235, two of the rods were replaced by rods of reduced diameter for convenience in carrying out kinetic measurements on the present cores.

The positions and allocations of rods for the plutonium cores of ZENITH are summarised in Appendix A, and illustrated in Fig. 1.6. Data on the dimensions of the control rods, which consist of boron carbide packed

between coaxial steel tubes, is also given in Appendix A.

The positions of the six U235 fission chambers which comprise the installed reactor instrumentation are also shown in Fig. 1.6. There are two low-flux and two high-flux pulse counting channels, and three current chambers forming the reactor shut-down channels. When the reactor is in hot operation the shut-down chambers are cooled by a current of air to prevent their temperature exceeding 250°C.

The reactor is heated by circulating nitrogen, which flows over an electrical heater of maximum power 250 kw located at the base of the reactor vessel, up through the interstitial channels in the core and end reflectors and down through the radial reflector. To achieve some measure of independent temperature control, a by-pass stream of cooler gas may be introduced into the top plenum to mix with the hot gas leaving the core before flowing through the reflector. A diagrammatic outline of the gas circuit is shown in Fig. 1.7 which also shows the ancillary plant associated with the reactor, for storage, circulation, purification and impurity analysis of the nitrogen.

Although the reactor is designed to run at maximum core and reflector temperatures in the region of 800°C and 400°C respectively, a restriction to a core temperature of 420°C was imposed in the present experiments to avoid the possibility of damage to the fuel. Special trip thermocouples were installed on selected fuel elements to prevent the limit being exceeded.

# CHAPTER 2

# THEORETICAL TREATMENT

## 2.1 Introduction

Calculations using multigroup methods in conjunction with basic nuclear data were carried out for the determination of spectrum, reactivity (as a function of temperature) and power distribution. The methods of calculation and nuclear data used are discussed below.

## 2.2 Methods of Calculation

The fuel element fine structure was treated by a calculation using the Winfrith DSN program in the energy range up to 1.5 eV (Ref. 2.1), while the group cross-sections for the plutonium resonance above this energy were obtained from the Monte Carlo code MOCUP (Ref. 2.2). The condensed data from those programs were fed into the diffusion theory codes MUPO and ANGIE for the overall reactor calculation.

The Winfrith DSN program (Ref. 2.3) solves the $S_n$-approximation to a set of multigroup one-dimensional Boltzmann transport equations in cylindrical geometry. The group structure and scattering matrix can be varied to suit the user, the main limitations being the restriction to one-dimensional geometry and the assumption of isotropic scattering. The present calculations were made in an $S_4$ approximation assuming a reflective boundary condition. In the group structure chosen, 20 of the 40 groups were clustered around the resonances of Pu239 at 0.3 eV and Pu240 at 1.06 eV. Scattering matrices were computed using the program PIXSE (Ref. 2.4), using both gas and Egelstaff representations for graphite. The manner in which the complex pattern of the spikes and spacers was converted to cylindrical geometry is discussed in Chapter 8 in connection with the results for spectrum and fine structure.

The cross-sections for the epithermal resonance region have been obtained for both ZENITH cores by applying the Monte Carlo technique to the first core only, using the same geometrical representation as in DSN. By tracing a total of 4096 neutrons, absorption and scattering events were counted separately for fuel and moderator to yield effective plutonium cross-sections in 10 energy groups. A calculation carried out for the first core with unshielded data gave a reactivity 0.5% higher than for the shielded case, so that any error due to inadequate treatment of the Pu239 self-shielding in the energy region above 1.5 eV is likely to be acceptably small.

The MUPO code (Ref. 2.5) solves a set of 43-group zero-dimensional diffusion equations for a homogenous medium, generates the spectrum in these groups, and condenses the input cross-sections to provide data for the two-dimensional diffusion code ANGIE (Ref. 2.6). Heterogeneity is treated by the use of group disadvantage factors. The disadvantage factors and group cross-sections were obtained from the DSN cell calculation as follows. The reaction rate R of a fuel atom from group i of the MUPO spectrum is given by:

$$R = \phi_{mi} \cdot \frac{\Sigma\, \phi_{fk}^{DSN}}{\Sigma\, \phi_{mk}^{DSN}} \cdot \frac{\Sigma\, [\sigma_{fk}^{DSN} \cdot \phi_{fk}^{DSN}]}{\Sigma\, \phi_{fk}^{DSN}}$$

$$= \phi_{mi}\, d_i\, \sigma_{fi}^{MUPO}$$

where: $\phi_{mi}$ is the MUPO moderator flux in group i;

$\Sigma\, \phi_{fk}^{DSN}$, $\Sigma\, \phi_{mk}^{DSN}$ are summations of the DSN fuel and moderator fluxes covering the same energy range as the MUPO group i considered;

$\sigma_{fk}^{DSN}$ is the fuel cross-section for group k of DSN.

Hence $d_i$, the disadvantage factor for group i of MUPO, and $\sigma_{fi}^{MUPO}$, the fuel cross-section for group i of MUPO, are given by the second and third factors in the expression.

Disadvantage factors are unity in the epithermal region since the self-shielding has been included in the group cross-sections derived from MOCUP.

The fundamental mode diffusion equations in MUPO covered the energy range up to 10 MeV. These were solved by a source iteration technique using energy-dependent bucklings obtained from ANGIE as discussed below. Separate calculations were carried out for core and reflector. In the reflector a weak fission source in the form of $0.7 \times 10^{15}$ atoms/cm$^3$ of U235 had to be inserted for the purposes of iteration. This extra material was removed before the condensation of the reflector cross-sections to six groups was performed.

The two-dimensional code ANGIE also uses a source iteration technique and calculates the effective multiplication factor as $\nu/\nu'$, where $\nu$ is the number of neutrons produced per fission and $\nu'$ is the value necessary to make the reactor just critical. The reactivity error arising from incomplete convergence was not greater than $10^{-4}$. The calculations were performed for a cylindrical model of the reactor, without control rods inserted and with the voidage smeared out in the selected regions (see Appendix B and Fig. 2.1). Equivalent radii were chosen on an area conservation basis.

Since the ANGIE code permits upscattering from one group only to the one immediately above, a rather coarse thermal group structure was necessary and altogether only six groups were used. The group structures used in MUPO and ANGIE are shown in Appendix B.

In order to improve the leakage representation in MUPO, the core and reflector were each sub-divided into two regions, and average bucklings for each ANGIE group were obtained for both regions from the results of the first ANGIE calculation. The bucklings were then fed back into the MUPO code and the group cross-sections re-evaluated. In the treatment of the second loading, the core was regarded as a single buckling region and the bucklings derived for the central region of the first core were applied in the MUPO stage. The reflector cross-sections derived for the first core were also used in the calculations on the second.

In the derivation of reaction rate distributions, unshielded 43-group cross-sections were used. Since the experimental (fission chamber)

measurements were performed at the cell edge position (i.e. in the interstitial channels between the fuel elements), the MUPO cross-sections were multiplied by the ratio of flux at edge of the cell to mean flux in moderator, which was available from the DSN calculation. These were condensed to 6 groups by flux weighting using the MUPO spectrum. The condensed cross-sections were multiplied by the ANGIE group fluxes at each position.

## 2.3 Nuclear Data

The combination of codes used entailed the use of data sources of different origin. As explained above, the Pu239 and Pu240 fission and absorption cross-sections were carried over to MUPO from WDSN (0.0112 - 1.375 eV) and MOCUP (4.565 - 1234 eV), while in the remaining energy intervals the MUPO cross-section data, based on the General Atomic Data Compilation GA-2451 (Ref. 2.7) were used. The data used yield a Pu239 $\eta$-value at 2200 m/s of 2.087.

The graphite scattering matrix in MUPO was based on the Schofield crystalline model (Ref. 2.8) below 1 eV and a monatomic gas model (A = 12) above. It is this model for graphite, therefore, that determines the spectrum used in the calculations of excess reactivity, reaction rate distributions and moderator temperature coefficients of reactivity. This model is an early representation of the effects of the crystalline structure of graphite and is known to predict somewhat softer spectra than experimentally observed in the ZENITH U235 cores or calculated using more recent scattering laws such as those of Parks (Ref. 8.13) or Egelstaff (Ref. 8.1). Scattering matrices based on these more recent developments were not, however, currently available for use with the MUPO code.

The graphite absorption cross-section in MUPO was adjusted, where necessary, by the addition of a small quantity of boron to bring it up to the value for the actual reactor (4.3 mb. for reflector and 4.2 mb. for core).

The composition of the stainless steel poison was determined by chemical analysis. The 2200 m/sec cross-section obtained on this basis agreed within experimental errors with that derived from oscillator measurements on the GLEEP reactor at Harwell. The error in calculation of steel absorption is estimated as not more than 3%, which corresponds to approximately 0.4% in reactivity. No account was taken of resonance self-screening of the steel. The effect of possible errors from this and other sources is discussed in detail in Chapter 8.

## CHAPTER 3

## REACTIVITY MEASUREMENTS

The first plutonium core was loaded by progressively substituting fuel boxes for graphite dummy boxes containing the same weight of graphite, the outer graphite sleeves remaining in the core. The pattern of fuel boxes was a good approximation to a uniform distribution over the fixed core size throughout the loading. After attainment of criticality the further excess reactivity added was held down by successive insertion of control rods to compensate each loading step. The second core was loaded by progressively replacing the fuel boxes of the first loading.

In the fully loaded cores, the source strength from the fuel, due primarily to the reaction of the Pu239 $\alpha$-particles with the aluminium plus a small contribution from the spontaneous fission of Pu240, was completely adequate for safety purposes at shut down. The source strength due to each fuel spike was measured in the early stages of the approach to criticality by comparing the count rate near the core centre due to the fuel alone with that due to the fuel plus a polonium-beryllium source averaged numerically over the actual fuel distribution. The value found was $(7.5 \pm 1.2) \times 10^3$ n/sec per spike, where most of the error arises from the uncertainty in the absolute calibration of the polonium-beryllium source. The total core neutron source was thus $1.8 \times 10^7$ n/sec for Core 1 and $3.5 \times 10^6$ n/sec for Core 2.

The measurement of the final excess reactivity of the clean core involved the determination of each step change of reactivity in terms of the control inserted for compensation. The method employed for calibration of the control rods was based on the diverging period measurement of reactivity. Since the total reactivity to be measured is of the order of several percent, thus involving the summation of a large number of individual steps of order 0.05% reactivity obtained from the period measurements, it is convenient to adopt a definition of the reactivity which is additive. It has been shown (Ref. 1.12) that a definition of the reactivity change between two states of multiplication factors $k_1$ and $k_2$ which allows a simple additive combination is:

$$\Delta\rho = \frac{k_2 - k_1}{\frac{1}{2}(k_2 + k_1)}$$

In the period measurements it is important to consider the criteria quoted by Toppel (Ref. 3.1) to ensure that the asymptotic period is measured without error arising from the initial transient due to the control rod movement, etc. An additional complication in the present experiments was the strong neutron source from the spikes. The Toppel criterion for the effect of a source can be ignored if the reactor period, T, is derived from the expression for the flux:

$$\phi = \phi_o e^{t/T} - \phi_s$$

where $\phi_s$ is a constant correction due to the source.

The conversion from period to reactivity is derived from the inhour equation using the delayed neutron data of Keepin et al. (Ref. 3.2). The

effectiveness of delayed relative to prompt neutrons, which is a function of the relative escape probabilities is:

$$\chi = 1.10 \pm 0.02$$

based on calculations on the first (Ref. 1.8) and the fourth (Ref. 1.13) U235 loadings of ZENITH, and assuming the same energy distribution for delayed neutrons from Pu239 and U235. The values for the U235 loadings are close to those calculated for the homogeneous U235-graphite reactor TREAT with similar buckling (Ref. 3.3). Combination of this factor with the 'nuclear' value ($\beta_o$) of Keepin et al. gives an effective delayed neutron fraction:

$$\beta = \chi \beta_o = 0.00231 \pm 0.00013.$$

The prompt neutron lifetime was measured using a rod oscillation technique (see Chapter 4). The values used were ($0.60 \pm 0.03$) milliseconds and ($1.28 \pm 0.07$) milliseconds for Core 1 and Core 2 respectively.

The most important complication in the measurement of excess reactivity is the high degree of interaction between the control rods in ZENITH. All reactivity changes were measured in terms of two standard rods (designated FCR and CCR) which were chosen to be at an azimuthal separation of approximately 90° on the control rod ring, as previous experience had shown that rods at this mutual separation suffered negligible interaction effect. By moving the FCR out of the reactor to provide a stepwise calibration by the diverging period method, and using the CCR to restore to the critical balance condition after each step, a complete calibration of reactivity against position was obtained for both rods. The worths of the standard rods depend on the overall rod configuration but were typically of the order of 1% in both cores.

These calibrations, when normalised to unit total rod worth, did not differ significantly from each other nor did they depend significantly upon either the interaction of other control rods or the temperature of the side reflector: the variation over a wide range of core loading and core temperature was small so that a linear interpolation with loading or temperature was adequate. Thus the worth of the FCR (or CCR) could be found from a single diverging period measurement using the interpolated relative calibration.

As loading proceeded from the initial critical state it was necessary to insert other control rods to compensate for the increase in reactivity. The insertion of each of these rods, of course, altered the worth of the two standard rods, but the worth of each loading step could still be obtained unambiguously by arranging that each step was approximately equivalent in reactivity to one standard rod, i.e. it was possible to determine the worths of the two standard rods before and after the loading change with the same configuration of the other rods in the reactor.

Since the worths of the FCR and CCR are redetermined after each loading step and after each change of overall rod configuration, this technique allows for changes in the worths of these rods both with insertion of other control rods and with the progressive change in absorption of the core. The method does not allow, however, for any change in the worths of the other rods inserted in the reactor as a result of the progressive change in core composition. Previous experience (Ref. 1.14) has shown that this

effect is small. It has also been found, and this is supported by a theoretical treatment due to Micheelsen (Ref. 1.7) designed to reproduce the essential features of the experimental technique, that the method may be applied most readily without correction when the reactivity change is due to loading either a thermal absorber, or better still, a resonance absorber. These considerations have been taken into account in the reactivity measurements whenever a significant error might otherwise arise due to changes in the worth of inserted control rods.

The error on reactivity measurement arising from the use of the diverging period technique is $\pm$ 3%, representing the error on rod calibration for comparison with other experimental results; taking the systematic uncertainties in delayed neutron data into account, the error appropriate to the comparison of experiment with theory is $\pm$ 6%.

During the loading of the first core a useful check of the accuracy of the technique of reactivity measurement was obtained. The system was built first with two stainless steel strips per fuel box and the reactivity perturbation was determined for the addition of two extra steel strips per element in two fuel elements at a time at radii 7.6, 22.9 and 38.1 cm; at 53.3 cm azimuthal variations were also investigated. The results were integrated graphically over the full core and this predicted a reactivity change of:

$$(-4.25 \pm 0.13)\%$$

for the loading of one extra steel strip in every element. The result subsequently obtained when actually loading an extra steel strip in every element by applying the technique described above for a large reactivity change gave:

$$(-4.37 \pm 0.13)\%$$

in excellent agreement. It should be noted that these errors are appropriate for comparison of experimental results; the error for comparison with theory would be $\pm$ 0.26% in either case.

The results obtained for the excess reactivities of both cores are summarised in Table 3.1 and are compared with theory in Chapter 8. Measurements of the reactivity perturbation due to graphite, fuel and copper as a function of position in the system were made. The details are given in Appendix C.

The pressure coefficient for the first loading found from reactivity measurements before and after replacing the atmosphere of air by nitrogen was:

$(-0.28 \pm 0.02)\%$ per atmosphere of air

or: $(-0.36 \pm 0.03)\%$ per atmosphere of nitrogen

which may be compared with the value:

$$(-0.43 \pm 0.02)\%$$

in the fifth U235 loading which had similar core absorption cross-section per graphite atom. The values derived by subcritical multiplication in the system when shut-down (10% reactivity held in control rods) were:

$(-0.29 \pm 0.04)\%$ per atmosphere of air

or: $(-0.38 \pm 0.05)\%$ per atmosphere of nitrogen.

As in the fifth U235 loading (Ref. 1.14), and contrary to the observations in the more dilute second (Ref. 1.10) and fourth (Ref. 1.13) U235 loadings, there is no significant difference between the result at critical and in the shut-down state.

TABLE 3.1

Excess Reactivity and Corrections

| Details | Excess Reactivity (%) | |
|---|---|---|
| | Core 1 | Core 2 |
| Excess Reactivity as Measured | $3.58 \pm 0.11$ | $4.03 \pm 0.12$ |
| Removal of Instruments, etc., from Side Reflector | $+0.70 \pm 0.11$ | $+1.0 \pm 0.26$ |
| Removal of Miscellaneous Graphite from Side Reflector | $-0.37 \pm 0.03$ | $-0.11 \pm 0.01$ |
| Replacing Air Atmosphere by Nitrogen | $-0.08 \pm 0.01$ | $-0.11 \pm 0.02$ |
| Excess Reactivity of Standard State B1* | 3.8 | 4.8 |
| Uncertainty due to Control Rod Calibration and Corrections | $\pm 0.16$ | $\pm 0.29$ |
| Uncertainty due to Delayed Neutron Data | $\pm 0.21$ | $\pm 0.26$ |
| Total Uncertainty | $\pm 0.3$ | $\pm 0.4$ |

*See Ref. 1.14. In this state all extraneous absorbers and instrumentation is assumed removed; all control rod channels and experimental holes in the reflector empty; nitrogen atmosphere; core edge region contains normal array of graphite fillers (367 Kg).

# CHAPTER 4

## PROMPT NEUTRON LIFETIME AND TRANSFER FUNCTION

### 4.1 Introduction

Measurements were made on the amplitude and phase of the reactor transfer function by studying the response of neutron flux level to a sinusoidal reactivity input provided by oscillation of the fine control rod.

If the reactivity input to the critical reactor is:

$$\Delta\rho = \Delta\rho_o \sin \omega t \qquad 4.1$$

the reactor power response for small $\Delta\rho_o$ may be written as:

$$N(t) = N_o + \Delta N_o \sin(\omega t + \phi) \qquad 4.2$$

where: $\Delta N_o$ is the amplitude of the fundamental component of the modulation of the reactor power (steady value $N_o$).

The fractional amplitude of power variation, $\Delta N_o/N_o$ is related to the reactivity input amplitude by the transfer function $A(\omega)$.

$$\frac{\Delta N_o}{N_o} = A(\omega)\,\Delta\rho_o \qquad 4.3$$

where: $A(\omega)$ is a complex function of the angular frequency $\omega$. The values of $A(\omega)$ and the tangent of the phase angle $\phi$ are given by the following expressions (Ref. 4.1):

$$\left|A(\omega)\right| = \frac{1}{\beta\omega}\left[\left\{\omega \sum_i \frac{a_i}{(\lambda_i^2+\omega^2)}\right\}^2 + \left\{\frac{l}{\beta} + \sum_i \frac{a_i\lambda_i}{(\lambda_i^2+\omega^2)}\right\}^2\right]^{-\frac{1}{2}} \qquad 4.4$$

$$\tan\phi = -\left\{\frac{l}{\beta} + \sum_i \frac{a_i\lambda_i}{(\lambda_i^2+\omega^2)}\right\} \Big/ \left\{\omega \sum_i \frac{a_i}{(\lambda_i^2+\omega^2)}\right\} \qquad 4.5$$

where: $l$ is the prompt neutron lifetime

$a_i$, $\lambda_i$ are the relative concentrations and decay constants of the delayed neutron precursors

$\beta$ is the effective delayed neutron fraction.

Although these expressions apply strictly to a bare reactor, it has been shown (Ref. 4.2) that a reflected system is adequately represented by these provided $l$ be taken as the effective prompt neutron lifetime (defined operationally as the result of uniform 1/v poisoning) and provided that angular frequencies well below the decay constant of the reflector are considered; at higher frequencies the bare core equivalence is no longer a satisfactory approximation (Ref. 4.3, 4.4). The object of the work reported here is to check the applicability of these zero-power kinetic equations in a

plutonium-fuelled system and to derive the effective neutron lifetime for the two cores using the measured phase of the transfer function.

A transfer function analyser is used to separate the fundamental mode of the reactor power variation from components of higher harmonic content. The phase angle is derived from the ratio of the quadrature to in-phase component, and the fractional power modulation of the fundamental mode is obtained from the sum of their squares.

## 4.2 Experimental Procedure

The reactor core flux was raised to $\sim 5 \times 10^7$ n/cm$^2$ sec, at which level the effect of the neutron source from the Pu/Al alloy fuel was trivial, and the fine control rod was set in oscillation. Any resulting drift in reactor power was corrected by moving the coarse control rod until the reactor mean power remained sufficiently constant.

In order to eliminate the effects of misalignment between the control rod and the synchro-resolver which makes the sine and cosine multiplication, the rod-drive mechanium was run alternately forward and in reverse. The mean of the measured phase angles was used in subsequent calculations. During the measurements on the first plutonium core this sequence was repeated at four different frequencies from 1 cycle/ sec to $\frac{1}{8}$ cycle/sec with the detector in the reflector, and with 5.04 cm amplitude of rod movement. In the second core a more detailed study was made to compare, in particular, the results obtained with the detector in the normal position in the side reflector and near the core centre. These measurements were carried out at 6 frequencies from 1 cycle/sec to 1/32 cycle/sec, with amplitudes of oscillation of 5.04 cm and 2.76 cm.

## 4.3 Results

The individual data obtained for both cores are summarised in Appendix D, Tables 1 and 2. The delayed neutron data used in the analysis were those of Keepin et al. (Ref. 3.2).

The more comprehensive set of measurements made in the second plutonium core showed that the phase lag of the transfer function was not significantly dependent upon:

(a) the amplitude of the rod oscillation

(b) whether the detector was in the side reflector position or the core position for any frequency except the highest (1 c/s).

For the highest frequency used there was a significant difference in phase lag at the two detector positions. This detector position dependence is due to the difference in the lifetime of neutrons in the core and the reflector regions. The kinetic contribution from the reflector can be regarded effectively as an additional delayed neutron group of decay constant $\sim 300\ \text{sec}^{-1}$ which would have dominant influence at frequencies of this order. The amplitude in the core would then be approximately independent of frequency and the phase would tend to zero, whereas in the reflector the amplitude would fall rapidly with frequency and the phase would be strongly negative. The observation of a small difference at 1 cycle/sec is due to the sensitivity of the phase measurement; it does not show up in the amplitude measurements. This sensitivity is greater in the

plutonium fuelled core due to the smaller delayed neutron fraction, which enhances the relative importance of the reflector component. The effect was not observed in the U235 loadings.

The values of tan $\phi$ plotted as a function of angular frequency for both cores are shown in Fig. 4.1. The curves are obtained using equation 4.5 with the value of $1/\beta$ giving the best fit to the experimental data. The phase angle for the reflector chamber at the highest frequency in the second core gives $1/\beta$ some 17% higher than the mean fit to the other points.

The signal to noise ratio in the experiments was such that the ratio had a maximum root mean square deviation of 0.4%. At the most sensitive phase angle this error in the tangent represents a phase error of approximately 0.1°, corresponding to $\pm$ 1% on the value of $1/\beta$.

As shown in Tables D1 and D2 the derived values of $1/\beta$ show no systematic dependence on frequency apart from the 1 c/s reflector measurement discussed above. The mean value of $1/\beta$ for Core 2 excluding the results showing spatial dependence is:

$$1/\beta = 0.553 \pm 0.009 \text{ sec}$$

i.e., $$l = 1.28 \pm 0.07 \text{ msec}$$

The rather restricted range of measurements for Core 1 gives:

$$1/\beta = 0.259 \pm 0.004 \text{ sec}$$

i.e., $$l = 0.60 \pm 0.03 \text{ msec}$$

where: $\beta$ has been taken as 0.00231 (see Chapter 3) for both cores.

The errors quoted on $1/\beta$ are in both cases the standard deviation of the individual values.

The amplitude of the transfer function was calculated for Core 2 as a function of frequency from equation 4.4. The mean ratio of experimental and calculated transfer function is 0.99 with a systematic uncertainty of $\pm$ 5%. The individual ratios have a standard deviation of $\pm$ 1½%. The comparison is made in graphical form in Fig. 4.2.

## CHAPTER 5

## TEMPERATURE COEFFICIENCTS OF REACTIVITY

The temperature coefficient of reactivity is defined as the change in reactivity per unit change in temperature. In ZENITH a considerable degree of separability of the core plus end reflectors and the side reflector temperatures is possible and so the temperature coefficient of each region may be determined independently. Full details of the experimental techniques and method of analysis are given for the fifth U235 Core (Ref. 1.14) so the description here will be brief.

Reactivity measurements by diverging period technique as described in Chapter 3 were carried out at each of a series of temperature states in the first loading. The only additional problem was that of ensuring that the extra error in reactivity arising from temperature drift of the reactor did not exceed the basic uncertainty of 1% applicable to the period measurement at room temperature. Careful control of the reactor heating system did in fact permit this criterion to be satisfied.

Temperatures were measured by chromel alumel thermocouples distributed on 25 fuel elements forming a representative array of fuel elements in the core (Fig. 1.5). Each of these elements carried one thermocouple at the half height position; additional thermocouples were placed on six of these at 72.4 cm above and below the centre position to provide information on the axial temperature variation.

The available positions in the side reflector were more restricted. Thermocouples were inserted into one control rod hole (radius 74.5 cm), one instrumentation hole (radius 78.4 cm), and two inner "depletion rod" holes (radii 97.3 and 103.6 cm) at the half height position and 76.2 cm above and below this. A further set of thermocouples was permanently fitted in the graphite in the region of lower statistical weight at radius 124.5 cm.

The calculations (see Chapter 2) were carried out for a system with uniform temperatures in the core (plus end reflectors) and in the side reflector. The actual temperature distribution in each of these two regions is ideally analysed to give the effective temperature, i.e. the uniform temperature which would give the same reactivity of the system. Since the number of thermocouple positions in the core was large and since their distribution was uniform, the radial temperature variation was satisfactorily accounted for by taking an unweighted mean. The temperature in the side reflector decreases with increasing radius and a simple analysis shows that the contribution to the reflector temperature coefficient decreases also; since the reflector coefficient is largely due to the absorption in this region, an effective temperature has been derived by weighting with the measured variation of a nearly $1/v$-absorber (copper) across the reflector. The systematic error in determining the uniform core temperature equivalent to the actual temperature distribution in the plutonium loading was taken as 1½%, as for the uranium-fuelled cores (Ref. 1.14); the systematic error due to temperature recording for the plutonium loading was found to be within the value of 2% estimated for the uranium loadings.

The data from a temperature coefficient study consist of a series of values of excess reactivity $\rho(\theta_C, \theta_R, P_o)$ where $(\theta_C + 20.4)$ and $(\theta_R + 20.4)$ are the weighted mean temperatures of core plus end reflectors and side reflector ($^oC$) and $P_o$ is the reactivity worth (%) at ambient temperature of

the particular configuration of inserted control rods. The measurements obtained with the first plutonium core are presented in Appendix E.

The dependence of reactivity on the parameters $\theta_C$, $\theta_R$ and $P_o$ was found by fitting a set of coefficients representing a physically reasonable dependence using a program written for the Ferranti Mercury Computer (Ref. 1.14). It was found that the measured data were represented adequately by the following expressions for the core plus end reflectors coefficient ($\alpha_C$) and side reflector coefficient ($\alpha_R$):

$$\alpha_C = (-0.33 + 0.0038\ \theta_C \pm 0.14) \times 10^{-5}$$ per °K for core temperatures between ambient and 670°K

$$\alpha_R = (5.09 - 0.0068\ \theta_R - 0.33\ P_o \pm 0.17) \times 10^{-5}$$ per °K for side reflector temperatures between ambient and 600°K,

i.e. the core coefficient is small and increases linearly with core temperature over this range, while the reflector coefficient is large and positive, falls linearly with temperature over the range and is reduced by the insertion of control rods. No improvement to the fit was obtained by the addition of other parameters representing either a dependence of the core coefficient upon the worth of inserted control rods or a dependence of the coefficient of one region upon the temperature of the other.

The uncertainties quoted are statistical and take into account approximately the correlation between the terms when used to evaluate the temperature coefficients with no control rod in the system. Additional uncertainties of 5½%, due to delayed neutron data (see Chapter 3) and due to the temperature recording and distribution (as noted above), are required for the total uncertainty.

The reproducibility of the reactivity of the system at the end of the temperature cycle is obtained by comparing the deviation of the fitted reactivity from the measurement at core and side reflector temperatures of 21.5 and 20.9°C, respectively, before heating and 25.3 and 25.0°C after heating. The reactivity change was less than 0.01% which over the 375°C temperature rise of the core would represent an average error of less than $3 \times 10^{-7}$/°K.

The coefficient of $P_o$ in the expression for the reflector coefficient may be used to derive the temperature coefficient of the worth of the inserted control rods. Using this value, a rod controlling 1% in reactivity with the reflector at room temperature would control 1.033% on raising the reflector temperature by 100°K. Similar values have been observed for the U235 cores (Ref. 1.14).

# CHAPTER 6

## SPECTRUM MEASUREMENTS WITH NEUTRON CHOPPER

### 6.1 Introduction

The WDSN cell calculation used to obtain the fine structure for the ZENITH fuel provides a directed neutron energy spectrum which may be compared with the measurements made using the neutron chopper time-of-flight spectrometer.

The detailed comparison with theory was complicated by the necessity of accounting adequately for the radial fine structure of the spectrum emergent from the source element, taking into consideration the spatial resolution function of the chopper and associated collimating system. Some consideration was given to the possibility of providing a source element of simpler geometry than the normal fuel element (e.g. a homogeneous cylindrical spine with fuel, absorber and moderator surrounded by an outer sleeve of graphite). Difficulty then arises, however, in the specification of the fuel content of the spine region in order to match the absorption characteristics of the standard element, and it was therefore decided to use the normal fuel element as the source and to adapt the theoretical model to take account of the detailed structure of the emergent beam.

The spectrum measurements were carried out on the first core only.

### 6.2 The Neutron Chopper and Source Element

The basic design of the ZENITH neutron chopper has been described elsewhere (Ref. 6.1, 6.2). In the present measurements, however, the rotor was incorporated in a redesigned housing with improved facilities for alignment of the assembly, and the provision for installing an auxiliary motor for making accurate small adjustments in rotor position during determinations of the dynamic background. The optical triggering system was also completely redesigned.

The chopper installation, with the in-pile collimator, rotor assembly, flight tube and detector bank, is shown in Fig. 6.1. Fig. 6.2 illustrates the rotor assembly; the fixed slits on either side of the rotor serve to reduce background. The chopper is capable of rotation at speeds up to 9600 r.p.m., at which speed the full width at half maximum of the (triangular))neutron burst is 40 μsec.

The neutron detectors used consisted of ten boron trifluoride proportional counters (96% B10) placed on top of the flight tube. The counters were 5 cm in diameter, had an active length of 15 cm and were filled to a pressure of 70 cm of Hg. The neutron pulses were fed to a 99-channel Phillips time analyser, the initiating pulse being obtained from a light signal reflected from a mirror on the chopper shaft.

The beam for the chopper measurement was extracted from a half length element (containing 5 spikes) which was inserted in place of the central element (K10). The spikes were separated by spacers of graphite and stainless steel, arranged in the same pattern as the normal element. Since the extreme end portion of the spike contained no fuel, being part of the aluminium envelope, the vertical location of the spikes was adjusted so that the top of the plutonium-bearing region was exactly level with the upper end of the graphite sleeve, which lay at the core mid-plane

(Fig. 6.3). A "top hat" of aluminium, 0.040" thick, formed a protective cover for the spikes.

## 6.3 The Measured Spectra

The details of the experiments have been given elsewhere (Ref. 6.5), and only the results are summarised in the present chapter. Two complete sets of measurements were carried out at ambient temperature (at chopper speeds of 2400, 4800 and 9600 r.p.m. and gate widths of 40, 20 and 10 μs), and one set at a core central region temperature of 645°K.

The spectra measured at core temperatures of 293°K and 645°K are shown in Fig. 6.4 normalised for comparison in the range above 10 eV. Each spectrum was produced from a combination of the runs at all three speeds. The low energy portion has been plotted from the runs at 2400 and 4800 r.p.m., since at these energies the cut-off correction for the higher chopper speed becomes inconveniently large. The limitation to the low energy end of the spectrum arises from the rapid deterioration in count to background ratio below about 0.01 eV. The runs at 9600 r.p.m. were used above 0.1 eV to obtain maximum resolution. The corresponding data are summarised in Appendix F.

The overall accuracy of the experimental spectrum is determined by the statistical errors on the individual points and by systematic factors such as the neutron transmission probability through the rotor (which is a function of rotor speed and neutron velocity) and the calibration of the neutron detectors as a function of neutron energy. The latter was obtained by comparison with the response of a 'thin' $1/v$ detector on the LIDO reactor at Harwell. Discrepancies between the most recent calibrations and earlier work suggest that there could be errors of order $\pm$ 10% in the flux at 0.01 eV relative to that above 1 eV in the spectra reported here.

The statistical error on the individual points is negligible at the higher energies, increasing to 5% at 0.02 eV. Below this energy the statistical error increases rapidly and is ~ 20% at 0.01 eV.

The curve of neutron transmission probability for different rotor speeds as a function of energy (or time-of-flight) was obtained using the method described in Ref. 6.3. The ratio of these curves for different rotor speeds was found to be in good agreement with that obtained from the comparison of chopper runs at different rotation speeds.

It was shown, using the formula of Stone and Slovacek (Ref. 6.4), that at the highest rotation speed, the correction for finite resolution was unimportant over the Pu239 resonance.

The effect of the Pu240 resonance at 1.06 eV is just apparent in the higher resolution runs. The resonance capture (calculated resonance escape probability = 0.93) is shown more clearly by the presentation used in Fig. 6.5, where $E.\phi(E)$ is plotted on a linear scale against energy.

# CHAPTER 7

## REACTION RATE DISTRIBUTIONS

### 7.1 Introduction

As a test of the treatment of the cell flux fine structure by the DSN calculation, measurements were carried out to find the relative activation of a detector of approximately $1/v$-dependent cross-section as a function of position in the fuel cell.

The axial and radial reaction rate distribution through the core and reflector regions was measured using a fission chamber containing Pu239, for comparison with the predictions of the ANGIE program. Additional measurements were made along the core axis using a fission chamber containing U235, the variation of Pu239/U235 fission ratio providing a useful indication of the ability of ANGIE to deal with spectrum changes over the reactor, particularly near the core-reflector interfaces.

### 7.2 Fine Structure Measurements

The most appropriate measurement of the fine structure would have been one where the spike reaction rate was measured by activation of plutonium foils, while that of the moderator was obtained by copper activation. The relative complexity of the foil intercalibrations required and the consequent larger experimental uncertainties led to the decision to perform the experiment with copper foils in both regions.

Special fine structure elements of the type shown in Fig. 7.1 were constructed, enabling measurements to be made at five different heights in the core. The reaction rate at each surface of the different components of the fuel bundle was obtained from 0.001 in. thick copper foils attached with Sellotape, the width of each being equal to that of the plutonium-bearing region of the spike (1.15"). The reaction rates in the graphite of the fuel box and sleeve were measured using foils of types 2 and 3, the former being accommodated as shown between sections of the fuel box and the latter inserted in 0.002 in. slits in the outer sleeve. After assembly, the fuel box was pinned in the sleeve in such a way that the measuring planes in box and sleeve were coincident and the sleeve foils covered the same $180^{\circ}$ sector as those in the box. The first measuring plane was 3.5 cm from the core centre, the others being spaced at intervals of 16.03 cm above the first foil.

The element was irradiated in the core centre location (K10) for 40 mins at a flux of $4 \times 10^7$ n/cm$^2$ sec. The activity counted was the 12.8 hr. $\beta$-decay of Cu64, using a single scintillator of 5 in. diameter coupled to an EMI 9530B photomultiplier. Since the type 3 foils had a diameter of 2.9 in., it was necessary to improve the radial flatness of response of the scintillator by applying thin layers of aluminium-covered PVC foil to the inner region.

Owing to the variation in area and thickness of the copper foils, it was necessary to include correction factors for geometrical efficiency of the counting system and for variation in $\beta$-ray self-absorption. These were made using a formula given by Hunt (Ref. 7.1) where the foil correction factor is of the form $g(1 + Kw/A)$, in which $g$ accounts for the foil geometry and $K$ for the self-absorption ($w$ is the foil weight, and $A$ the foil area).

All three types of foils were intercalibrated to find the values of g and K by irradiation in the thermal column of the NESTOR reactor.

While in the second core no significant difference was found between the fine structure measurements at different heights, in the first the measuring plane at the core boundary did show a significant variation from the others. In obtaining the disadvantage factor for comparison with theory, the values at this position have not been included. These values were combined with those of the element sleeve and fuel box and integrated over the appropriate volumes of fuel, steel and moderator to give the disadvantage factors quoted in Table 7.1 below. For the second core, where the single spike is surrounded by the graphite of the fuel element, a factor of 0.985 ± 0.004 has been taken for the ratio of activation in spike relative to activation at surface, based on the discussion by Carter et al. (Ref. 1.1). The errors quoted include the effects of uncertainty in the geometrical and self-shielding factors, and random sources such as counting statistics, and are consistent with the variation in ratios at the selected heights of measurement.

TABLE 7.1

Copper Activation Ratios

| Core | Ratio | Mean of all but Boundary Cell | Boundary Cell |
|---|---|---|---|
| 1 | $\frac{\text{Cu reaction rate in fuel}}{\text{Cu reaction rate in moderator}}$ | 0.821 ± 0.006 | 0.785 ± 0.008 |
| | $\frac{\text{Cu reaction rate in steel}}{\text{Cu reaction rate in moderator}}$ | 0.832 ± 0.007 | 0.794 ± 0.008 |
| | $\frac{\text{Cu reaction rate in steel}}{\text{Cu reaction rate in fuel}}$ | 1.014 ± 0.002 | 1.012 ± 0.003 |
| 2 | $\frac{\text{Cu reaction rate in fuel}}{\text{Cu reaction rate in moderator}}$ | 0.878 ± 0.007 | - |

Since the measurements with fission chambers were carried out in the interstitial positions between the fuel elements, it was of interest to obtain the ratio of copper activation on the surface of the element relative to the mean moderator value. For this purpose additional foils were placed on the element surface at each plane of measurement. The ratios of the reaction rate at this position relative to mean cell graphite are quoted in Table 7.2.

TABLE 7.2

Copper Reaction Rate at Surface of Element

(Mean of two foils at each axial height)

| Core | Position in cm (Axial height above core centre plane) | $\left(\frac{\text{Copper reaction rate at surface of element}}{\text{Copper reaction rate in cell graphite, mean}}\right)$ |
|---|---|---|
| 1 | 3.5 | 1.036 |
| | 35.6 | 1.036 |
| | 51.6 | 1.036 |
| | 67.6 | 1.051 |
| 2 | 3.5 | 1.012 |
| | 35.6 | 1.021 |
| | 51.6 | 1.021 |
| | 67.6 | 1.023 |

The comparison of the measured fine structure with theory is discussed in Chapter 8.

## 7.3 Fission Chamber Measurements

The axial and radial variation of both Pu239 and U235 reaction rates were measured at ambient temperature using 0.6 cm diameter fission chambers. Each chamber contained approximately 0.5 mgm of fissile material in an active length of 2.0 cm. Measurements were made axially at core centre and edge, and radially on the core centre plane and on a plane 24.5 cm above centre.

At each position four 100-sec counts were taken. Simultaneously the counts on the reactor instrumentation channels were taken to be used as a correction for drift in reactor power. Three of the fission chamber counts were made at an operational gain setting on the bias plateau and the fourth at reduced gain. Since this latter count was taken on the steep portion of the bias curve a sensitive indication was provided of variation of operating characteristics, a change of 10% in the ratio of the count rates at the two amplifier gains corresponding to a change in count rate on the plateau of 1%. The variation in this ratio was always less than $\pm$ 4% corresponding to less than $\pm$ 0.4% variation in count rate at operating bias.

The axial scans were performed at intervals of 5 cm in height in a sequence such that the counter was returned several times to the core centre position for physical position check and renormalisation of count rate. Bias curves were taken at the top and bottom positions and on each occasion when the chamber was at core centre position. The Pu239 radial scans were performed along a radius giving as symmetrical an azimuthal control rod distribution as possible. The sequence of positions was such that every fourth measurement was made in J9* channel to allow renormalisation of count rate. Before each measurement in J9* a bias curve was taken. The radial measurements of Pu239/U235 ratio were performed independently of the radial scans using a Pu239 and a U235 chamber simultaneously.

In all the measurements reported the error due to counting statistics was less than ± 0.3%. The error arising from changes in electronic operating conditions was obtained by examination of repeated measurements at the core centre (axial scans) or J9* channel (radial scans) and was estimated at ± 0.3%. This figure is consistent with the variations in the ratio of the counts at different gain values recorded above. Errors due to counter positioning uncertainty are most significant in the inner and outer reflector regions, where the slopes of the count rate vs position curve is greatest. The most sensitive indication of error in counter position is the difference between the Pu239/U235 ratios in the top and bottom reflector. The differences in these regions can be explained by assuming an overall positional uncertainty of ± 0.2 cm. Throughout most of the core the contribution to the error on the reaction rate of a single fissile nuclide relative to core centre is ± 0.2% but the error rises appreciably in the high flux gradient regions of the reflector, particularly in the region beyond 110 cm.

Measurements using a fission chamber covered with a 0.040 in. sheath of Nimonic 75 have shown that the nimonic wall of the chamber produces no detectable differential effect on the reaction rate of a single fissile nuclide over the extent of the core, but that in the outer reflector the chamber wall absorption reduces the reaction rate by ~ 0.5% relative to the core centre. No corrections have been made to the data presented for this effect which, within the experimental errors, will produce a negligible effect on the Pu239/U235 ratios.

Reaction rate distributions measured with Pu239 and U235 chambers in the first core are shown in Fig. 7.2 to 7.4. Fig. 7.2 and 7.3 show the axial distributions of the fission rates of Pu239 and U235 respectively in channel K10. Fig. 7.4 shows the radial Pu239 distribution on the core centre plane, taken with the control rod settings shown in Fig. 7.5. The variation of Pu239/U235 fission ratio in channel K10 is illustrated in Fig. 7.6. The data for the fission chamber scans are summarised in Appendix G, Tables G.1 to G.5.

As in the U235 cores there is asymmetry in the axial distribution with a peak to peak ratio of 1.15 for the Pu239 reaction rate and 1.16 for the U235. The sharp peak in the axial scans at the core centre is due to the 1.44 cm gap between plutonium spikes in the fuel elements. The radial scan was repeated in the plane 24.5 cm above core centre in order to obtain a scan free from the effects of this singularity; the higher side reflector peak in this scan is due to the absence of the peak at the central normalisation position in the plane. The slight increase in the Pu239/U235 in the graphite region at core centre position is presumably explained by the reduced shielding of the plutonium resonance flux due to the absence of fuel in this region.

The Pu239/U235 fission ratio in the interstitial channel nearest to the core centre, relative to the value in the outermost reflector position (R61) was 1.81 ± 0.04. It is known from measurements with Lu/Mn detectors that the spectrum at this latter position can be represented by a Maxwellian with a neutron temperature of 313 ± 7°K. A correction has been made to the experimental result, using Westcott data, to normalise to a reflector temperature of 300°K. A similar correction has been applied to normalise the core centre ratio, measured at a physical temperature of 293°K, for comparison with the MUPO prediction. The final value is then 1.83 ± 0.04 at 300°K.

A useful check of experimental consistency is provided by the measurements of fission ratio in a plutonium-spike fuelled exponential stack of very similar C/Pu239 ratio (2420) and calculated spectrum where a value of 1.79 $\pm$ 0.02 was obtained (Ref. 1.1).

The detailed comparison of these results with theory is given in Chapter 8.

# CHAPTER 8

## COMPARISON OF EXPERIMENT AND THEORY

### 8.1 Introduction

For design of an enriched-fuel reactor the calculational accuracies should be of the following order:

| | |
|---|---|
| On reactivity | ± 1% |
| On temperature coefficients of reactivity | ± $10^{-5}$/°K |
| On power distribution | ± 5%. |

In this chapter, comparisons of experiment and theory are made to assess the adequacy of the data and methods of calculation employed in meeting these requirements.

### 8.2 Neutron Spectrum

Two representations of the scattering characteristics of graphite have been used in the derivation of the thermal spectrum from the DSN cell calculation. The free gas model, which takes account of the thermal motion of the scattering atoms but assumes no interaction between atoms, has been used as a reference. This spectrum has been compared with that obtained from a crystal model based on the theory of Egelstaff and Schofield (Ref. 8.12), using a phonon spectrum derived from the experimental scattering law experiments of Egelstaff (Ref. 8.1)*.

From the equilibrium spectrum given by the DSN calculation the vertically directed flux $\phi_v(E, \underline{r})$ was calculated using a neutron balance argument as follows. Assuming a reactor core is infinite in the vertical direction, the number of neutrons of energy E scattered from 1 $cm^3$ into a small angle $d\Omega$ about the vertical direction is:

$$\frac{d\Omega}{4\pi} \int \phi(E', \underline{r})\ \Sigma_s\ (E' \longrightarrow E, \underline{r})\ dE'$$

The number of neutrons removed from 1 $cm^3$ in an angle $d\Omega$ about the vertical direction is:

$$\phi_v\ (E, \underline{r})\ \Sigma_t\ (E, \underline{r})\ d\Omega$$

where: $\Sigma_t(E)$ is the total cross-section at energy E.

For neutron balance:

$$\phi_v\ (E, \underline{r}) = \frac{1}{4\pi\ \Sigma_t\ (E, \underline{r})} \int \phi(E', \underline{r})\ \Sigma_s\ (E' \longrightarrow E, \underline{r})\ dE'$$

---

*All calculations of the neutron spectrum using WDSN were carried out by Mr. H. H. W. Pitcher of General Reactor Physics Division.

The surface of the source element was divided into eight concentric zones and this expression provided the vertically directed flux in each zone. In deriving the spectrum for comparison with experiment it was necessary to superimpose on the calculated vertical fluxes the spatial response function of the chopper collimating assembly which was a maximum for neutrons leaving the centre of the source element and decreased to zero at the edge. In the calculation of this response function, account had to be taken not only of the basic geometry of the main collimator, and of the slit system of the rotor and sub-collimators, but also of the relative transmission probability of neutrons of different velocity through the moving rotor. The details of the calculation have been given by Reed and Symons (Ref. 6.3).

In order to ensure the validity of the basic comparison of experimental and theoretical spectra it was necessary to check the adequacy of the geometrical approximation used in the DSN calculation to treat the complex configuration of the fuel bundle. The influence of the geometrical model was investigated by cylindricalising the source element in two different ways. In the first of these the Pu/Al spike, steel and graphite spacers were homogenised into an inner cylinder surrounded by the remaining graphite in the form of an outer sleeve. In the second model the plutonium was distributed in two annular regions, chosen so as to preserve the thickness of the plutonium alloy in the spike and the area of the fuel-bearing region of the element, while the aluminium sheath, steel and internal graphite were homogenised in the enclosed regions.

The directed spectra calculated using these two representations are shown in Fig. 8.1, the Egelstaff scattering model being used in both cases. The spectrum from the homogenised source element shows much more pronounced dips at the 0.3 eV and 1.06 eV resonances. This model would be expected to over-estimate the depressions caused by the resonances since in the actual fuel element (and in the annular geometrical model), although the depression in the spikes themselves is large, the contribution of neutrons to the directed beam from this region is small in comparison with that from the remaining graphite regions of the spine. For the homogeneous fuel region model, on the other hand, the depression exists over the entire central region.

The factor to which the derived spectra are most sensitive is in fact, the choice of scattering law, as is indicated in Fig. 8.2, where the spectra based on the gas model and on the Egelstaff scattering data, both with annular source geometry, are compared with the experimental spectrum (normalised at 1.45 eV). As expected the Egelstaff prediction is in better general agreement over the whole energy range than the gas model, which on account of its over-estimate of the energy transfer in the energy region where crystal binding effects are important, predicts too many neutrons below 0.1 eV. While even with the Egelstaff model there are still experimentally significant differences between the measured and calculated spectra (there is an indication that the spectra are still "too well thermalised") the practical importance of the residual discrepancy should not be exaggerated; the difference in steel/Pu239 absorption ratio calculated in the Egelstaff and in the experimental spectrum for example, is only 3%, corresponding to a reactivity error for this core loading of approximately 0.4%.

The reasonable adequacy of the Egelstaff model demonstrated here, is consistent with the results quoted by Macdougall (Ref. 8.2) and by Poole et al (Ref. 8.3).

## 8.3 Reactivity

### 8.3.1 Introduction

The excess reactivity data are first compared directly with experiment in Section 8.3.2. Subsequent sections deal with those particular aspects of the calculations which are less reliable and where special treatment is necessary.

### 8.3.2 Excess Reactivity

The data for comparison are given in Table 8.1. The reactivities calculated using MUPO and ANGIE are somewhat sensitive to the DSN calculation of flux fine structure in the fuel from which the MUPO group disadvantage factors for plutonium and steel are derived. The experimental measurement of the relative copper foil activation in plutonium, steel and moderator is compared with calculations of these quantities using the DSN fluxes. It will be seen that the differences between experiment and theory correspond to about $2\frac{1}{2}\%$ and 5% in fuel/moderator ratio for the two cores and, for the first core, $1\frac{1}{2}\%$ in steel to plutonium ratio. The theoretical ratios quoted for the first core have been obtained using the 'homogeneous' representation of the fuel region of the element (which of course results in equality of fuel spike and steel fluxes). With the 'annular' model the fuel/moderator and steel/fuel copper activation ratios were 0.836 and 1.008, i.e. not greatly different from the 'homogeneous' values.

The reactivity differences due to these differences in fine structure are determined by making use of a fitting formula due to Kalnaes (Ref. 8.4) to derive group disadvantage factors for plutonium and steel consistent with the experimental copper reaction rate ratios. (In the groups covering the Pu240 resonance the DSN-based disadvantage factors have been retained since the copper activation is insensitive to the actual fine structure there). For the first core the reactivity difference is 0.5%, most of which is due to the difference in thermal utilisation, which depends on the steel/plutonium flux ratio, and the remainder to the discrepancy in plutonium/moderator ratio which affects the thermal leakage. For the second core the reactivity difference in Table 8.1 is 1.0%, due largely to the change in thermal leakage. The unsatisfactory representation of the fine structure in the second core is probably due to the poor representation of the spike for the DSN calculation; this was done by converting the spike into an annulus of the same thickness. A more sophisticated calculation of fine structure using collision probability technique is desirable to improve the representation of fine structure, though it must be noted that the problem of heterogeneity is particular to the experiments with this fuel in ZENITH and would not arise in this form in a power reactor.

TABLE 8.1

Excess Reactivity of ZENITH Plutonium Loadings

| Loading | Excess Reactivity (%) | | Conditions of Theoretical Prediction | | | |
|---|---|---|---|---|---|---|
| | Experimental | Theoretical Prediction | ANGIE Energy Group Boundaries* | Mean Copper Activation Ratio ⁄ | | |
| | | | | Fuel Spike / Graphite | Steel / Fuel Spike | Origin |
| First | 3.8 ± 0.3 | 4.0 | a | 0.841 | 1.000 | DSN |
| | | 3.5 | b | 0.841 | 1.000 | DSN |
| First ø | 7.9 ± 0.6 | 3.5 | a | 0.821 (± 0.006) | 1.014 (± 0.002) | Experiment |
| | | 7.7 | a | 0.841 | 1.000 | DSN |
| Second | 4.8 ± 0.4 | 5.3 | a | 0.835 | – | DSN |
| | | 6.3 | a | 0.878 (± 0.007) | – | Experiment |
| | | 6.1 | b | 0.878 | – | Experiment |

* a 0.001, 0.0225, 0.1787, 1.00 4.564, 24780 and $10^7$ eV

b 0.001, 0.0225, 0.3568, 1.00, 4.564, 24780 and $10^7$ eV

⁄ Consistent with the group disadvantage factors used for MUPO. In the experiment-based set, the disadvantage factors used for the energy groups between 0.712 eV and 4.564 eV, i.e. around the Pu240 resonance, were taken from the DSN set.

ø With all radial regions outside the core modified to have the same mean graphite density and nitrogen content as the main side reflector (i.e. standard state C of Ref. 1.14). Perturbation measurements were used to adjust the experimental value.

The choice of energies for the ANGIE group boundaries is conditioned by the restriction on upscattering to the next group only. This limits the number of thermal groups to two and for these plutonium systems the upper energy boundary for the second group is also important as is indicated in Table 8.1 where the difference in calculated reactivity for the first core with two different group boundaries is 0.5%. The fractions of neutrons absorbed in each group for both cores are shown in Table 8.2.

TABLE 8.2

Fractions of Absorptions and Fissions in ANGIE Groups

| ANGIE Group | Energy Range (eV) | Fractional Absorptions | | Fractional Fissions | |
|---|---|---|---|---|---|
| | | 1st Core | 2nd Core | 1st Core | 2nd Core |
| 1 | 0.001 - 0.0225 | 0.043 | 0.187 | 0.048 | 0.198 |
| 2 | 0.0225 - 0.1787 | 0.342 | 0.586 | 0.378 | 0.608 |
| 3 | 0.1787 - 1.000 | 0.363 | 0.170 | 0.392 | 0.160 |
| 4 | 1.000 - 4.564 | 0.081 | 0.022 | 0.020 | 0.004 |
| 5 | 4.565 - 24780 | 0.155 | 0.033 | 0.148 | 0.028 |
| 6 | 24780 - $10^7$ | 0.016 | 0.002 | 0.014 | 0.002 |

A one-dimensional comparison, using CRAM (Ref. 8.11), of the two 6-group sets and an 18-group subdivision has been carried out for the first core. The two 6-group sets differ in reactivity by 0.3% (c.f. 0.5% in the 2-dimensional ANGIE comparison) and 6-group set "a" agrees within 0.01% with the 18-group set. Thus, apart from any difference which might be obscured by the one-dimensional representation, set "a", which avoids the undesirably wide 0.0225-0.3568 eV group, is clearly preferred.

When the experiment-based disadvantage factors are used, the predicted excess reactivity of the first core is consistent within experimental error ($\pm$ 0.3%), while the reactivity of the second core is overestimated by $(1.5 \pm 0.4)$%.

### 8.3.3 Reactivity Effect of Steel in the Core

A calculation of the reactivity effect of removing one third of the steel from the first core was carried out; using the experiment-based disadvantage factors the experimental reactivity change of $(4.31 \pm 0.26)$% was overestimated by $(0.40 \pm 0.26)$%. Uncertainties in the calculation due to the thermal cross-section of steel (0.13%) and neglect of the self-screening of the steel resonances (0.03%) seem insufficient to explain this discrepancy, and other systematic inaccuracies in the calculation, such as the representation of ZENITH voidage, for example, should largely cancel out. The difference could arise from either an overestimate of the reaction rate of steel relative to that of Pu239 or, rather improbably, from the use of a delayed neutron fraction for Pu239 which is $(10 \pm 3)$% low.

In fact, an overestimate of the effect of steel is consistent with the other observation that the measured Pu239/U235 fission ratio (relative to 300°K Maxwellian) at the core centre is $1.83 \pm 0.04$,

compared to the MUPO prediction of 1.67. Since steel and U235 have similar low energy cross-section dependence (approximating to $^1/_v$) the Pu239/steel reaction rate ratio will be similarly underestimated, resulting in an overestimate of the relative absorption in steel by some 10%. The error in fission ratio is apparently due to the inadequacy of the Schofield scattering data for graphite used in the MUPO library, and has been noted elsewhere (Ref. 1.14). There is evidence that the more recent models of Parks (Ref. 8.13) or Egelstaff (Ref. 8.1) give more satisfactory agreement.

When the differences between experiment and theory for the first loading are extrapolated to a system containing no steel, the excess reactivity would be overestimated by 0.9% with the experiment-based disadvantage factors, closer to the difference observed in the second core where no steel was present.

### 8.3.4 Reactivity Effects of Graphite in the Side Reflector

The inner part of the ZENITH side reflector contains several regions of quite high voidage and the treatment of these presents a problem in diffusion theory calculations. The effect of voidage in the core edge region (Fig. 1.5) has been investigated in considerable detail both experimentally and by the theoretical methods available here. The experimental results (Fig. 8.3) show that the reactivity variation is linear in the weight of graphite (when this is removed in an axially uniform manner) and this implies that the effects of streaming are not great, since the small side fillers are of significantly different thickness from the large fillers (Fig. 1.5) and the large fillers were removed alternately. The calculation of the homogenized region with density appropriately reduced, predicts a reactivity change which for small amounts of graphite removed is approximately linear and is about $\frac{3}{4}$ of the experimental value. The theoretical curve crosses the experimental line when approximately $^2/_3$ of the graphite has been removed and thereafter the theoretical reactivity change becomes much greater (numerically). Although the shape of the theoretical curve can be explained on the basis of inadequacy of diffusion theory, the disagreement between the initial slope of the theoretical curve and the experimental line is unsatisfactory and respresents a potentially more serious failure of the theoretical model. A similar disagreement is observed in the control rods region where the effect of adding 205 Kg of graphite (equivalent to 230 Kg of graphite of full axial height) into the region of mean voidage 0.7 was calculated. The ratio of the theoretical to the experimental reactivity was 0.57, compared with the value 0.75 derived from the data for the core edge region over the same density range.

On this evidence, the ratio of theoretical and experimental reactivity change in Fig. 8.3 may be assumed to be valid for the lampblack insulation barrier region and may be used to estimate the effect on the comparison of theoretical and experimental reactivity. The effect of changing the lampblack density to the same value as the main side reflector (1.55 gm/cc) would increase the reactivity difference between theory and experiment by 0.8%. The effect of making the same change in the control rods region would reduce the difference by 0.7%. Although these largely cancel, direct comparison of a theoretical calculation in which the lampblack and control rods

region have the same mean density as the main side reflector with the experimental value corrected for these changes in graphite content is preferable. Such a calculation is included in Table 8.1, showing that eliminating the regions of high voidage from the calculations shifts the difference between calculation and experiment by 0.4%.

The uncertainty in the density of the reflector graphite (see Appendix A) is estimated to contribute an uncertainty of 0.2% in excess reactivity.

### 8.3.5 Plutonium Data

The Pu239 cross-sections stored in the MOCUP library yield fission and absorption resonance integrals in good agreement with a recent calculation by Brissenden (Ref. 8.5) using resonance parameters recommended by Story (Ref. 8.6). In the calculations carried out here, MUPO data are used above and below this range. The MOCUP-MUPO data differ somewhat from those recently recommended by Hanna and Walker from which Critoph (Ref. 8.7) has derived 2-group cross-sections for the amendment to the Westcott compilation. The values are given in Table 8.3.

TABLE 8.3

Pu239 Resonance Integrals

| Origin | Resonance Integral* from 0.45 eV | | | |
|---|---|---|---|---|
| | Fission Barns | Absorption Barns | Capture / Fission | $\bar{\eta}$ |
| Data used in present work | 300 | 494 | 0.65 | 1.76 |
| Hanna and Walker | 321 | 516 | 0.61 | 1.80 |

*Including $^1/_v$ component

The effect of changing to data consistent with the Hanna and Walker recommendation would increase the reactivity of the first core by 0.8%.

The effect of neglecting resonance self-screening of the Pu239, which is calculated by MOCUP, is to increase the excess reactivity of the first core by 0.5%. It is estimated that the uncertainty on the reactivity of the system due to the uncertainty in the self-screening calculation is < 0.1%.

### 8.3.6 Comparison with U235 Cores

The comparison of Pu239 and U235 fuelled cores of comparable spectra with the same conditions for the reflector should eliminate in large measure the uncertainty due to the effects of the core edge and reflector voidage on the excess reactivity of the system. The fifth U235 core and the first Pu239 core had similar absorption per scattering atom, as also did the fourth U235 and second Pu239 cores.

Table 8.4 shows the comparisons. For the harder spectrum systems the agreement of the reactivity difference between calculation and experiment is better when the plutonium core is taken with all steel removed; this supports the conclusions reached in Section 8.3.3.

The comparison given in Table 8.4 shows that, for both the dilute and the heavy loadings, the accuracy of calculation of reactivity with Pu239 fuel (in the absence of competitive absorber) does not differ from that achieved with U235 by more than one percent.

TABLE 8.4

Comparison of Excess Reactivities of U235 and Pu239 Cores

| Core | $\Sigma_a/\xi\Sigma_s$ | Excess Reactivity (%) in Standard State B1 (Ref. 1.14) | | |
|---|---|---|---|---|
| | | Experiment | Calculation* | Calculation–Experiment |
| 1st Plutonium | 0.51 | 3.8 ± 0.3 | 3.5 | −0.3 ± 0.3 |
| 1st Plutonium with all steel removed | | see Section 8.3.3 | | +0.9 ± 0.8 |
| 5th U235 | 0.84 | 5.3 ± 0.4 | 6.5 | +1.2 ± 0.4 |
| 2nd Plutonium | 0.09 | 4.8 ± 0.4 | 6.3 | +1.5 ± 0.4 |
| 4th U235 | 0.12 | 9.3 ± 0.8 | 10.4 | +1.1 ± 0.8 |

*Using disadvantage factors based on experiment as in Table 8.1. For U235 Cores, the data have been corrected to $\eta = 2.078$ (Ref. 8.8) at 2200 m/sec from the value 2.057 in the MUPO library.

## 8.4 Temperature Coefficients of Reactivity

The comparison of experimental temperature coefficients of reactivity for the first core with calculation is given in Table 8.5. The reactor state for the measurements differed from those for the excess reactivity in three important respects: the graphite content of the core edge region was 110 Kg instead of the normal full loading of 367 Kg; the steel/Pu atomic ratio in the core was 83 and the control rods region contained instrumentation, etc. controlling 0.75% in reactivity. The calculations take these into account.

The ANGIE calculations use the disadvantage factors from the DSN calculation with homogenised fuel region and set "a" energy group boundaries.

The theoretical temperature coefficients are obtained by differencing reactivity calculations made with the MUPO graphite scattering matrices at the appropriate temperatures. The incomplete convergence of the ANGIE program results in a numerical error of $0.1 \times 10^{-5}$ per $^{o}K$ in the quoted data.

Doppler broadening of the Pu240 resonance was not included directly in the MUPO-ANGIE calculations and an additional calculation was needed to obtain the contribution due to this. By carrying out reactivity calculations with and without the Pu240 it was found that the absorption in this isotope (which occurs predominantly at the 1.06 eV resonance) controls 5.0% reactivity, so that the core-average resonance escape probability $\bar{p} = 0.95$. Then the Doppler coefficient is approximately:

$$-\left(\frac{1-\bar{p}}{\bar{p}}\right)\frac{1}{I}\frac{dI}{d\theta} = -0.053\,\frac{1}{I}\frac{dI}{d\theta}$$

where I is the Pu240 effective resonance integral.

Using the tabulation given by Blake (Ref. 8.9) with a reasonable $\sigma_p$ (based on a smeared fuel region), $\frac{1}{I}\frac{dI}{d\theta}$ is found to be $1.0 \times 10^{-4}$ per °K so that the Doppler reactivity coefficient is $-0.5 \times 10^{-5}$ per °K. A more sophisticated calculation using the SPECTROX code by R. G. Harper (Ref. 8.10) gave a very similar result. The Doppler contribution is included in the calculated data in Table 8.5.

No detailed account has been taken in the calculations of the thermal expansion of the core; such effects, which are normally neglected in solid moderator systems, are of some significance in ZENITH due to the small core size and to the fact that the support structure (Fig. 1.1) at the base of the core is made of nimonic alloy and is heated to a temperature exceeding that in the core. An estimate based on the difference in fuel element worth at core edge compared with core average gives a contribution from expansion of $-(0.5 \pm 0.2) \times 10^{-5}$ per °K (see Appendix H).

TABLE 8.5

Temperature Coefficients of Reactivity in the First Core

| Region | Temperature Range (°K) | Temperature Coefficient of Reactivity ($10^{-5}$ per °K) | | |
|---|---|---|---|---|
| | | Experiment | Theory | Theory, with Expansion Correction |
| Core plus End Reflectors | 300 - 500<br>500 - 700 | +0.1 ± 0.2<br>+0.8 ± 0.2 | 1.3<br>1.1 | 0.8 ± 0.2<br>0.6 ± 0.2 |
| Side Reflector | 300 - 500<br>500 - 700 | +4.4 ± 0.3<br>+3.0 ± 0.3 | 3.6<br>2.2 | -<br>- |

The effect of altering the ANGIE energy group boundaries to set "b" is negligible for the side reflector coefficient and for the core plus end reflectors coefficient in the 300-500°K temperature range, though in the higher temperature range the core coefficient increases by $1.0 \times 10^{-5}$ per °K, a significant change. The coefficients using the experiment-based set of disadvantage factors have not been calculated directly, though it is estimated that the resulting change in steel/plutonium reaction rate would increase the calculated core coefficient by approximately $+0.1 \times 10^{-5}$ per °K

and the change in plutonium/graphite reaction rate would decrease the coefficient by a similar amount.

In summary the agreement with experiment for the core temperature coefficient is approximately 1 x $10^{-5}$ °K, which is comparable with that observed in the U235 loadings (Ref. 1.14). The agreement with the side reflector coefficient is similar and represents an improvement on the comparison for the U235 loadings where the effect of the neutron absorption by the instrumentation in the control rod region and the nitrogen content of the pores in the graphite was not included directly.

## 8.5 Reaction Rate Distribution

The six group fluxes given by the ANGIE program were used to provide the spatial variation of the reaction rate of Pu239 in the core and reflector regions. Six group cross-sections for each of the buckling regions were obtained by condensation using the appropriate 43-group MUPO spectrum. The calculation was performed using both of the thermal group structures discussed above in the reactivity comparisons.

The comparison of experiment with theory for the first core is given in Appendix G, Tables G.1 - G.5, and in Figs. 7.2 - 7.6. It is seen that the two calculations differ significantly from one another and from the experimental measurements, the discrepancy between experiment and theory at the interface between the two buckling regions (at about 2/3 core radius) being about 5% with either choice of groups. It is evident that a more satisfactory prediction of the core power distribution would require the use of a 2-dimensional diffusion code allowing the use of a finer thermal group structure.

The overall change of spectrum as a function of position in the reactor, is predicted reasonably well by the ANGIE 6-group calculation, even near the core-reflector boundary, as is shown in Fig. 7.6, where the ANGIE prediction of the Pu239/U235 fission ratio along the reactor axis (using the preferred choice of thermal group boundary) is compared with experiment. The slight peaking effect at the core centre plane is caused by the absence of plutonium from the small region separating the fuel spikes in the axial direction.

## 8.6 Conclusions

The primary conclusion which may be drawn from the comparisons of theory with experiment is that the general agreement is comparable with that found for the U235 cores previously investigated, and is of the order of the suggested design requirements of 1% in reactivity, $10^{-5}$ per °K in temperature coefficient and 5% in power distribution. It is important to note, however, that this refers to plutonium containing only a small abundance of 240 isotope.

More specific points are:

(a) The Schofield representation of graphite used in the MUPO code gives spectra in which the ratio of Pu239 to $1/v$ absorber reactions is 10% low in the heavier loading (consistent with the experience in the exponential experiments with this fuel), and this results in correspondingly overestimated reactivity worth of steel. The reasonable agreement observed between the chopper measurements and spectra predicted using the more recent Egelstaff

scattering law, as well as other evidence, implies that the use of this would significantly reduce the discrepancy.

(b) The comparison of relative reactivities of plutonium and U235 cores of similar overall spectrum avoids some of the sources of systematic error (e.g. treatment of core boundary region) on the absolute reactivity of a core considered in isolation. The accuracy of reactivity calculation for plutonium is shown to differ from that for U235 fuel by not more than about one percent. This is not inconsistent with the rather lower accuracy measurements in the exponential assemblies.

(c) As is often the case, the treatment by cylindricalisation of a rather complex experimental fuel element geometry is not adequate and introduces some uncertainty into the comparisons of reactivity and spectra.

(d) The use of a two-dimensional diffusion code allowing more detailed thermal group structure (say below 2 eV) than ANGIE, is very desirable, and would avoid the necessity for buckling iteration. The excess reactivity and core temperature coefficient are noticeably changed when the thermal group boundaries are altered.

(e) The kinetic behaviour of the plutonium fuelled cores for frequencies less than $\frac{1}{2}$ cps does not differ from that for a bare reactor with constant effective neutron lifetime. At 1 cps, some dependence of the phase of the transfer function on detector position is noted.


## Acknowledgements

It is a pleasure to acknowledge the unremitting efforts of the ZENITH Operations team under Mr. L. J. Brading.

The authors are also indebted to Dr. J. E. Sanders for guidance and encouragement.

## REFERENCES


1.1 D. H. Carter et al. "Measurements of Buckling and Relative Reaction Rates in some Plutonium-Graphite Assemblies". J. Nucl. En. 18, 105 (1964).

1.2 K. J. Mitchell and R. A. Geary. "The High Temperature Zero Energy Reactor ZENITH". P.I.C.G. 10, 1463 (1958).

1.3 G. Gunnill and G. H. Kinchin. "ZENITH". Nucl. Eng., November 1959.

1.4 O.E.E.C. Dragon Project First Annual Report (1959-60)

1.5 O.E.E.C. Dragon Project Second Annual Report (1960-61).

1.6 O.E.E.C. Dragon Project Third Annual Report (1961-62).

1.7 B. W. Micheelson. "Control Rod Studies for the ZENITH Reactor". Proceedings of a Symposium on Physics and Material Problems of Reactor Control Rods, I.A.E.A., Vienna, (1963) 107

1.8 R. M. Absalom et al. "A Report on the First Loading of ZENITH". AEEW - R 50 (1960).

1.9 R. M. Absalom et al. A.E.E. Winfrith Internal Report.

1.10 F. R. Barclay et al. A.E.E. Winfrith Internal Report.

1.11 M. H. Burgess et al. A.E.E. Winfrith Internal Report.

1.12 R. Caro Manso, R. G. Freemantle and J. D. Rogers. "Temperature Coefficients of Reactivity in the Fourth Loading of ZENITH". AEEW - R 208 (1962).

1.13 I. R. Cameron et al. "Reactivity and Reaction Rate Studies on the Fourth Loading of ZENITH". AEEW - R 237 (1963).

1.14 F. R. Barclay et al. "A Report on Core 5 of ZENITH". AEEW - R 328.

1.15 I. R. Cameron. A.E.E. Winfrith Internal Report.

2.1 H. H. W. Pitcher. Private Communication.

2.2 G. W. Bannister, J. C. Basher and I. C. Pull. "MOCUP, a Monte Carlo Programme". To be published as AEEW - R 243.

2.3 S. Francescon. "The Winfrith DSN Programme". AEEW - R 273 (1963).

2.4 J. D. Macdougall. "PIXSE". AEEW - M 318 (1963).

2.5 J. Schlösser. Internal Dragon Project Report.

2.6 R. Stuart and S. Stone. "ANGIE, a Two-Dimensional Multigroup Neutron Diffusion Code for IBM-704". UCRL-5019 (1957).

2.7 G. D. Joanou et al. "Nuclear Data for GAM-I Data Tape".

2.8 P. Schofield and A. Hassitt. P.I.C.G. 16, Paper 18 (1958).

3.1 B. J. Toppel. "Sources of Error in Reactivity Determinations by Means of Asymptotic Period Measurements". Nucl. Sci. & Eng., 5, 2, 88 (1959).

3.2 G. R. Keepin, T. F. Wimmett and R. K. Ziegler. "Delayed Neutrons from Fissionable Isotopes of Uranium, Plutonium and Thorium". J. Nucl. En. 6, 1 (1957).

3.3 D. Okrent et al. "The Reactor Kinetics of the Transient Reactor Test Facility (TREAT)". ANL-6174 (1960).

4.1 D. J. Littler. "Measurements of the Change in Cross-Section of Irradiated Uranium made by Modulating the Power of a Nuclear Reactor". RS/R 2092.

4.2 C. E. Cohn. "Reflected-Reactor Kinetics". Nucl. Sci. & Eng., 13, 1, 12 (1962).

4.3 A. Wassermann, in Quarterly Technical Report, SPERT Project, IDO 16606 (1960).

4.4 R. W. Keaton and C. W. Griffin, "Reflected Reactor Kinetics", NAA-SR-7263

6.1 F. R. Barclay et al. "Time-of-Flight Neutron Spectra Measurements in ZENITH". AEEW - R 89 (1962).

6.2 F. R. Barclay and D. L. Reed. "Time-of-Flight Neutron Spectra Measurements on Core 4 of ZENITH". AEEW - R 193 (1962).

6.3 D. L. Reed and C. R. Symons. "A Method for Comparison of Experimental and Theoretical Differential Neutron Spectra in the ZENITH Reactor". AEEW - M 453.

6.4 R. S. Stone and R. E. Slovacek. Nucl. Sci. & Eng., 6, 466 (1959).

6.5 F. R. Barclay et al. "Spectrum Measurements in the ZENITH Plutonium Core 7 using a Neutron Chopper" AEEW - R 375.

7.1 C. Hunt. Private Communication.

8.1 P. A. Egelstaff. Private Communication.

8.2 J. D. Macdougall. "The Effect of Moderator Scattering Law on the Physics of Graphite-Moderated Thermal Reactors". React. Sci. & Tech., 17, 481 (1963).

8.3 M. J. Poole, P. Schofield and R. N. Sinclair. "Some Measurements of Thermal Neutron Spectra". Proceedings of a Symposium on Exponential and Critical Experiments, Amsterdam, 1963. Vol. III, P 87.

8.4 O. Kalnaes. Internal Dragon Project Report.

8.5 R. J. Brissenden. Private Communication.

8.6 J. S. Story. Private Communication.

8.7 E. Critoph. "Effective Cross-Sections for U235 and Pu239". CRRP-1191. (Addendum to AECL-1101) (1964).

8.8 N-G. Sjostrand and J. S. Story. "Neutron Cross-Sections and Fission Parameters of U233, U235 and Pu239 at 2200 m/sec". AEEW - M 125 (1961).

8.9 J. P. H. Blake. "Resonance Integral Calculations for High Temperature Reactors". AEEW - R 25 (1960).

8.10 R. G. Harper. Private Communication.

8.11 A. Hassitt. "A Computer Programme to Solve the Multigroup Diffusion Equations". TRG Report 229 (R).

8.12 P. A. Egelstaff and P Schofield. "On the Evaluation of the Thermal Neutron Scattering Law". AERE - R 3803.

8.13 D.E. Parks, J.R. Beyster and N.F. Wikner. "Thermal Neutron Spectra in Graphite". N.S.E. (1962) 13, 306.

## APPENDIX A

### Physics Data for ZENITH Plutonium Cores

1. FUEL ELEMENTS

| | | |
|---|---|---|
| Effective overall length | 246.2 | cm |
| Length of fuel region* | 139.9 | cm |
| Outside diameter of graphite sleeve | 7.37 | cm |
| Inside diameter of graphite sleeve | 4.59 | cm |

2. SPIKE

| | | |
|---|---|---|
| Total length of spike | 71.36 | cm |
| Length of Pu-Al alloy core | 69.22 | cm |
| Total width of spike | 3.10 | cm |
| Width of Pu-Al alloy core | 2.94 | cm |
| Thickness of Pu-Al alloy core | 0.051 | cm |
| Thickness of Al sheath | 0.051 | cm |
| Wt. of Pu in spike core | 6.50 | gm |
| Wt. of Al in spike core | 26.47 | gm |
| Wt. of Al sheath | 61.30 | gm |

| Plutonium atomic composition: | | No. of Spikes per Fuel Element | |
|---|---|---|---|
| Pu239 | 97.4% | Core 1 | : 10 |
| Pu240 | 2.5% | Core 2 | : 2 |
| Pu241 | 0.1% | | |

3. STEEL (Core 1 only)

| | |
|---|---|
| Total length of steel | 139.6 cm |
| Width | 2.50 cm |
| Thickness | 0.142 cm (17 SWG) |
| Density | 7.85 gm/cm$^3$ |

*This length includes the central gap of 1.44 cm, made up of a graphite spacer of 0.20 cm length and the aluminium end terminations of the spikes.

Steel Composition (wt. %)

| Constituent | Wt. % |
|---|---|
| Fe | 69.1 |
| Cr | 18.7 |
| Ni | 10.3 |
| Mn | 0.8 |
| Ti | 0.5 |
| Mo | 0.2 |
| Co | 0.1 |
| Si | 0.1 |
| Al | 0.1 |
| C | 0.1 |

4. REACTOR CORE

| | |
|---|---|
| Effective diameter of core | 122.7 cm |
| Height of core (loaded region) | 139.9 cm |
| No. of fuel elements in fully loaded core | 235 |
| Triangular lattice pitch | 7.62 cm |
| Voidage fraction in core | 0.187 |
| Capture cross-section of fuel element graphite | 4.2 mb |
| Density of sleeve graphite | 1.634 $gm/cm^3$ |
| Density of fuel box graphite | 1.669 $gm/cm^3$ |

5. EFFECTIVE DIAMETERS IN RADIAL REFLECTOR REGIONS

| | |
|---|---|
| Barrier tiles inside | 127.90 cm |
| Barrier tiles outside<br>Lampblack inside | 135.62 cm |
| Lampblack outside<br>"Control Rod Zone" inside | 144.18 cm |
| "Control Rod Zone" outside<br>Main reflector inside | 167.32 cm |
| Main reflector outside | 318.46 cm |

6. LAMPBLACK

| | |
|---|---|
| Density | 0.24 ± 0.03 gm/cm$^3$ |
| Absorption cross-section | 4 mb |

7. MAIN REFLECTOR

| | |
|---|---|
| Voidage fraction | 0.074 |
| Graphite cross-section (2200 m/s) | 4.3 cm |
| Graphite density | 1.68 ± 0.02 gm/cm$^3$ |

8. CONTROL RODS

(a) Normal rods

| | |
|---|---|
| Length | 169.9 cm |
| Length of boron carbide loaded region | 153.3 cm |
| Inner tube | 4.6 cm OD x 20 SWG (0.091 cm) |
| Material | B.S. 980 C.D.S.2 |
| Length | 168.7 cm |
| Outer tube | 6.19 cm OD x 20 SWG (0.091 cm) |
| Material | B.S. 980 C.D.S.2 |
| Length | 159.8 cm |
| Boron carbide density | 1.33 gm/cm$^3$ |
| Total boron carbide weight | 1600 gm |
| Diameter of control rod channel in reflector graphite | 7.77 cm |

(b) Special smaller rods

| | |
|---|---|
| Length | 169.9 cm |
| Length of boron carbide loaded region | 153.3 cm |
| Inner tube | 1.905 cm OD x 13 SWG (0.234 cm) |
| Material | B.S. 980 C.D.S.2 |
| Length | 168.7 cm |
| Outer tube | 3.175 cm OD x 17 SWG (0.142 cm) |
| Material | B.S. 980 C.D.S.2 |
| Length | 159.8 cm |
| Boron carbide density | 1.33 gm/cm$^3$ |
| Total boron carbide weight | 570 gm |
| Diameter of control rod channel in reflector graphite | 7.77 cm |

TABLE B1

Mesh Points at which Mesh Spacing Changes

(see Fig. 2.1)

| Axial Position (cm) | Axial Mesh Point | | Regions* |
|---|---|---|---|
| | CRAM in 1 dimension | ANGIE | |
| -10.00 | - | 0 | |
| | | | 15, 16 |
| 0.00 | 0 | 2 | |
| | | | 1, 10, 11, 12, 14, 17 |
| 31.51 | 4 | 6 | |
| | | | 1, 10, 11, 12, 13, 14 |
| 41.51 | | 8 | |
| | | | 1, 10, 11, 12, 13, 14 |
| 51.51 | 7 | 11 | |
| | | | 2, 10, 11, 12, 13, 14 |
| 53.35 | 8 | 12 | |
| | | | 3, 10, 11, 12, 13, 14 |
| 73.35 | 12 | 18 | |
| | | | 3, 10, 11, 12, 13, 14 |
| 122.56 | 18 | 27 | |
| | | | 4, 10, 11, 12, 13, 14 |
| 124.00 | 19 | 29 | |
| | | | 3, 10, 11, 12, 13, 14 |
| 171.60 | 25 | 38 | |
| | | | 3, 10, 11, 12, 13, 14 |
| 191.60 | 29 | 44 | |
| | | | 5, 10, 11, 12, 13, 14 |
| 193.21 | 30 | 45 | |
| | | | 6, 10, 11, 12, 13, 14 |
| 197.24 | 31 | 47 | |
| | | | 7, 10, 11, 12, 13, 14 |
| 203.59 | 32 | 49 | |
| | | | 8, 10, 11, 12, 13, 14 |
| 214.18 | 34 | | |
| | | | 8 |
| 219.47 | | 52 | |
| | | | 8, 10, 11, 12, 13, 14 |
| 239.47 | 36 | 54 | |
| | | | 9, 10, 11, 12, 13, 14 |
| 246.23 | 37 | 55 | |

*Regions 10-17 do not apply to CRAM

| Radial Position (cm) | Radial Mesh Point (ANGIE) | Regions |
|---|---|---|
| 0.00 | 0 | |
| | | 1, 2, 3, 4, 5, 6, 7, 8, 9, 15 |
| 40.00 | 8 | |
| | | 1, 2, 3, 4, 5, 6, 7, 8, 9, 15 |
| 61.33 | 14 | |
| | | 10, 16 |
| 63.95 | 15 | |
| | | 11, 16 |
| 67.81 | 16 | |
| | | 12, 16 |
| 72.09 | 17 | |
| | | 13, 16, 17 |
| 83.66 | 20 | |
| | | 14, 16 |
| 93.66 | 22 | |
| | | 14, 16 |
| 103.66 | 23 | |
| | | 14, 16 |
| 159.23 | 28 | |

TABLE B2

Number Densities of Atoms

| Region | Plutonium Loading | Pu239 ($\times 10^{19}$) | Pu240 ($\times 10^{17}$) | Pu241 ($\times 10^{16}$) | C ($\times 10^{22}$) | Al ($\times 10^{21}$) | Fe ($\times 10^{21}$) | Cr ($\times 10^{20}$) | Ni ($\times 10^{20}$) | Mn ($\times 10^{19}$) | Co ($\times 10^{18}$) | Mo ($\times 10^{18}$) | Ti ($\times 10^{19}$) | N (300°K) ($\times 10^{19}$) |
|---|---|---|---|---|---|---|---|---|---|---|---|---|---|---|
| 1 | Both | | | | 6.837 | | | | | | | | | 1.778 |
| 2 | First | | | | 6.153 | 2.196 | 0.220 | | | | | | | 2.090 |
| 2 | Second | | | | 6.515 | 0.843 | 0.220 | | | | | | | 1.896 |
| 3 | First | 2.291 | 5.837 | 2.680 | 6.106 | 2.753 | 1.214 | 3.532 | 1.625 | 1.466 | 1.579 | 2.360 | 1.060 | 1.740 |
| 3 | Second | 0.4582 | 0.1167 | 0.536 | 6.669 | 0.551 | | | | | | | | 1.816 |
| 4 | First | | | | 6.301 | 1.236 | 1.214 | 3.532 | 1.625 | 1.466 | 1.579 | 2.360 | 1.060 | 1.740 |
| 4 | Second | | | | 6.729 | 0.247 | | | | | | | | 1.816 |
| 5 | First | 2.291 | 5.837 | 2.680 | 6.132 | 2.753 | 0.558 | 1.625 | 0.747 | 0.674 | 0.726 | 1.080 | 0.487 | 1.740 |
| 5 | Second | 0.4582 | 0.1167 | 0.536 | 6.669 | 0.551 | | | | | | | | 1.816 |
| 6 | First | | | | 6.093 | 1.047 | | | | | | | | 2.121 |
| 6 | Second | | | | 6.227 | 0.209 | | | | | | | | 1.955 |
| 7 | Both | | | | 6.404 | | | | | | | | | 1.987 |
| 8 | Both | | | | 6.755 | | | | | | | | | 1.778 |
| 9 | Both | | | | 5.945 | | | | | | | | | 2.151 |
| 10 | Both | | | | 7.310 | | | | | | | | | 1.612 |
| 11 | Both | | | | 8.417 | | | | | | | | | 1.066 |
| 12 | Both | | | | 1.202 | | | | | | | | | 4.372 |
| 13 | Both | | | | 5.892 | | | | | | | | | 2.213 |
| 14 | Both | | | | 7.794 | | | | | | | | | 1.349 |
| 15 | Both | | | | 0 | | 1.97 | 80.2 | 26.81 | | | | | 0 |
| 16 | Both | | | | 0 | | 1.59 | 65.0 | 21.74 | | | | | 0 |
| 17 | Both | | | | 8.417 | | | | | | | | | 1.066 |

## APPENDIX C

### TABLE C1

Reactivity Perturbations due to Graphite and Fuel in the Core Region

| Position in Core | Radius (cm) | Reactivity Change (%) on loading | | | |
|---|---|---|---|---|---|
| | | Graphite* | | Fuel/ | |
| | | Core 1 | Core 2 | Core 1 | Core 2 |
| T17 | 53.3 | 0.012 | 0.016 | 0.042 | 0.089 |
| S16 | 45.7 | 0.017 | | 0.024 | |
| R15 | 38.1 | 0.019 | | 0.018 | |
| P14 | 30.5 | 0.021 | 0.023 | 0.015 | 0.104 |
| N13 | 22.9 | 0.023 | | 0.013 | |
| M12 | 15.2 | 0.024 | 0.027 | 0.015 | 0.122 |
| L11 | 7.6 | 0.025 | | 0.015 | |
| K10 | 0 | 0.025 | 0.027 | 0.017 | 0.131 |
| J9 | 7.6 | 0.025 | | 0.016 | |
| H8 | 15.2 | 0.024 | 0.027 | 0.015 | 0.122 |
| G7 | 22.9 | 0.026 | | 0.012 | |
| F6 | 30.5 | 0.024 | 0.024 | 0.013 | 0.101 |
| E5 | 38.1 | 0.023 | | 0.016 | |
| D4 | 45.7 | 0.020 | | 0.022 | |
| C3 | 53.3 | 0.015 | 0.016 | 0.048 | 0.088 |

*1 kg uniformly distributed between 78.4 cm above the core centre plane and 74.0 cm below.

/The plutonium, aluminium and steel content of a standard fuel element.

TABLE C2

Radial Variation of Reactivity Perturbation due to Full Length Graphite

| Position | Radius (cm) | *Reactivity Change (% per kg) | |
|---|---|---|---|
| | | Core 1 | Core 2 |
| K10 | 0 | 0.0213 | 0.0247 |
| P14 | 30.5 | 0.0181 | 0.0211 |
| T17 | 53.3 | 0.0102 | 0.0148 |
| Core Edge | 62.6 | 0.0053† | 0.0082 |
| Instrument Holes | 74.5 | 0.0039 | 0.0043 |
| Control Rod Holes | 78.4 | 0.0030ø | 0.0036 |

*On loading 1 kg uniformly distributed over the full axial height.

†The result was found to be constant over the whole range of graphite content of the core edge region (367 kg) showing that streaming effects were not important. There was some dependence on the reactivity held in control rods and when rods controlling reactivity P (%, taken as positive) were inserted the reactivity worth of 1 kg of graphite was increased to

$$(0.0053 \pm 0.0003P)\%$$

øNo significant change in this value was observed when the reactivity held by control rods was changed by 0.8%.

TABLE C3

Radial Variation of Reactivity Perturbation due to Copper in the First Core

| Position | Radius | Copper Tube Diameters (cm) | | Reactivity Change (%) on loading 1 kg/ |
|---|---|---|---|---|
| | | Inside | Outside | |
| R61 | 155.9 | 1.31 | 1.51 | -0.0005 |
| R56 | 143.2 | 1.31 | 1.51 | -0.0015 |
| R50 | 128.0 | 1.31 | 1.51 | -0.005 |
| R44 | 112.7 | 1.31 | 1.51 | -0.015 |
| R38 | 97.5 | 1.31 | 1.51 | -0.034 |
| East Instrument Hole | 74.5 | 1.31 | 1.51 | -0.065 |
| T16* | 53.5 | 1.01 | 1.19 | -0.054 |
| S15* | 45.9 | 1.01 | 1.19 | -0.050 |
| P13* | 30.8 | 1.01 | 1.19 | -0.060 |
| M11* | 15.9 | 1.01 | 1.19 | -0.071 |
| H7* | 15.9 | 1.01 | 1.19 | -0.069 |
| F5* | 30.8 | 1.01 | 1.19 | -0.057 |
| D3* | 45.9 | 1.01 | 1.19 | -0.048 |
| R35 | 89.9 | 1.31 | 1.51 | -0.043 |
| R41 | 105.1 | 1.31 | 1.51 | -0.021 |
| R47 | 120.3 | 1.31 | 1.51 | -0.009 |
| R53 | 135.6 | 1.31 | 1.51 | -0.003 |

/Uniformly distributed over the full length of the reactor.

TABLE C4

Axial Variation of Reactivity due to Copper in the Core and End Reflectors of the First Core

| Height Above Core Centre Plane | Reactivity Change on Loading Copper* |
|---|---|
| -113.2 | -0.004 |
| - 92.8 | -0.044 |
| - 72.4 | -0.065 |
| - 52.0 | -0.049 |
| - 31.6 | -0.064 |
| - 11.2 | -0.078 |
| + 9.3 | -0.078 |
| + 29.7 | -0.064 |
| + 50.1 | -0.049 |
| + 70.5 | -0.056 |
| + 90.9 | -0.041 |
| +111.7 | -0.007 |

*1 kg uniformly distributed in the interstitial holes between fuel elements.

## APPENDIX D

### TABLE D1

### Neutron Lifetime and Transfer Function (First Core)

| Detector Position | Period (sec) | $\phi$ (radian) | $1/\beta$ (sec) | Length of Rod oscillated (cm) |
|---|---|---|---|---|
| Reflector | 1 | 1.0524 | 0.269 | 10.09 |
| " | 2 | 0.7442 | 0.254 | 10.09 |
| " | 4 | 0.5386 | 0.258 | 10.09 |
| " | 8 | 0.4585 | 0.264 | 10.09 |

TABLE D2

Neutron Lifetime and Transfer Function (Second Core)

| Set | Detector Position | Period (sec) | $\phi$ (radian) | $1/\beta$ (sec) | Length of Rod oscillated (cm) | Fractional Amplitude of Power Variation | Amplitude of Reactivity Perturbation (%) | Amplitude of Transfer Function | |
|---|---|---|---|---|---|---|---|---|---|
| | | | | | | | | Exp. | Calculated with $1/\beta$ = 0.553 |
| C1 | Core | 1 | 1.298 | 0.559 | 10.08 | 0.0438 | 0.0833 | 116 | 120 |
| | " | 1 | 1.299 | 0.561 | 10.08 | 0.0457 | " | 113 | 120 |
| | " | 2 | 1.078 | 0.547 | 10.08 | 0.0855 | " | 211 | 211 |
| | " | 4 | 0.8258 | 0.546 | 10.08 | 0.1280 | " | 316 | 317 |
| | " | 8 | 0.6455 | 0.545 | 10.08 | 0.1642 | " | 406 | 407 |
| | " | 16 | 0.5930 | 0.541 | 10.08 | 0.1971 | " | 487 | 493 |
| | " | 32 | 0.6256 | 0.536 | 10.08 | 0.2461 | " | 608 | 618 |
| R1 | Reflector | 1 | 1.340 | 0.664* | 10.07 | 0.0454 | 0.0832 | 120 | 120 |
| | " | 2 | 1.090 | 0.564 | 10.07 | 0.0840 | " | 208 | 211 |
| | " | 4 | 0.8312 | 0.553 | 10.07 | 0.1263 | " | 313 | 317 |
| | " | 8 | 0.6550 | 0.561 | 10.07 | 0.1571 | " | 416 | 407 |
| | " | 8 | 0.6501 | 0.553 | 10.07 | 0.1620 | " | 401 | 407 |
| | " | 16 | 0.6006 | 0.561 | 10.07 | 0.1890 | " | 500 | 493 |
| | " | 16 | 0.6003 | 0.561 | 10.07 | 0.1893 | " | 501 | 493 |
| | " | 16 | 0.5951 | 0.546 | 10.07 | 0.1970 | " | 488 | 493 |
| | " | 32 | 0.6287 | 0.550 | 10.07 | 0.2356 | " | 623 | 618 |
| | " | 32 | 0.6273 | 0.544 | 10.07 | 0.2470 | " | 611 | 618 |
| C2 | Core | 1 | 1.295 | 0.552 | 5.52 | 0.0253 | 0.0457 | 122 | 120 |
| | " | 1 | 1.296 | 0.554 | 5.52 | 0.0258 | " | 118 | 120 |
| | " | 1 | 1.295 | 0.552 | 5.52 | 0.0265 | " | 119 | 120 |
| | " | 2 | 1.078 | 0.547 | 5.52 | 0.0456 | " | 220 | 211 |
| | " | 2 | 1.069 | 0.535 | 5.52 | 0.0461 | " | 211 | 211 |
| | " | 2 | 1.073 | 0.540 | 5.52 | 0.0461 | " | 208 | 211 |
| | " | 4 | 0.8298 | 0.551 | 5.52 | 0.0682 | " | 313 | 317 |
| | " | 4 | 0.8290 | 0.550 | 5.52 | 0.0700 | " | 315 | 317 |
| | " | 8 | 0.6473 | 0.548 | 5.52 | 0.0883 | " | 405 | 407 |
| | " | 8 | 0.6480 | 0.549 | 5.52 | 0.0897 | " | 404 | 407 |
| | " | 16 | 0.5944 | 0.545 | 5.52 | 0.1072 | " | 492 | 493 |
| | " | 16 | 0.5960 | 0.549 | 5.52 | 0.1094 | " | 493 | 493 |
| | " | 32 | 0.6280 | 0.547 | 5.52 | 0.1385 | " | 624 | 618 |
| R2 | Reflector | 1 | 1.338 | 0.659* | 5.52 | 0.0255 | 0.0464 | 121 | 120 |
| | " | 1 | 1.336 | 0.653* | 5.52 | 0.0260 | " | 117 | 120 |
| | " | 1 | 1.339 | 0.662* | 5.52 | 0.0272 | " | 121 | 120 |
| | " | 2 | 1.090 | 0.565 | 5.52 | 0.0452 | " | 214 | 211 |
| | " | 2 | 1.089 | 0.562 | 5.52 | 0.0459 | " | 208 | 211 |
| | " | 2 | 1.096 | 0.572 | 5.52 | 0.0470 | " | 209 | 211 |
| | " | 4 | 0.8432 | 0.568 | 5.52 | 0.0702 | " | 317 | 317 |
| | " | 4 | 0.8420 | 0.567 | 5.52 | 0.0721 | " | 320 | 317 |
| | " | 8 | 0.6531 | 0.558 | 5.52 | 0.0884 | " | 400 | 407 |
| | " | 8 | 0.6540 | 0.559 | 5.52 | 0.0905 | " | 402 | 407 |
| | " | 16 | 0.5998 | 0.559 | 5.52 | 0.1068 | " | 483 | 493 |
| | " | 16 | 0.6010 | 0.562 | 5.52 | 0.1089 | " | 483 | 493 |
| | " | 32 | 0.6320 | 0.564 | 5.52 | 0.1396 | " | 602 | 618 |

*these values not included in means

| Measurement Set | Mean $1/\beta$ (sec) | Standard Deviation of Individual Values | Mean of Ratios of Experimental and Theoretical Amplitude of Transfer Function | Standard Deviation of Individual Ratios |
|---|---|---|---|---|
| C1 | 0.548 | 0.009 | 0.982 | 0.021 |
| R1 | 0.555 | 0.007 | 1.000 | 0.015 |
| C2 | 0.548 | 0.005 | 1.000 | 0.011 |
| R2 | 0.564 | 0.005 | 0.990 | 0.013 |

## APPENDIX E

### Excess Reactivity Measurements for Temperature Coefficients of Reactivity in the First Core

| Effective Temperature (°C) | | Reactivity Worth (%) at Ambient Temperature of Inserted Control Rods | Excess Reactivity (%) |
|---|---|---|---|
| Core plus End Reflectors | Side Reflector | | |
| 21.5 | 20.9 | 0 | 0.3572 |
| 93.5 | 40.5 | 0 | 0.4230 |
| 129.1 | 60.1 | 0 | 0.5182 |
| 96.1 | 60.7 | 0 | 0.5220 |
| 184.1 | 97.8 | 0 | 0.7135 |
| 258.9 | 96.6 | 0 | 0.7641 |
| 342.7 | 102.2 | 0 | 0.8467 |
| 354.6 | 169.5 | 0 | 1.1353 |
| 352.9 | 227.2 | 0 | 1.3593 |
| 273.6 | 231.0 | 0 | 1.3273 |
| 186.2 | 169.3 | 0 | 1.0336 |
| 264.2 | 170.5 | 0 | 1.0784 |
| 130.5 | 97.8 | 0 | 0.7080 |
| 97.6 | 59.4 | 0 | 0.5131 |
| 25.3 | 25.0 | 0 | 0.3675 |
| 354.6 | 169.5 | 0.830 | 0.2754 |
| 352.9 | 227.2 | 0.830 | 0.4836 |
| 396.9 | 315.3 | 0.830 | 0.7881 |
| 359.7 | 316.1 | 0.830 | 0.7440 |
| 273.6 | 231.0 | 0.830 | 0.4338 |
| 186.2 | 169.3 | 0.830 | 0.1645 |
| 264.2 | 170.5 | 0.830 | 0.2035 |
| 21.5 | 20.9 | 0.737 | -0.3879 |
| 93.5 | 40.5 | 0.737 | -0.3276 |
| 129.1 | 60.1 | 0.737 | -0.2282 |
| 96.1 | 60.7 | 0.737 | -0.2207 |
| 184.1 | 97.8 | 0.737 | -0.0497 |
| 258.9 | 96.6 | 0.737 | 0.0115 |
| 342.7 | 102.2 | 0.737 | 0.0622 |
| 354.6 | 169.5 | 0.737 | 0.3387 |
| 352.9 | 227.2 | 0.737 | 0.5364 |
| 273.6 | 231.0 | 0.737 | 0.4933 |
| 186.2 | 169.3 | 0.737 | 0.2278 |
| 264.2 | 170.5 | 0.737 | 0.2753 |
| 130.5 | 97.8 | 0.737 | -0.0562 |
| 97.6 | 59.4 | 0.737 | -0.2297 |
| 352.9 | 227.2 | 1.602 | -0.3480 |
| 396.9 | 315.3 | 1.602 | -0.0606 |
| 359.7 | 316.1 | 1.602 | -0.0851 |
| 273.6 | 231.0 | 1.602 | -0.3943 |
| 186.2 | 169.3 | 1.602 | -0.6463 |
| 264.2 | 170.5 | 1.602 | -0.5921 |

| Effective Temperature (°C) | | Reactivity Worth (%) at Ambient Temperature of Inserted Control Rods | Excess Reactivity (%) |
|---|---|---|---|
| Core plus End Reflectors | Side Reflector | | |
| 21.5 | 20.9 | 0.698 | -0.3478 |
| 93.5 | 40.5 | 0.698 | -0.2894 |
| 129.1 | 60.1 | 0.698 | -0.1885 |
| 96.1 | 60.7 | 0.698 | -0.1824 |
| 184.1 | 97.8 | 0.698 | -0.0084 |
| 258.9 | 96.6 | 0.698 | 0.0235 |
| 342.7 | 102.2 | 0.698 | 0.1051 |
| 354.6 | 169.5 | 0.698 | 0.3828 |
| 352.9 | 227.2 | 0.698 | 0.5863 |
| 273.6 | 231.0 | 0.698 | 0.5483 |
| 186.2 | 169.3 | 0.698 | 0.2744 |
| 264.2 | 170.5 | 0.698 | 0.3185 |
| 130.5 | 97.8 | 0.698 | -0.0159 |
| 97.6 | 59.4 | 0.698 | -0.1912 |
| 25.3 | 25.0 | 0.698 | -0.3365 |
| 354.6 | 169.5 | 1.601 | -0.5276 |
| 352.9 | 227.2 | 1.601 | -0.3579 |
| 396.9 | 315.3 | 1.601 | -0.0732 |
| 359.7 | 316.1 | 1.601 | -0.0979 |
| 273.6 | 231.0 | 1.601 | -0.3992 |
| 186.2 | 169.3 | 1.601 | -0.6567 |
| 264.2 | 170.5 | 1.601 | -0.5959 |
| 21.5 | 20.9 | 1.435 | -1.0929 |
| 93.5 | 40.5 | 1.435 | -1.0400 |
| 129.1 | 60.1 | 1.435 | -0.9349 |
| 96.1 | 60.7 | 1.435 | -0.9251 |
| 184.1 | 97.8 | 1.435 | -0.7716 |
| 258.9 | 96.6 | 1.435 | -0.7561 |
| 342.7 | 102.2 | 1.435 | -0.6784 |
| 354.6 | 169.5 | 1.435 | -0.4143 |
| 352.9 | 227.2 | 1.435 | -0.2387 |
| 273.6 | 231.0 | 1.435 | -0.2857 |
| 186.2 | 169.3 | 1.435 | -0.5314 |
| 264.2 | 170.5 | 1.435 | -0.4917 |
| 130.5 | 97.8 | 1.435 | -0.7806 |
| 97.6 | 59.4 | 1.435 | -0.9353 |
| 25.3 | 25.0 | 1.435 | -1.0825 |
| 354.6 | 169.5 | 2.373 | -1.3226 |
| 352.9 | 227.2 | 2.373 | -1.1895 |
| 396.9 | 315.3 | 2.373 | -0.9219 |
| 359.7 | 316.1 | 2.373 | -0.9235 |
| 273.6 | 231.0 | 2.373 | -1.2273 |
| 186.2 | 169.3 | 2.373 | -1.4675 |
| 264.2 | 170.5 | 2.373 | -1.3915 |

## APPENDIX F

### TABLE F1

Spectrum Measured by Chopper at Ambient Temperature

| N(E) | E | N(E) | E |
|---|---|---|---|
| 5.930, 1 | 5.701, 1 | 1.617, 4 | 7.996, -2 |
| 1.233, 2 | 2.469, 1 | 1.677, 4 | 7.408, -2 |
| 2.062, 2 | 1.371, 1 | 1.682, 4 | 6.883, -2 |
| 3.081, 2 | 8.709, 0 | 1.693, 4 | 6.412, -2 |
| 4.357, 2 | 6.018, 0 | 1.701, 4 | 5.987, -2 |
| 5.881, 2 | 4.405, 0 | 1.686, 4 | 5.604, -2 |
| 7.664, 2 | 3.364, 0 | 1.656, 4 | 5.256, -2 |
| 9.615, 2 | 2.652, 0 | 1.610, 4 | 4.939, -2 |
| 1.180, 3 | 2.145, 0 | 1.564, 4 | 4.650, -2 |
| 1.426, 3 | 1.770, 0 | 1.583, 4 | 4.386, -2 |
| 1.676, 3 | 1.486, 0 | 1.528, 4 | 4.144, -2 |
| 1.867, 3 | 1.265, 0 | 1.518, 4 | 3.921, -2 |
| 2.073, 3 | 1.089, 0 | 1.497, 4 | 3.716, -2 |
| 2.326, 3 | 9.484, -1 | 1.438, 4 | 3.526, -2 |
| 2.670, 3 | 8.330, -1 | 1.460, 4 | 3.351, -2 |
| 3.053, 3 | 7.375, -1 | 1.373, 4 | 3.188, -2 |
| 3.412, 3 | 6.575, -1 | 1.254, 4 | 3.037, -2 |
| 3.770, 3 | 5.898, -1 | 1.254, 4 | 2.897, -2 |
| 4.064, 3 | 5.321, -1 | 1.194, 4 | 2.766, -2 |
| 4.397, 3 | 4.825, -1 | 1.194, 4 | 2.643, -2 |
| 4.621, 3 | 4.395, -1 | 1.130, 4 | 2.529, -2 |
| 4.740, 3 | 4.020, -1 | 1.108, 4 | 2.422, -2 |
| 4.807, 3 | 3.691, -1 | 1.110, 4 | 2.321, -2 |
| 4.786, 3 | 3.400, -1 | 9.906, 3 | 2.227, -2 |
| 4.743, 3 | 3.143, -1 | 9.928, 3 | 2.138, -2 |
| 4.924, 3 | 2.914, -1 | 9.540, 3 | 2.055, -2 |
| 5.129, 3 | 2.709, -1 | 8.233, 3 | 1.976, -2 |
| 5.300, 3 | 2.525, -1 | 8.765, 3 | 1.902, -2 |
| 5.786, 3 | 2.359, -1 | 8.264, 3 | 1.831, -2 |
| 6.149, 3 | 2.209, -1 | 8.106, 3 | 1.765, -2 |
| 6.717, 3 | 2.073, -1 | 7.748, 3 | 1.702, -2 |
| 7.295, 3 | 1.949, -1 | 7.261, 3 | 1.643, -2 |
| 7.984, 3 | 1.836, -1 | 7.047, 3 | 1.586, -2 |
| 8.412, 3 | 1.732, -1 | 5.933, 3 | 1.533, -2 |
| 8.886, 3 | 1.637, -1 | 6.078, 3 | 1.482, -2 |
| 9.810, 3 | 1.549, -1 | 6.262, 3 | 1.433, -2 |
| 1.034, 4 | 1.469, -1 | 4.996, 3 | 1.387, -2 |
| 1.052, 4 | 1.394, -1 | 4.717, 3 | 1.343, -2 |
| 1.137, 4 | 1.325, -1 | 5.307, 3 | 1.302, -2 |
| 1.179, 4 | 1.261, -1 | 4.527, 3 | 1.262, -2 |
| 1.252, 4 | 1.202, -1 | 4.237, 3 | 1.224, -2 |
| 1.294, 4 | 1.147, -1 | 3.903, 3 | 1.187, -2 |
| 1.345, 4 | 1.095, -1 | 4.018, 3 | 1.152, -2 |
| 1.387, 4 | 1.047, -1 | 3.503, 3 | 1.119, -2 |
| 1.400, 4 | 1.025, -1 | 3.739, 3 | 1.088, -2 |
| 1.502, 4 | 9.402, -2 | 2.742, 3 | 1.057, -2 |
| 1.554, 4 | 8.657, -2 | 2.780, 3 | 1.027, -2 |

TABLE F2

Spectrum Measured by Chopper at Core Temperature of 645°K

| N(E) | E | N(E) | E |
|---|---|---|---|
| 5.797, 1 | 5.852, 1 | 1.212, 4 | 7.996, -2 |
| 1.204, 2 | 2.512, 1 | 1.210, 4 | 7.408, -2 |
| 2.036, 2 | 1.389, 1 | 1.184, 4 | 6.883, -2 |
| 3.089, 2 | 8.798, 0 | 1.139, 4 | 6.412, -2 |
| 4.419, 2 | 6.069, 0 | 1.123, 4 | 5.987, -2 |
| 5.925, 2 | 4.437, 0 | 1.070, 4 | 5.604, -2 |
| 7.722, 2 | 3.385, 0 | 1.060, 4 | 5.256, -2 |
| 9.795, 2 | 2.667, 0 | 1.000, 4 | 4.939, -2 |
| 1.204, 3 | 2.155, 0 | 9.641, 3 | 4.650, -2 |
| 1.454, 3 | 1.778, 0 | 9.552, 3 | 4.386, -2 |
| 1.704, 3 | 1.492, 0 | 9.146, 3 | 4.144, -2 |
| 1.934, 3 | 1.270, 0 | 8.599, 3 | 3.921, -2 |
| 2.153, 3 | 1.093, 0 | 8.482, 3 | 3.716, -2 |
| 2.423, 3 | 9.515, -1 | 8.498, 3 | 3.526, -2 |
| 2.815, 3 | 8.356, -1 | 7.680, 3 | 3.351, -2 |
| 3.202, 3 | 7.396, -1 | 7.967, 3 | 3.188, -2 |
| 3.635, 3 | 6.593, -1 | 7.629, 3 | 3.037, -2 |
| 3.971, 3 | 5.914, -1 | 6.973, 3 | 2.897, -2 |
| 4.387, 3 | 5.335, -1 | 6.623, 3 | 2.766, -2 |
| 4.660, 3 | 4.836, -1 | 6.441, 3 | 2.643, -2 |
| 4.912, 3 | 4.405, -1 | 6.067, 3 | 2.529, -2 |
| 5.088, 3 | 4.028, -1 | 6.039, 3 | 2.422, -2 |
| 5.272, 3 | 3.698, -1 | 5.717, 3 | 2.321, -2 |
| 5.388, 3 | 3.407, -1 | 5.495, 3 | 2.227, -2 |
| 5.503, 3 | 3.149, -1 | 5.418, 3 | 2.138, -2 |
| 5.696, 3 | 2.919, -1 | 5.447, 3 | 2.055, -2 |
| 6.050, 3 | 2.714, -1 | 4.741, 3 | 1.976, -2 |
| 6.516, 3 | 2.529, -1 | 4.321, 3 | 1.902, -2 |
| 6.941, 3 | 2.363, -1 | 4.748, 3 | 1.831, -2 |
| 7.532, 3 | 2.213, -1 | 4.219, 3 | 1.765, -2 |
| 8.031, 3 | 2.078, -1 | 3.352, 3 | 1.702, -2 |
| 8.580, 3 | 1.952, -1 | 4.092, 3 | 1.643, -2 |
| 9.059, 3 | 1.838, -1 | 3.192, 3 | 1.586, -2 |
| 9.617, 3 | 1.734, -1 | 3.212, 3 | 1.533, -2 |
| 1.009, 4 | 1.639, -1 | 3.072, 3 | 1.482, -2 |
| 1.059, 4 | 1.552, -1 | 2.957, 3 | 1.433, -2 |
| 1.082, 4 | 1.471, -1 | 2.284, 3 | 1.387, -2 |
| 1.121, 4 | 1.396, -1 | 2.620, 3 | 1.343, -2 |
| 1.156, 4 | 1.327, -1 | 2.656, 3 | 1.302, -2 |
| 1.182, 4 | 1.263, -1 | 2.371, 3 | 1.262, -2 |
| 1.153, 4 | 1.203, -1 | 2.545, 3 | 1.224, -2 |
| 1.224, 4 | 1.148, -1 | 2.479, 3 | 1.187, -2 |
| 1.223, 4 | 1.096, -1 | 1.683, 3 | 1.152, -2 |
| 1.245, 4 | 1.048, -1 | 1.884, 3 | 1.119, -2 |
| 1.296, 4 | 1.003, -1 | 1.188, 3 | 1.087, -2 |
| 1.226, 4 | 9.402, -2 | 1.607, 3 | 1.057, -2 |
| 1.228, 4 | 8.657, -2 | | |

## APPENDIX G

### TABLE G1

### Axial Variation of Pu239 Fission Rate (First Core)

| Position (cm from Centre) | In K10 Channel | | | | | | In D4 Channel |
|---|---|---|---|---|---|---|---|
| | Experiment | | Angie | | | | Experiment |
| | + | − | + | | − | | − |
| | | | *Set (a) | *Set (b) | *Set (a) | *Set (b) | |
| 0 | 1.000 | 1.000 | 1.000 | 1.000 | 1.000 | 1.000 | 1.000 |
| 5 | 0.956 | 0.965 | 0.941 | 0.929 | 0.941 | 0.928 | 0.966 |
| 10 | 0.924 | 0.935 | 0.921 | 0.903 | 0.921 | 0.907 | 0.940 |
| 15 | 0.898 | 0.912 | 0.900 | 0.882 | 0.903 | 0.887 | 0.917 |
| 20 | 0.872 | 0.883 | 0.880 | 0.861 | 0.886 | 0.868 | 0.897 |
| 25 | 0.848 | 0.857 | 0.858 | 0.840 | 0.866 | 0.848 | 0.875 |
| 30 | 0.811 | 0.837 | 0.835 | 0.818 | 0.842 | 0.827 | 0.854 |
| 35 | 0.785 | 0.815 | 0.810 | 0.796 | 0.816 | 0.806 | 0.832 |
| 40 | 0.757 | 0.791 | 0.781 | 0.775 | 0.790 | 0.784 | 0.810 |
| 45 | 0.730 | 0.761 | 0.751 | 0.761 | 0.763 | 0.772 | 0.787 |
| 50 | 0.707 | 0.743 | 0.764 | 0.625 | 0.780 | 0.631 | 0.770 |
| 55 | 0.699 | 0.734 | 0.756 | 0.645 | 0.773 | 0.657 | 0.764 |
| 60 | 0.730 | 0.764 | 0.788 | 0.690 | 0.804 | 0.709 | 0.795 |
| 65 | 0.829 | 0.869 | 0.887 | 0.814 | 0.917 | 0.820 | 0.908 |
| 70 | 1.068 | 1.130 | 1.103 | 1.020 | 1.148 | 1.052 | 1.170 |
| 75 | 1.312 | 1.454 | 1.352 | 1.285 | 1.438 | 1.364 | 1.492 |
| 80 | 1.450 | 1.630 | 1.486 | 1.411 | 1.577 | 1.541 | 1.663 |
| 85 | 1.478 | 1.684 | 1.515 | 1.489 | 1.615 | 1.594 | 1.711 |
| 90 | 1.431 | 1.648 | 1.476 | 1.460 | 1.585 | 1.580 | 1.669 |
| 95 | 1.310 | 1.532 | 1.369 | 1.297 | 1.477 | 1.410 | 1.548 |
| 100 | 1.140 | 1.364 | 1.200 | 1.153 | 1.307 | 1.260 | 1.381 |
| 105 | 0.948 | 1.147 | 0.987 | 0.947 | 1.095 | 1.072 | 1.157 |
| 110 | 0.731 | 0.907 | 0.744 | 0.708 | 0.863 | 0.846 | 0.916 |
| 115 | 0.507 | 0.648 | 0.488 | 0.464 | 0.615 | 0.595 | 0.660 |
| 120 | 0.291 | 0.377 | 0.236 | 0.236 | 0.342 | 0.342 | 0.378 |

"See Table 8.1 for explanation of energy group structure

TABLE G2

Axial Variation of U235 Fission Rate in K10 Channel (First Core)

| Position (cm from centre) | Experiment | | Angie | | | |
|---|---|---|---|---|---|---|
| | + | - | + | | - | |
| | | | *Set (a) | *Set (b) | *Set (a) | *Set (b) |
| 0 | 1.000 | 1.000 | 1.000 | 1.000 | 1.000 | 1.000 |
| 5 | 0.963 | 0.979 | 0.979 | 0.995 | 0.981 | 0.996 |
| 10 | 0.943 | 0.951 | 0.957 | 0.970 | 0.960 | 0.973 |
| 15 | 0.915 | 0.926 | 0.935 | 0.950 | 0.940 | 0.955 |
| 20 | 0.886 | 0.904 | 0.915 | 0.930 | 0.920 | 0.936 |
| 25 | 0.858 | 0.875 | 0.893 | 0.908 | 0.900 | 0.917 |
| 30 | 0.825 | 0.857 | 0.870 | 0.883 | 0.827 | 0.895 |
| 35 | 0.799 | 0.838 | 0.845 | 0.857 | 0.852 | 0.874 |
| 40 | 0.772 | 0.814 | 0.819 | 0.834 | 0.830 | 0.845 |
| 45 | 0.755 | 0.796 | 0.804 | 0.823 | 0.812 | 0.830 |
| 50 | 0.746 | 0.788 | 0.879 | 0.958 | 0.889 | 0.915 |
| 55 | 0.761 | 0.805 | 0.905 | 0.984 | 0.922 | 1.004 |
| 60 | 0.826 | 0.873 | 0.980 | 1.062 | 1.007 | 1.084 |
| 65 | 0.995 | 1.047 | 1.178 | 1.255 | 1.211 | 1.275 |
| 70 | 1.373 | 1.443 | 1.511 | 1.568 | 1.560 | 1.613 |
| 75 | 1.769 | 1.954 | 1.930 | 1.965 | 2.045 | 2.096 |
| 80 | 2.024 | 2.301 | 2.175 | 2.211 | 2.333 | 2.373 |
| 85 | 2.137 | 2.464 | 2.279 | 2.294 | 2.438 | 2.463 |
| 90 | 2.120 | 2.485 | 2.242 | 2.243 | 2.422 | 2.444 |
| 95 | 1.980 | 2.375 | 2.159 | 2.174 | 2.336 | 2.357 |
| 100 | 1.777 | 2.154 | 1.931 | 1.931 | 2.100 | 2.115 |
| 105 | 1.495 | 1.858 | 1.595 | 1.595 | 1.810 | 1.810 |
| 110 | 1.166 | 1.492 | 1.196 | 1.196 | 1.398 | 1.398 |
| 115 | 0.816 | 1.079 | 0.800 | 0.800 | 0.985 | 0.985 |
| 120 | 0.459 | 0.632 | 0.405 | 0.405 | 0.554 | 0.554 |

*See Table 8.1 for explanation of energy group structure

TABLE G3

Radial Variation of Pu239 Fission Rate (First Core)

| Position | Radius | On Core Centre plane | | | At Axial height + 24.5 cm. | |
|---|---|---|---|---|---|---|
| | | Experiment | Angie | | Experiment | Angie |
| | (cm.) | | *Set (a) | *Set (b) | | *Set (a) |
| J9* | 4.4 | 1.000 | 1.000 | 1.000 | 1.000 | 1.000 |
| H8* | 11.6 | 0.977 | 0.984 | 0.985 | 0.991 | 0.983 |
| G7* | 19.2 | 0.954 | 0.954 | 0.959 | 0.951 | 0.956 |
| F6* | 26.8 | 0.914 | 0.914 | 0.926 | 0.898 | 0.918 |
| F6 | 30.8 | 0.899 | 0.893 | 0.912 | 0.880 | 0.894 |
| E5* | 34.4 | 0.886 | 0.873 | 0.904 | 0.861 | 0.875 |
| E5 | 38.35 | 0.858 | 0.855 | 0.908 | 0.845 | 0.855 |
| D4 | 45.9 | 0.840 | 0.886 | 0.868 | 0.845 | 0.893 |
| C3* | 49.6 | 0.899 | 0.911 | 0.924 | 0.888 | 0.930 |
| C3 | 53.5 | 1.011 | 0.989 | 1.032 | 0.995 | 1.012 |
| B2* | 57.2 | 1.212 | 1.110 | 1.220 | 1.233 | 1.156 |
| W. Inst. | 74.2 | 1.910 | 1.831 | 1.813 | 2.022 | 2.022 |
| R35 | 89.9 | 1.822 | 1.905 | 1.862 | 2.004 | 2.096 |
| R41 | 105.1 | 1.367 | 1.477 | 1.477 | 1.518 | 1.615 |
| R47 | 120.3 | 0.925 | 0.972 | 0.972 | 1.013 | 1.064 |
| R53 | 135.4 | 0.543 | 0.553 | 0.560 | 0.589 | 0.605 |
| R59 | 150.8 | 0.228 | 0.308 | 0.308 | 0.253 | 0.225 |

*See Table 8.1 for explanation of energy group structure

TABLE G4

Axial Variation of Pu239/U235 Ratio in K10 Channel (First Core)

| Position (cm from centre) | Experiment | | Angie | |
|---|---|---|---|---|
| | + | − | + | − |
| | | | *Set (a) | |
| 0 | 1.000 | 1.000 | 1.000 | 1.000 |
| 5 | 0.993 | 0.986 | 0.960 | 0.960 |
| 10 | 0.980 | 0.983 | 0.961 | 0.960 |
| 15 | 0.981 | 0.985 | 0.961 | 0.960 |
| 20 | 0.984 | 0.977 | 0.961 | 0.962 |
| 25 | 0.988 | 0.979 | 0.961 | 0.962 |
| 30 | 0.983 | 0.977 | 0.960 | 0.960 |
| 35 | 0.982 | 0.973 | 0.958 | 0.958 |
| 40 | 0.980 | 0.972 | 0.950 | 0.953 |
| 45 | 0.967 | 0.956 | 0.934 | 0.946 |
| 50 | 0.948 | 0.943 | 0.871 | 0.878 |
| 55 | 0.919 | 0.912 | 0.836 | 0.838 |
| 60 | 0.884 | 0.875 | 0.799 | 0.800 |
| 65 | 0.833 | 0.830 | 0.752 | 0.757 |
| 70 | 0.778 | 0.783 | 0.729 | 0.736 |
| 75 | 0.742 | 0.744 | 0.702 | 0.701 |
| 80 | 0.716 | 0.708 | 0.682 | 0.679 |
| 85 | 0.692 | 0.683 | 0.667 | 0.664 |
| 90 | 0.675 | 0.663 | 0.652 | 0.649 |
| 95 | 0.662 | 0.645 | 0.635 | 0.633 |
| 100 | 0.642 | 0.633 | 0.629 | 0.625 |
| 105 | 0.634 | 0.617 | 0.624 | 0.621 |
| 110 | 0.627 | 0.608 | 0.620 | 0.620 |
| 115 | 0.621 | 0.601 | 0.617 | 0.620 |
| 120 | 0.634 | 0.597 | 0.614 | 0.638 |

*See Table 8.1 for explanation of energy group structure

TABLE G5

Spatial Variation of Pu239/U235 Ratio normalised to R61 (First Core)

| Position | Radius | Axial Height | Experiment | Angie *Set (a) |
|---|---|---|---|---|
| J9* | 4.4 | 0 | 1.809 | 1.713 |
| D4 | 45.9 | 0 | 1.639 | 1.523 |
| J9* | 4.4 | -55 | 1.670 | 1.438 |
| J9* | 4.4 | +55 | 1.637 | 1.432 |
| J9* | 4.4 | +24.5 | 1.774 | 1.647 |
| D4 | 45.9 | -55 | 1.523 | - |

*See Table 8.1 for explanation of energy group structure

## APPENDIX H

### Estimate of the Contribution of Core Expansion to the Core Temperature Coefficient of Reactivity

The effect of expansion on the temperature coefficient of a large reactor with solid moderator is normally negligible. In ZENITH, however, the small, high leakage core is formed of fuel elements carried on a nimonic support grid (Fig. 1); the expansion of this grid and the rather higher temperature of the grid than the average in the core leads to an effective mean radial expansion coefficient of the core of $1.1 \times 10^{-5}/^{\circ}K$ between 20 and 800°C. (The reflector is carried on a bedplate whose temperature is virtually independent of the core temperature).

Let $r_o$ be the radius of the core, let R be the reactivity worth of a fuel element at radius r, let $\overline{R}$ be the mean worth of a fuel element averaged over the whole core and let the effective radial expansion coefficient be $\alpha$. Then for temperature rise $\theta(^{\circ}K)$ the core expands to radius:

$$r_o (1 + \alpha\theta)$$

and the core density decreases uniformly by a factor $(1-2\alpha\theta)$. This may be treated as the transfer of a proportion $2\alpha\theta$ of the core material from within the original core radius to the edge of the core. In terms of fuel elements, the 'number' transferred is $470\alpha\theta$; the reactivity change is then $470\alpha\theta (R_o - \overline{R})$ whence the temperature coefficient is:

$$470\alpha (R_o - \overline{R})$$

Table H1 gives the result for the first plutonium loading and for the three U235 loadings for which data are available (note that corrections have not formerly been applied to the U235 core data). The uncertainty of these data is estimated to be about $\pm 0.2 \times 10^{-5}$; this is due primarily to the uncertainty in $R_o$ since the reactivity is a fast varying function of radius at the core edge.

TABLE H1

Contribution of Expansion to the ZENITH Core Temperature Coefficients

| System | | Worth of Fuel Element (%) | | Contribution to Core Coefficient $10^{-5}$ per °K |
|---|---|---|---|---|
| Fuel | Core | At Radius 61.6 cm | Mean over Core | |
| Pu239 | 1 | 0.14 | 0.24 | -0.5 |
| U235 | 2 | 0.23 | 0.42 | -1.0 |
| U235 | 4 | 0.26 | 0.45 | -1.0 |
| U235 | 5 | 0.17 | 0.27 | -0.5 |

The contribution from axial expansion of the graphite fuel element sleeves will be much less than the radial effect since, firstly, the expansion coefficient is only that of the graphite itself ($\sim 3.10^{-6}/^{o}K$, a factor of three lower than the effective radial coefficient) and, secondly, the axial neutron leakage from the core is considerably smaller than the radial leakage (bare core bucklings are = 15 $m^{-2}$ radial, 5 $m^{-2}$ axial). The axial effect has therefore been neglected.

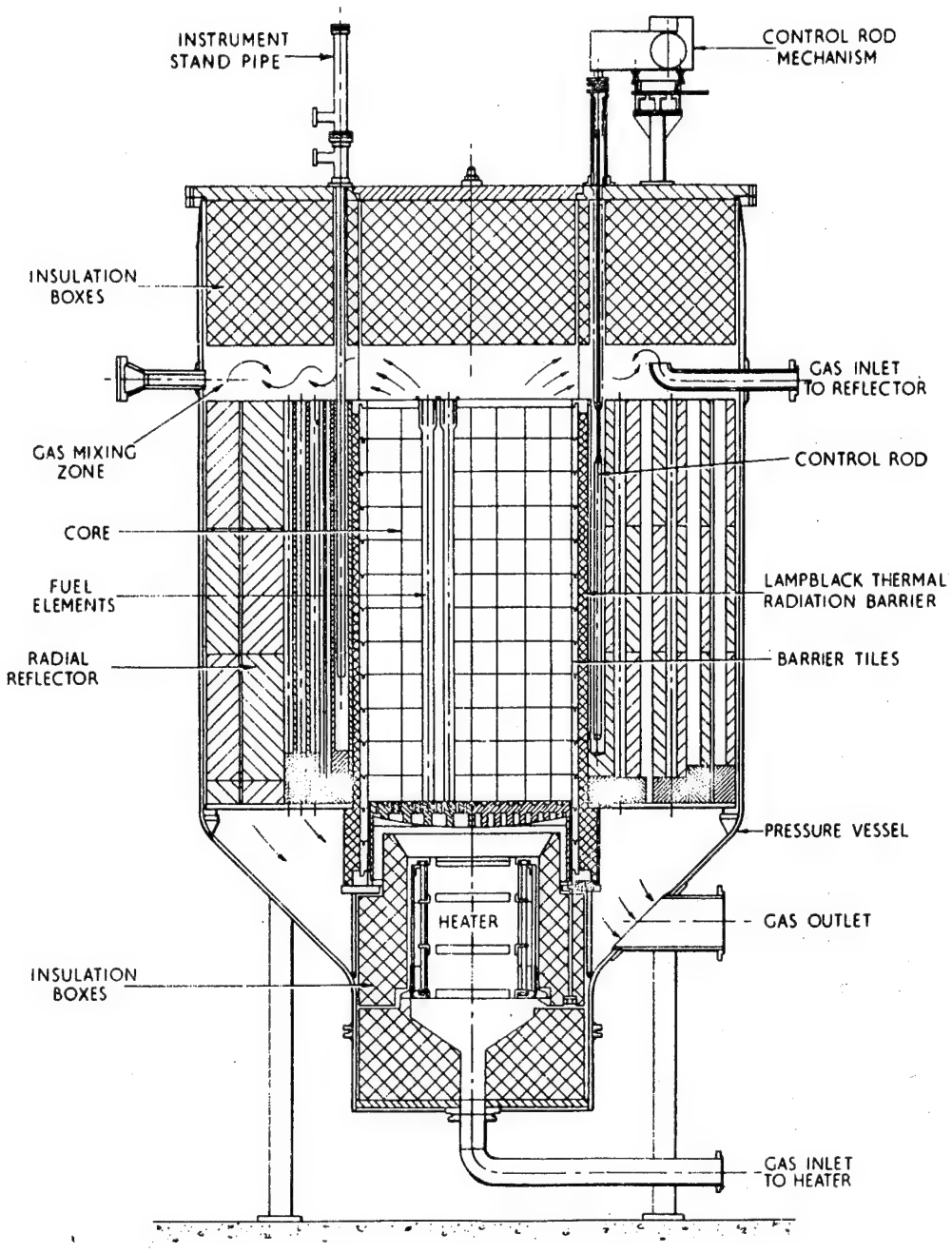


FIG. 1·1. SECTION THROUGH REACTOR VESSEL

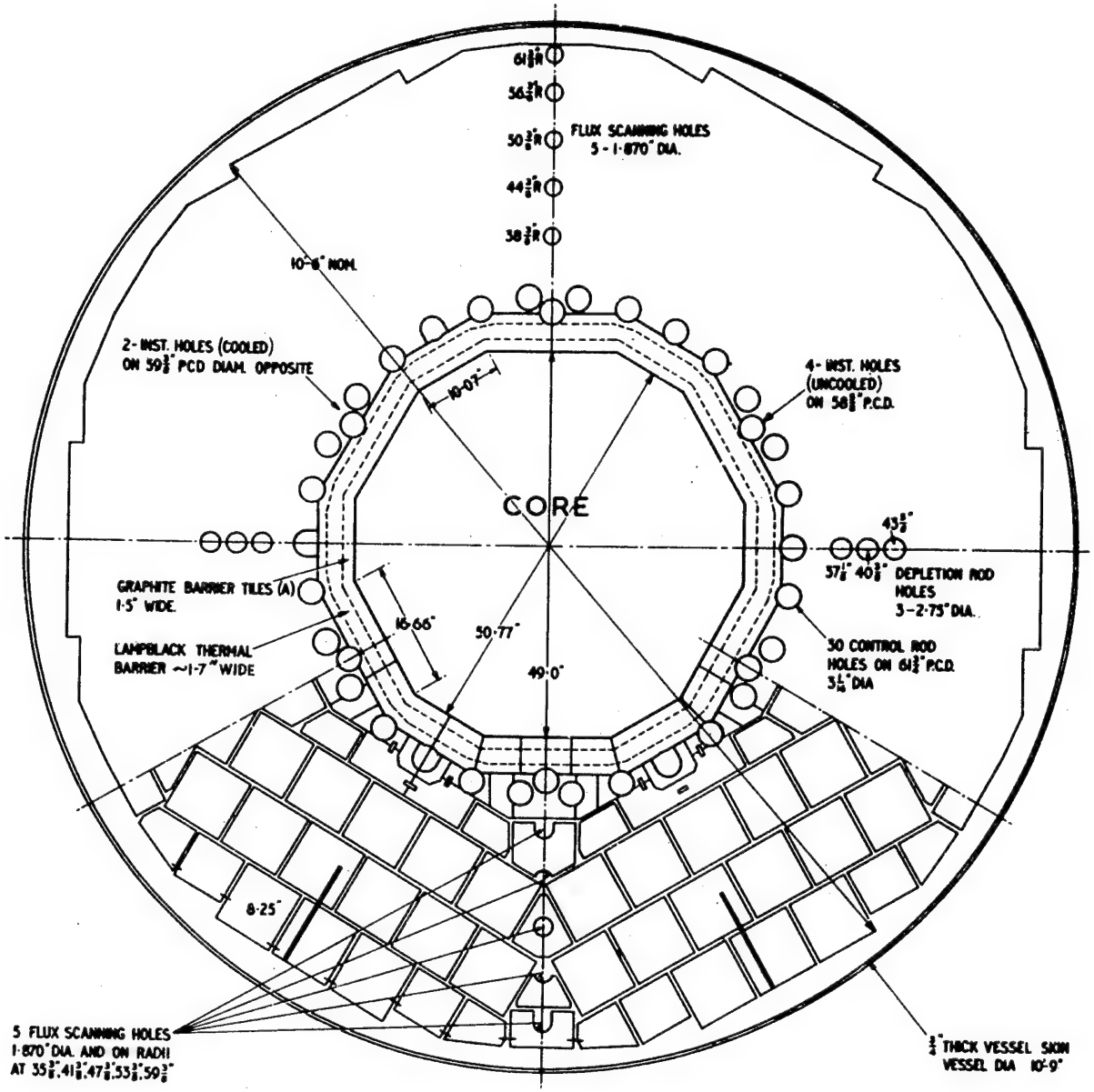


FIG. 1·2 PLAN VIEW OF ZENITH CORE & REFLECTOR

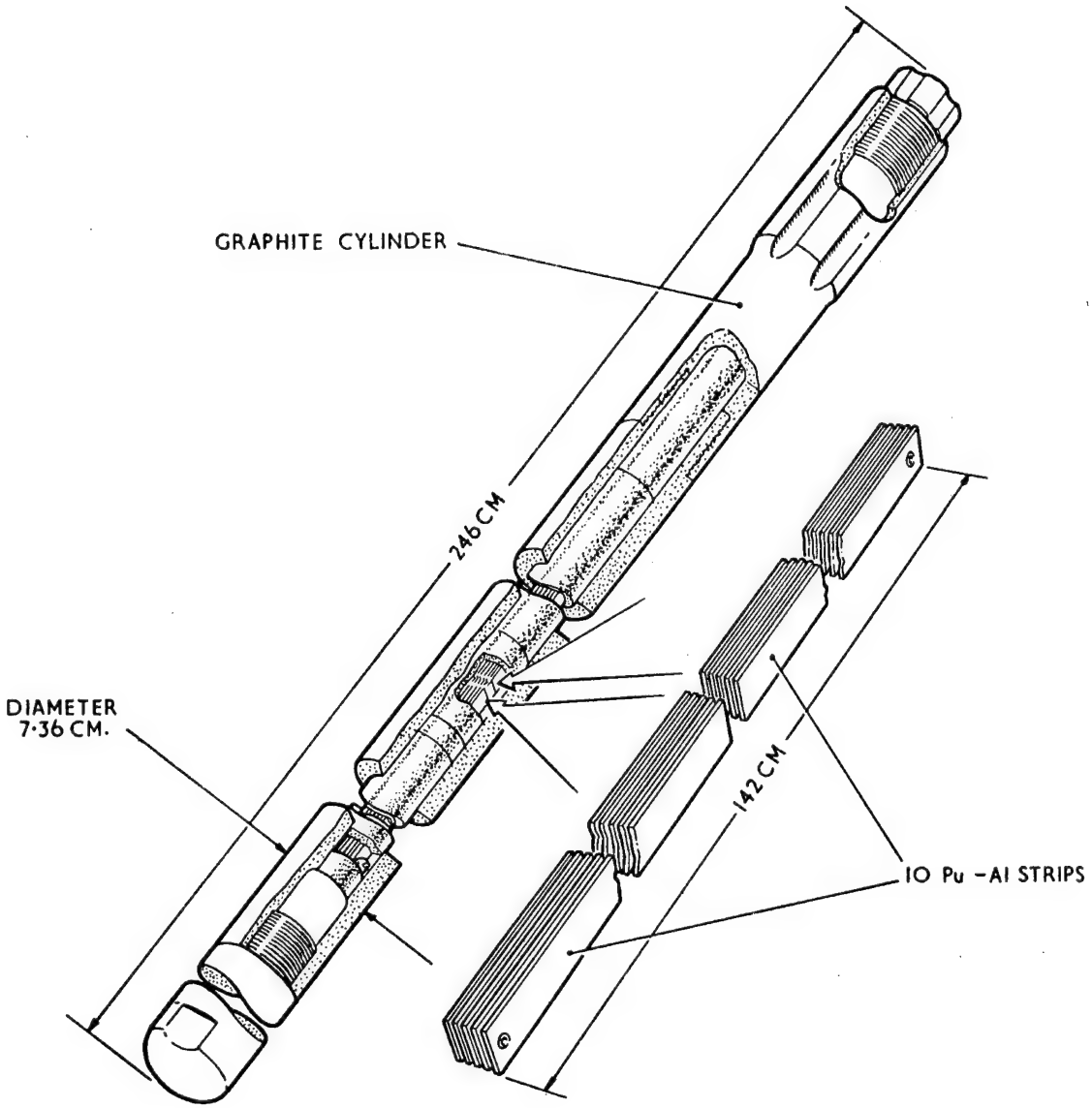


FIGURE I.3. FUEL ELEMENT FOR ZENITH PLUTONIUM CORE

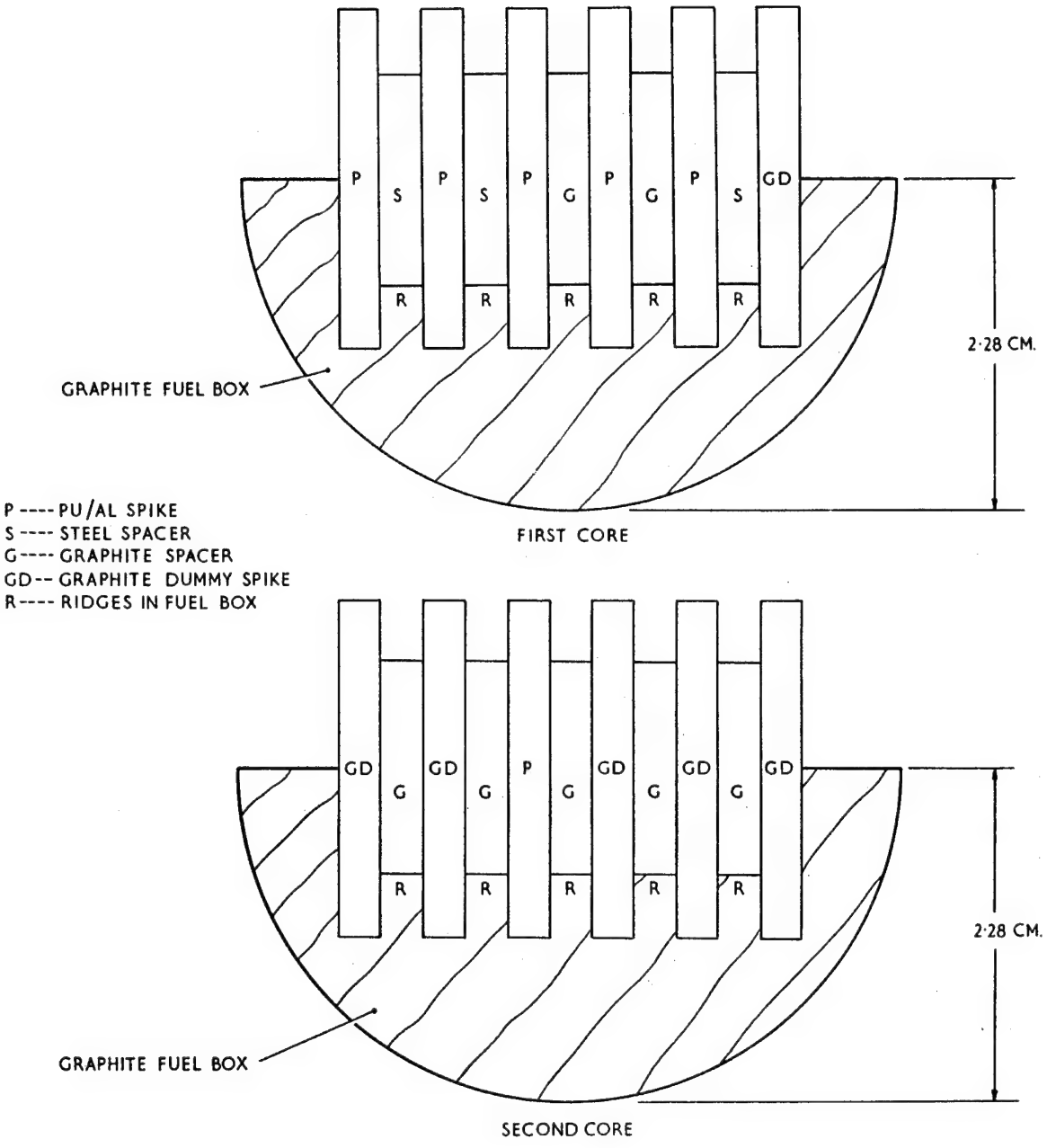


FIGURE 1.4. FUEL ARRANGEMENT FOR ZENITH PLUTONIUM CORES(SECTION ACROSS ELEMENT)

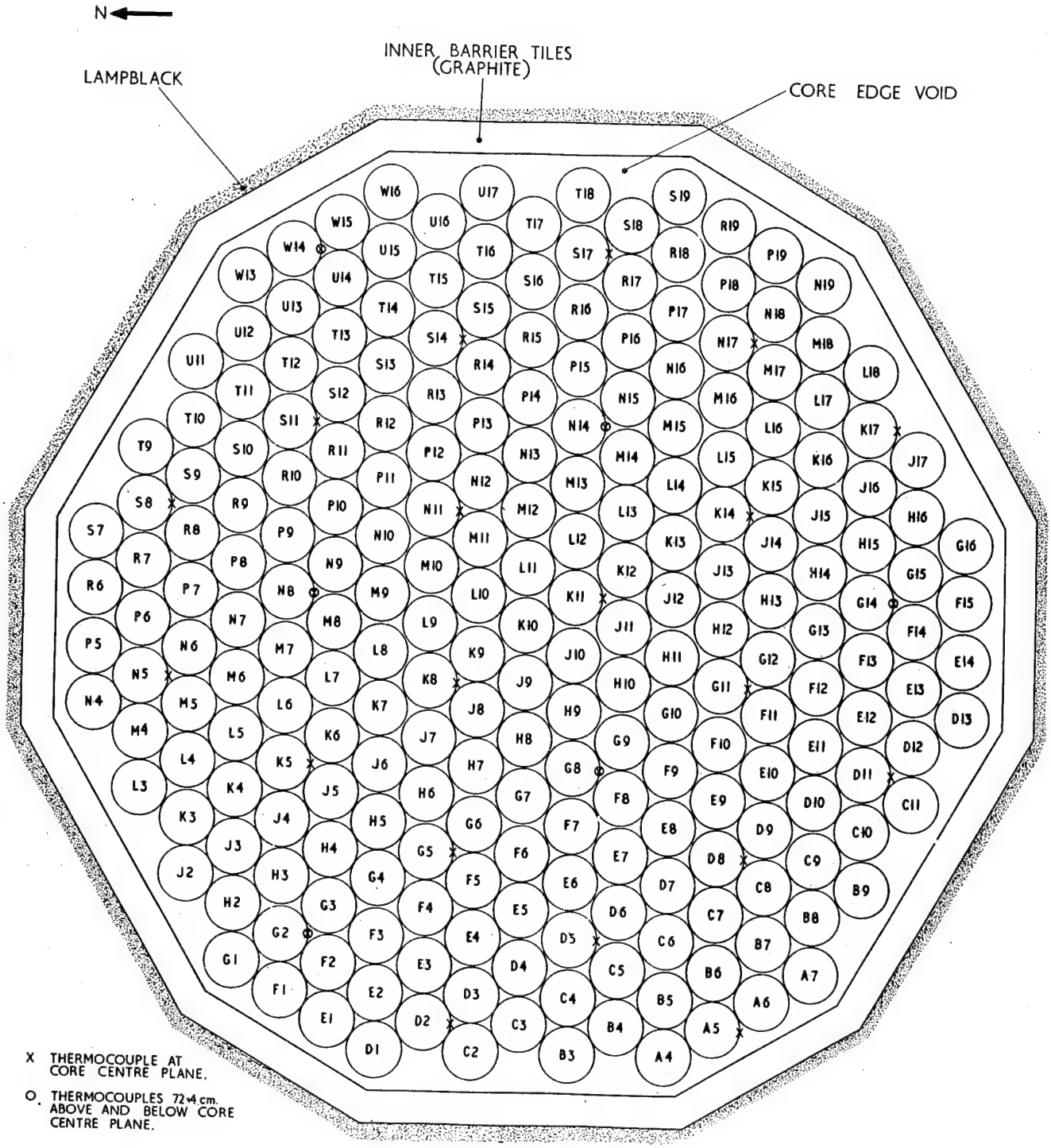


FIG. 1·5 ZENITH CORE ARRANGEMENT

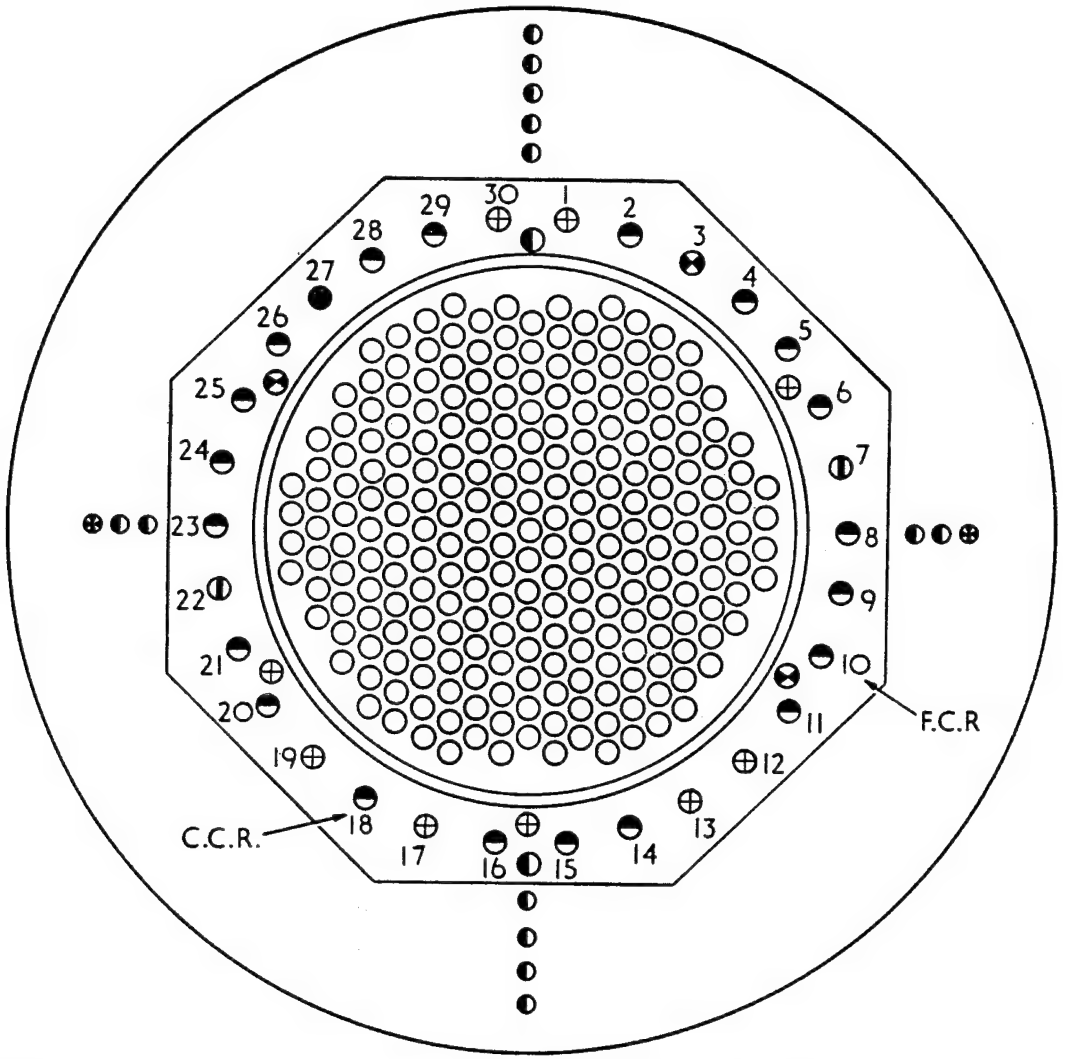


FUEL ELEMENTS ... ... ... ... ... ○
GRAPHITE FILLED CONTROL ROD HOLES ⊕
CONTROL RODS ... ... ... ... ... ◓
LOW FLUX INSTRUMENT ... ... ... ... ◑
HIGH FLUX INSTRUMENT ... ... ... ... ⊛
SHUT DOWN INSTRUMENT ... ... ... ⊗
EXPERIMENTAL HOLES ... ... ... ... ◐
CHAMBER FOR TRANSFER FUNCTION ANALYSER ●

FIGURE I.6. CONTROL ROD AND INSTRUMENT POSITIONS

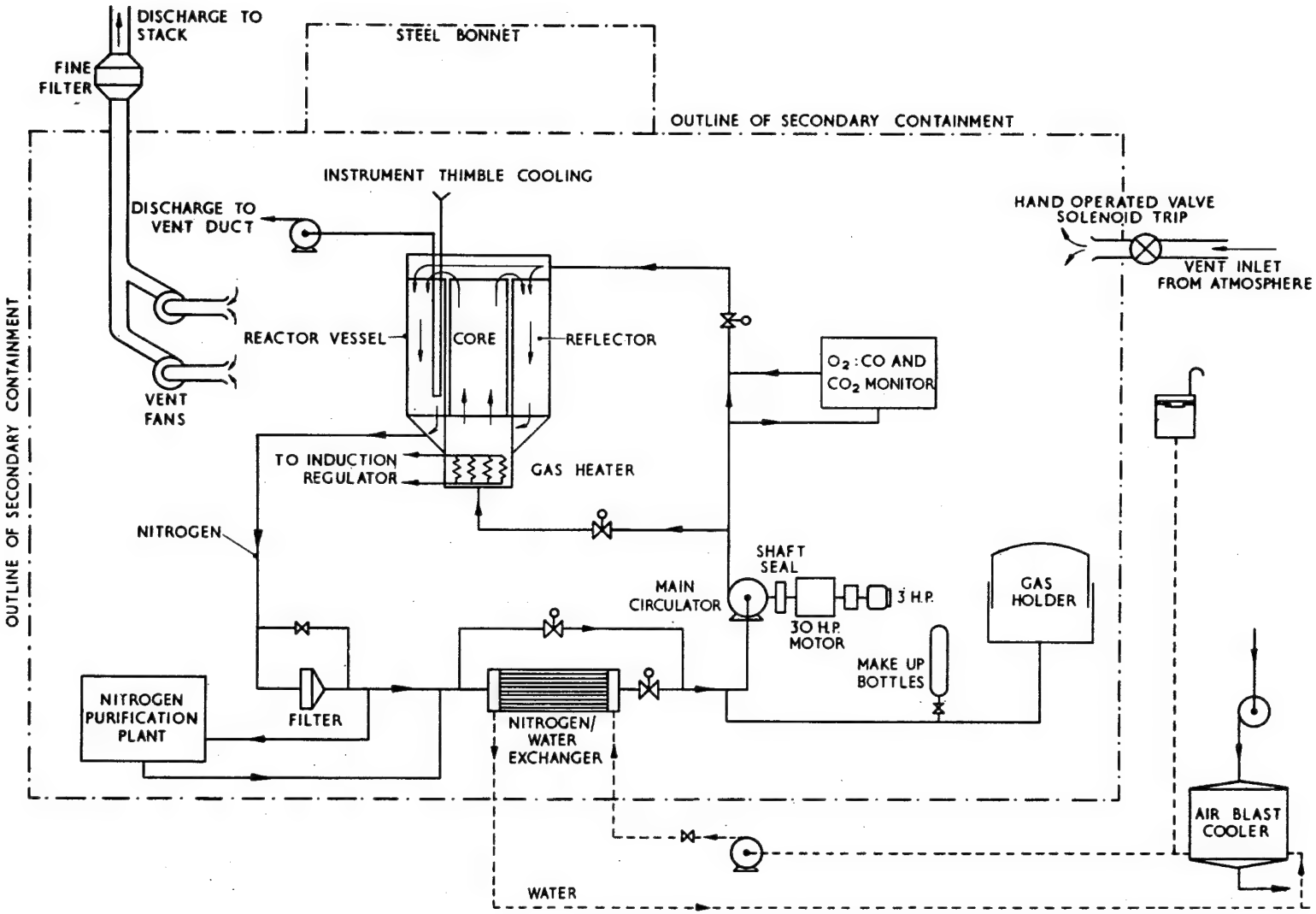


FIG. 1·7 ZENITH FLOW DIAGRAM

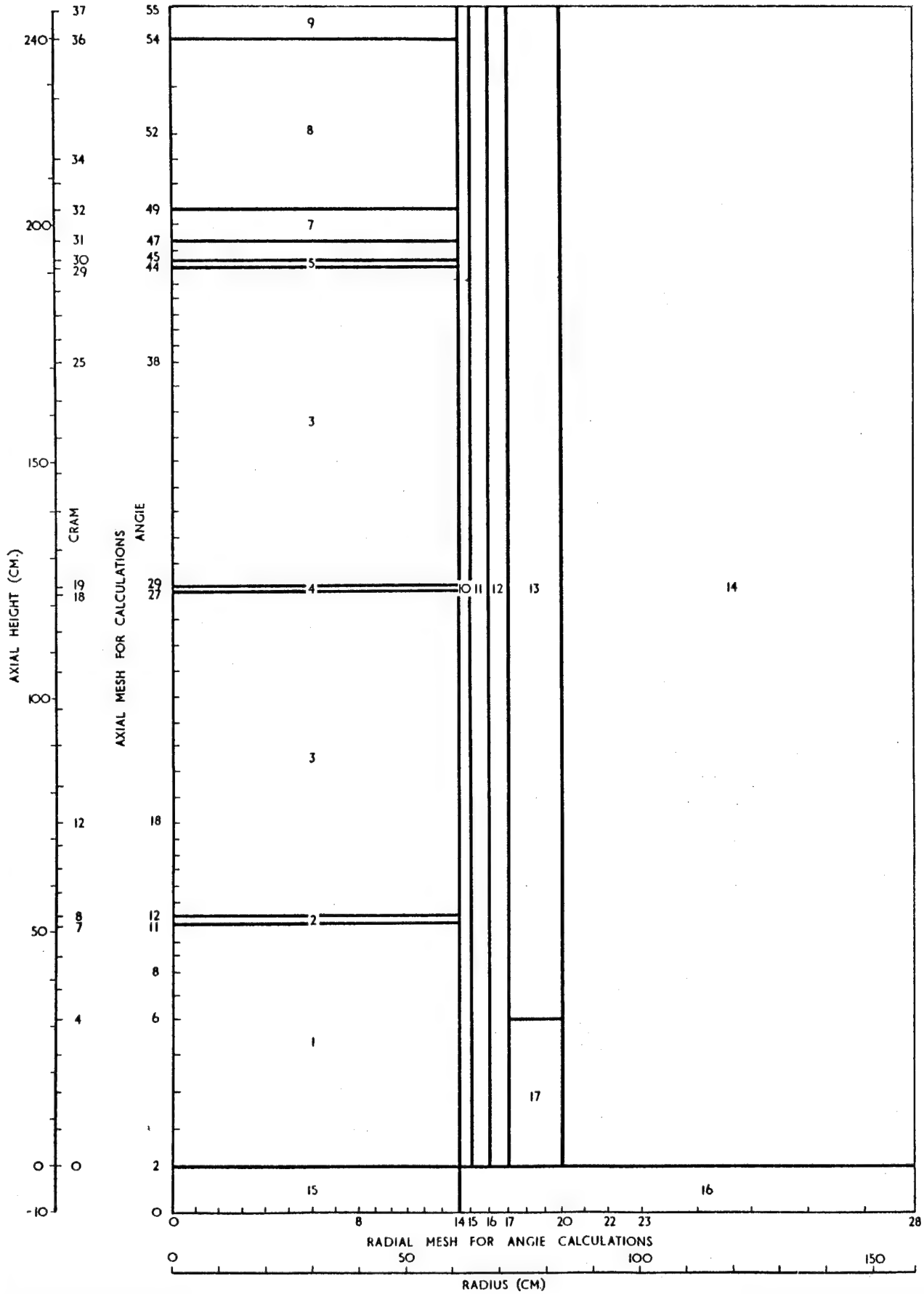


FIGURE 2.1 GEOMETRICAL ARRANGEMENT FOR CALCULATIONS

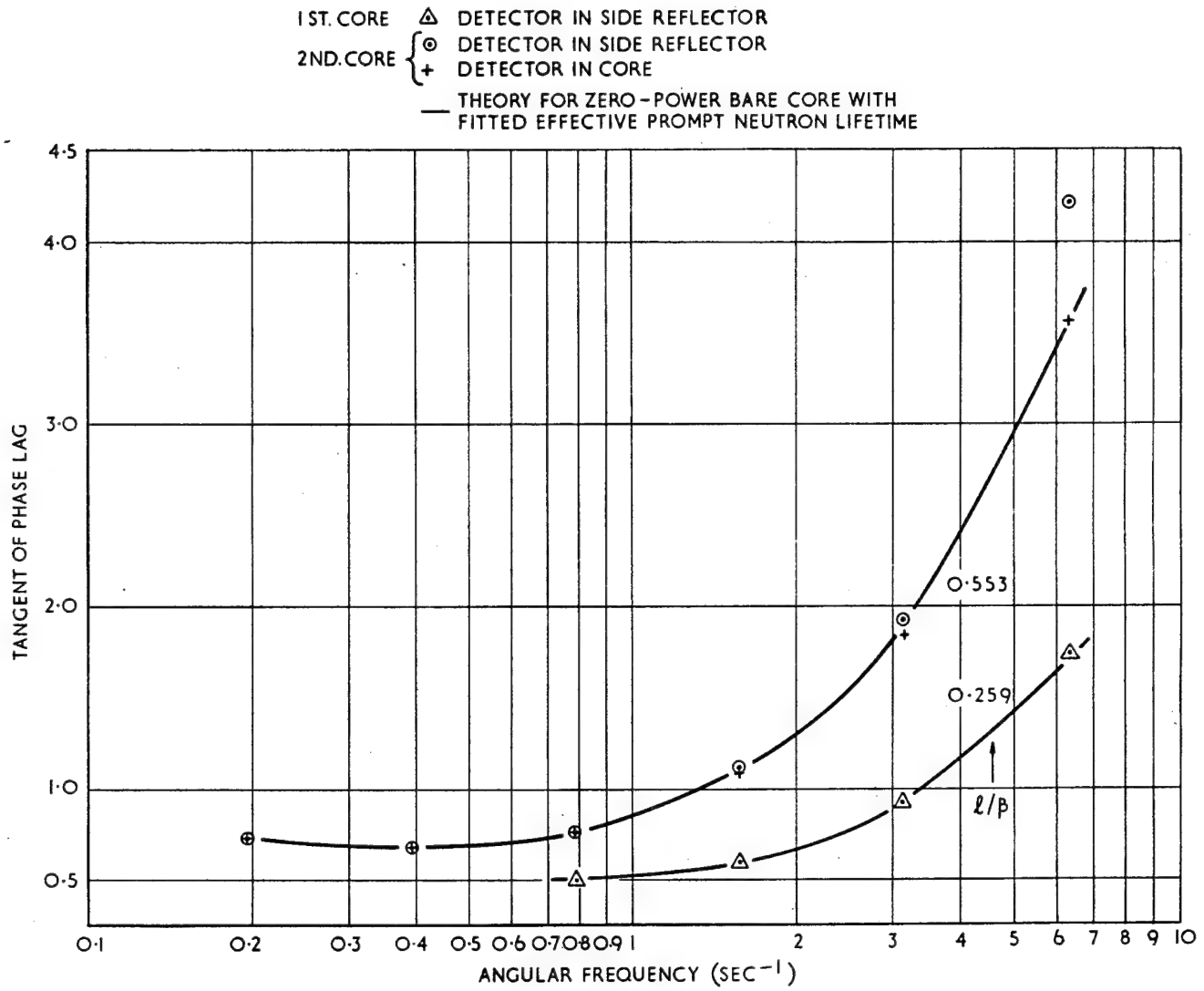


FIGURE 4.1. PHASE OF TRANSFER FUNCTION

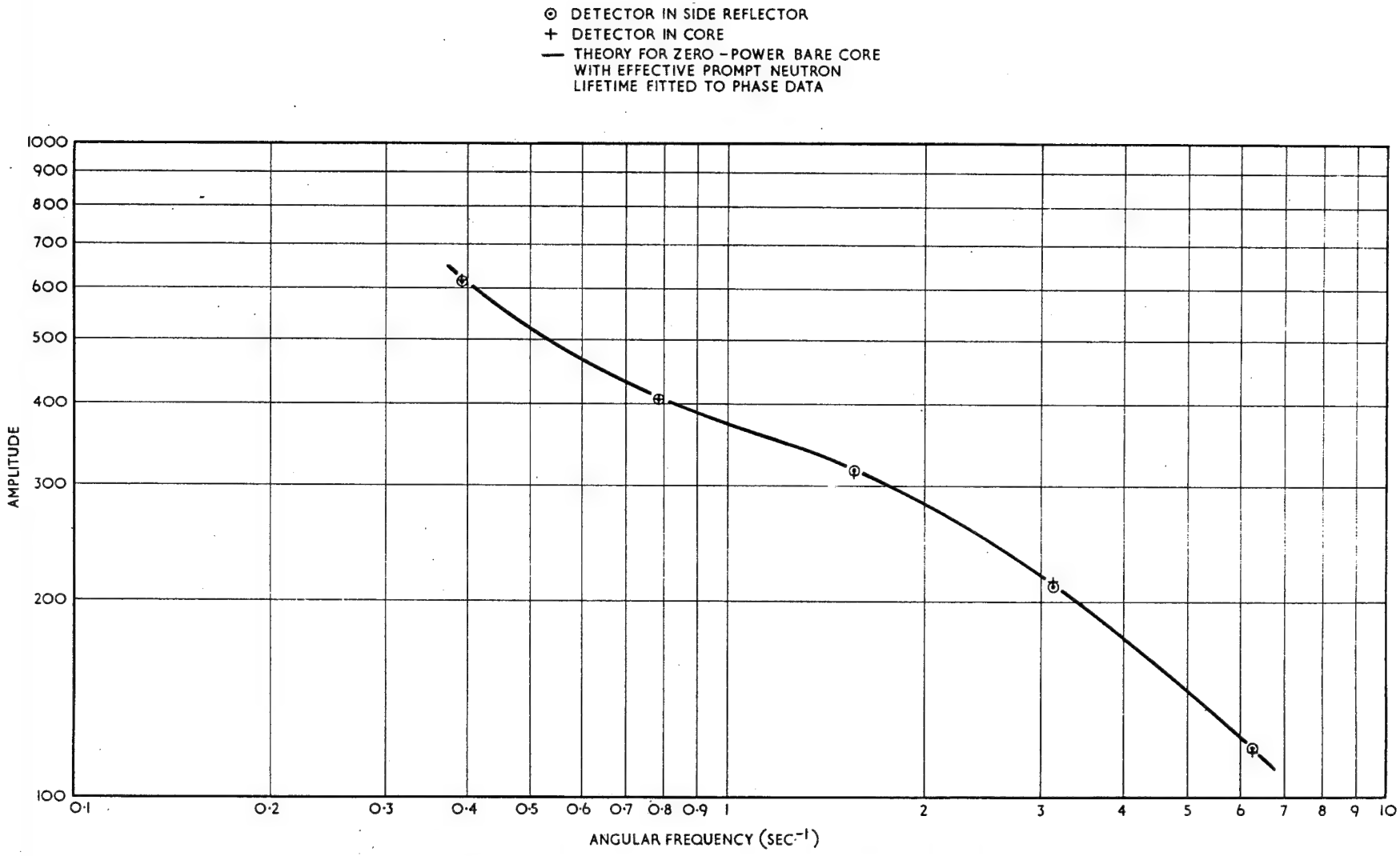


FIGURE 4.2. AMPLITUDE OF TRANSFER FUNCTION FOR SECOND CORE

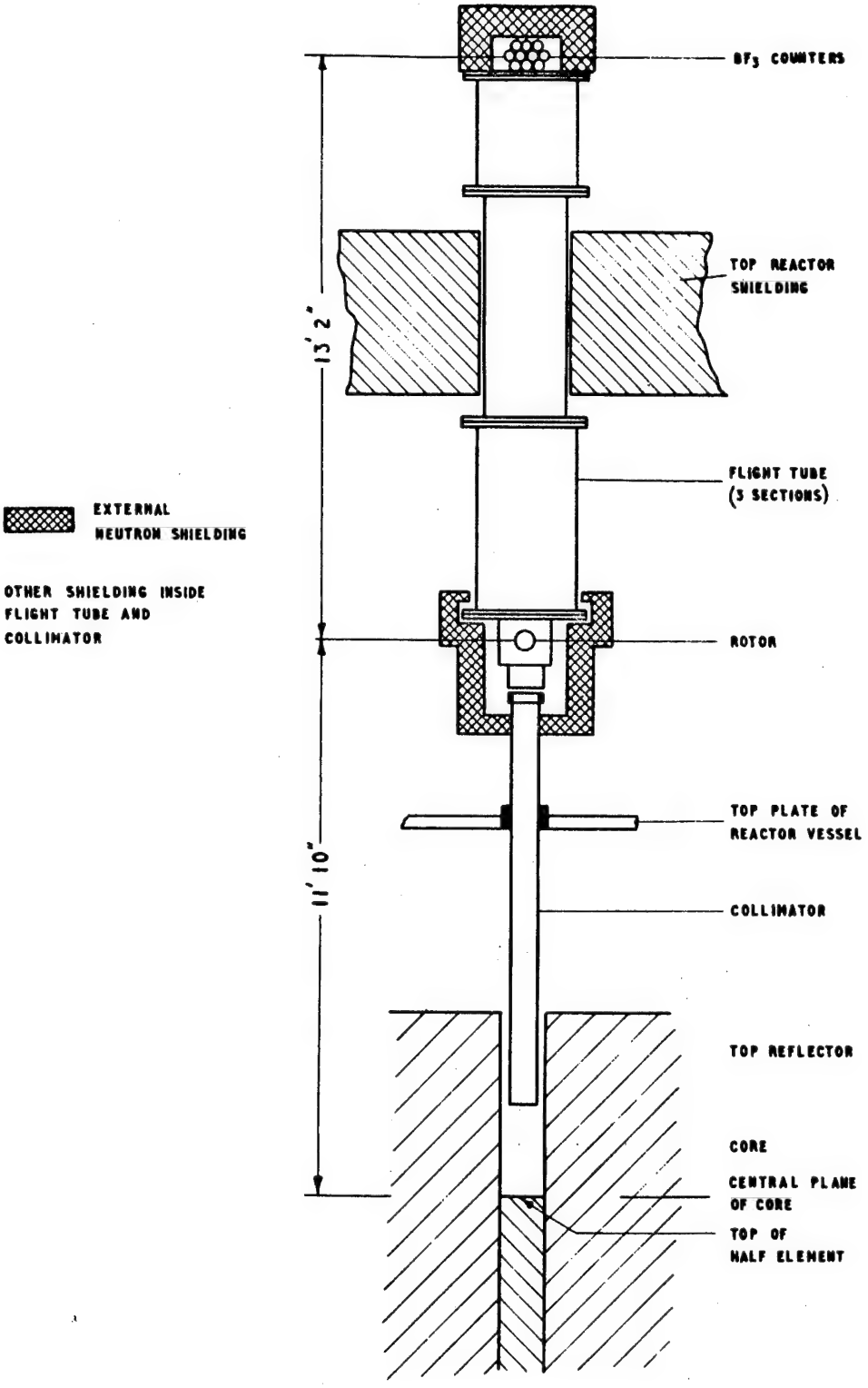


FIG. 6.1 GENERAL ASSEMBLY OF CHOPPER.

APPROXIMATELY TO SCALE VERTICALLY

NOT TO SCALE HORIZONTALLY

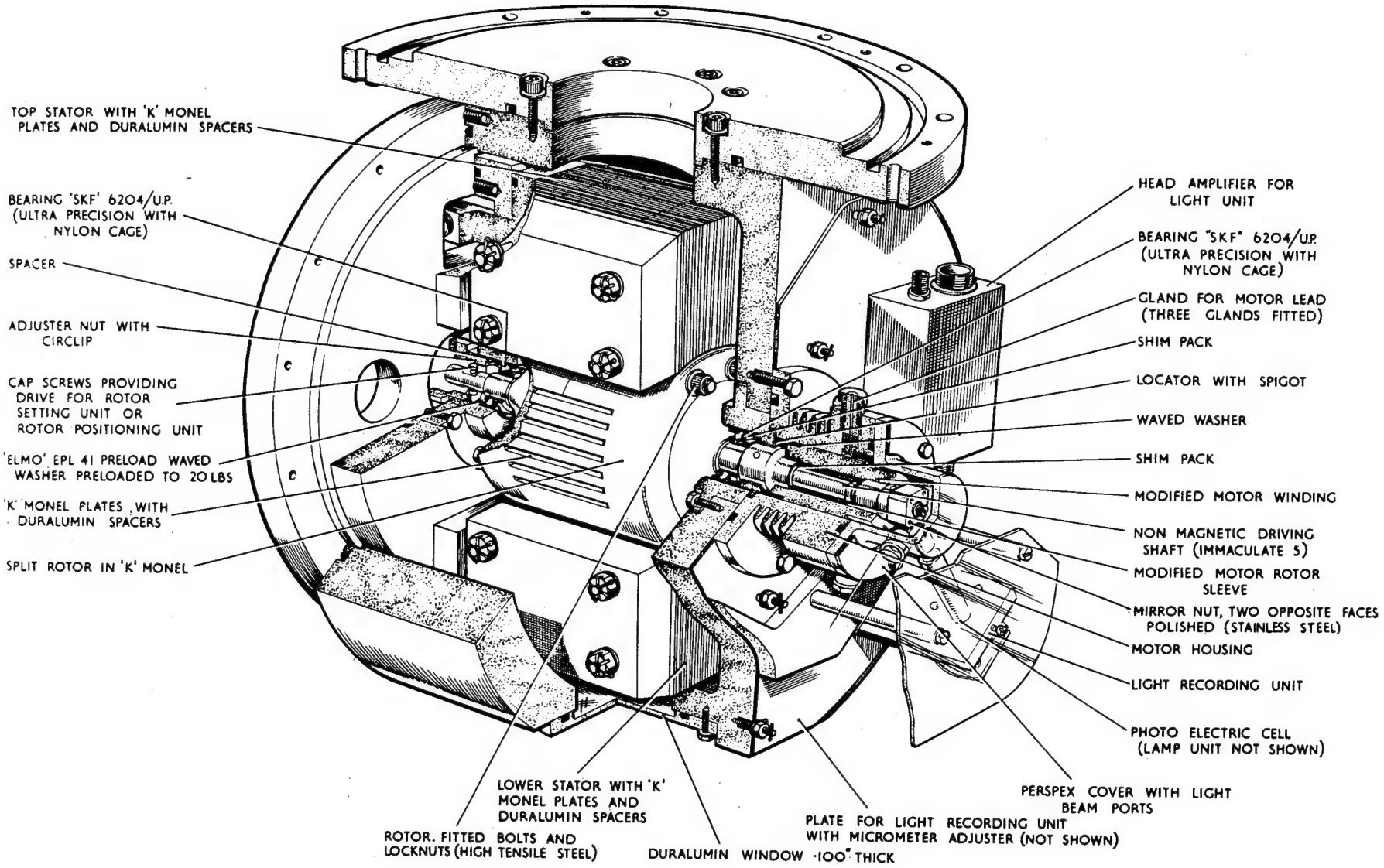


FIG.6.2 ROTOR ASSEMBLY

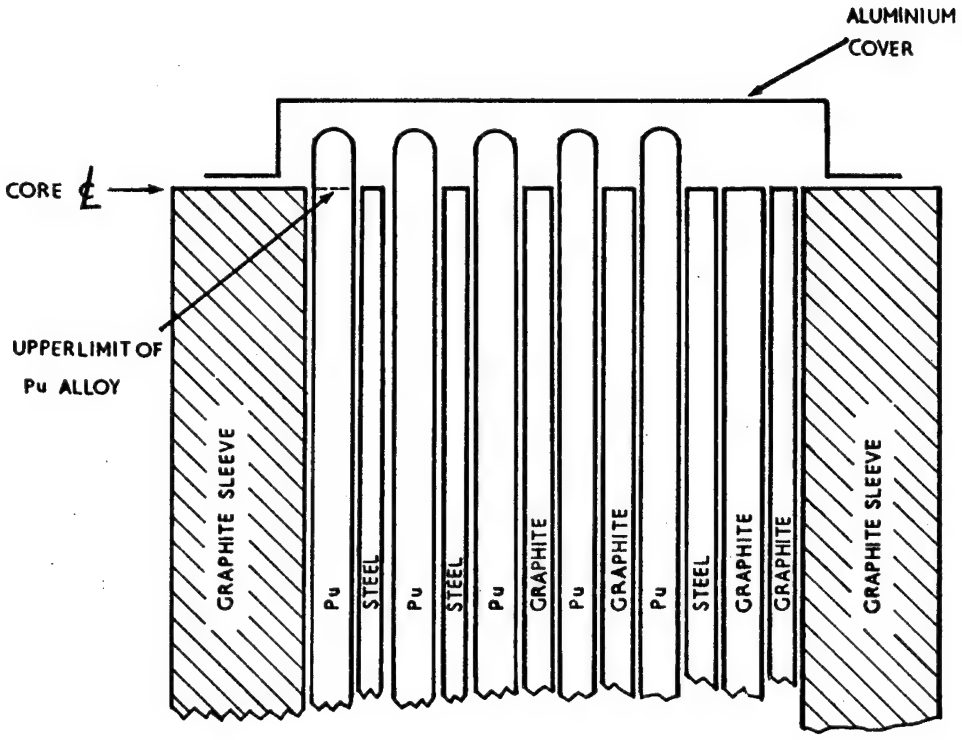


FIGURE 6.3 TOP OF SOURCE ELEMENT.

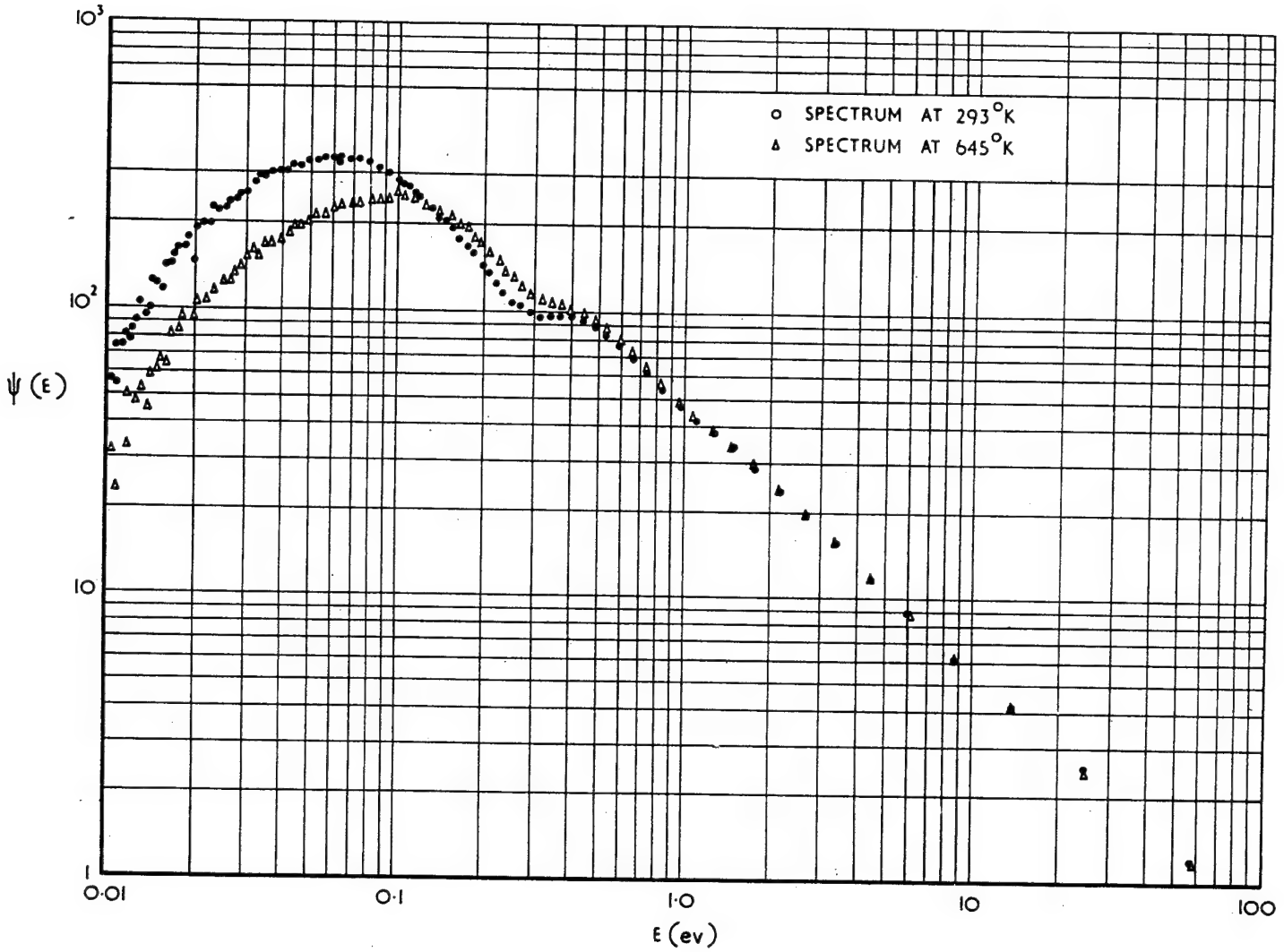


FIG. 6.4 EXPERIMENTAL SPECTRA AT 293°K AND 645°K.

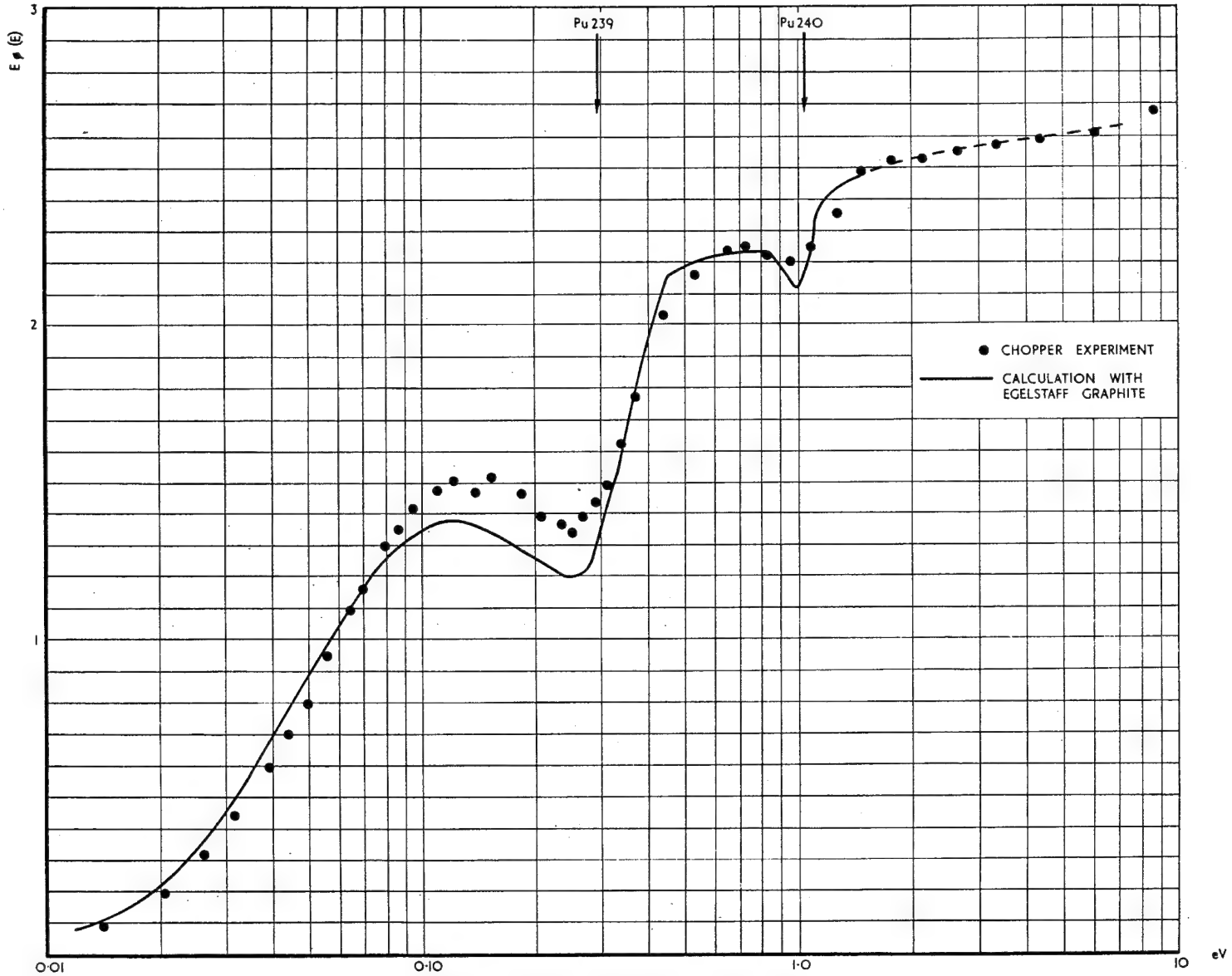


FIGURE 6·5 ZENITH PLUTONIUM CORE E.ø (E) vs E

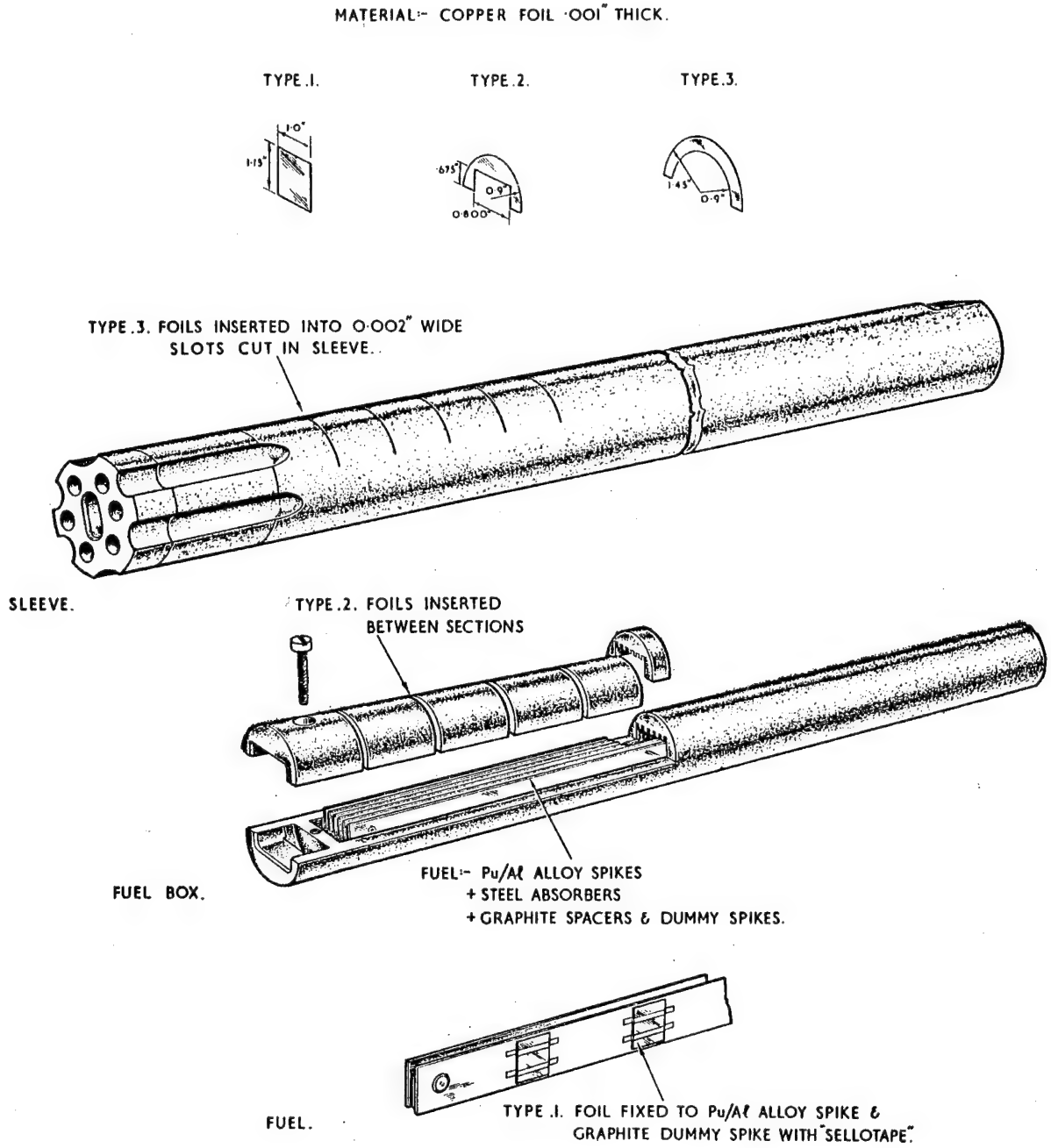


FIG. 7.1. FINE STRUCTURE ELEMENT FOR PLUTONIUM CORES.

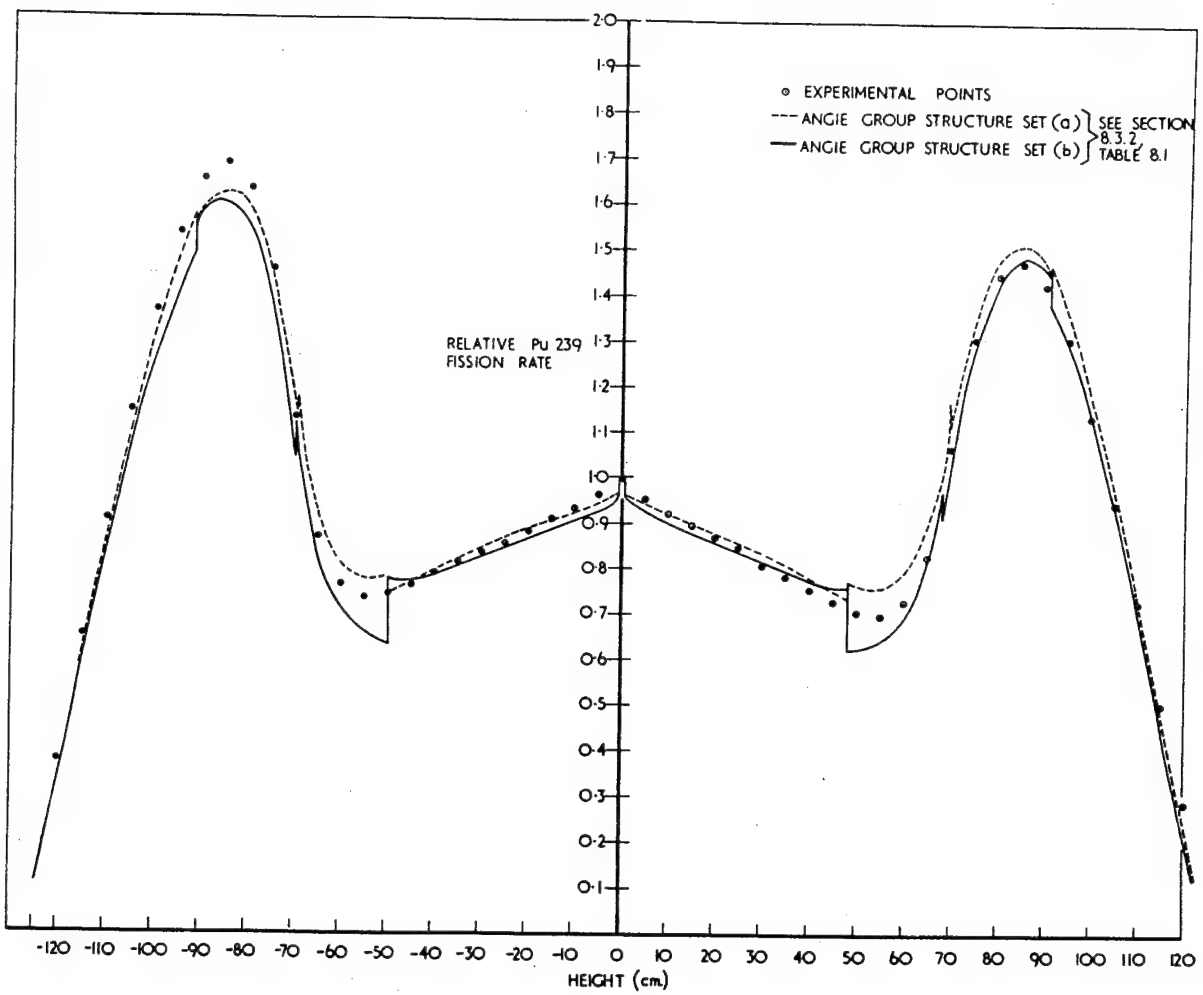


FIG. 7.2 AXIAL DISTRIBUTION OF Pu 239 FISSION RATE IN K10 CHANNEL (FIRST CORE)

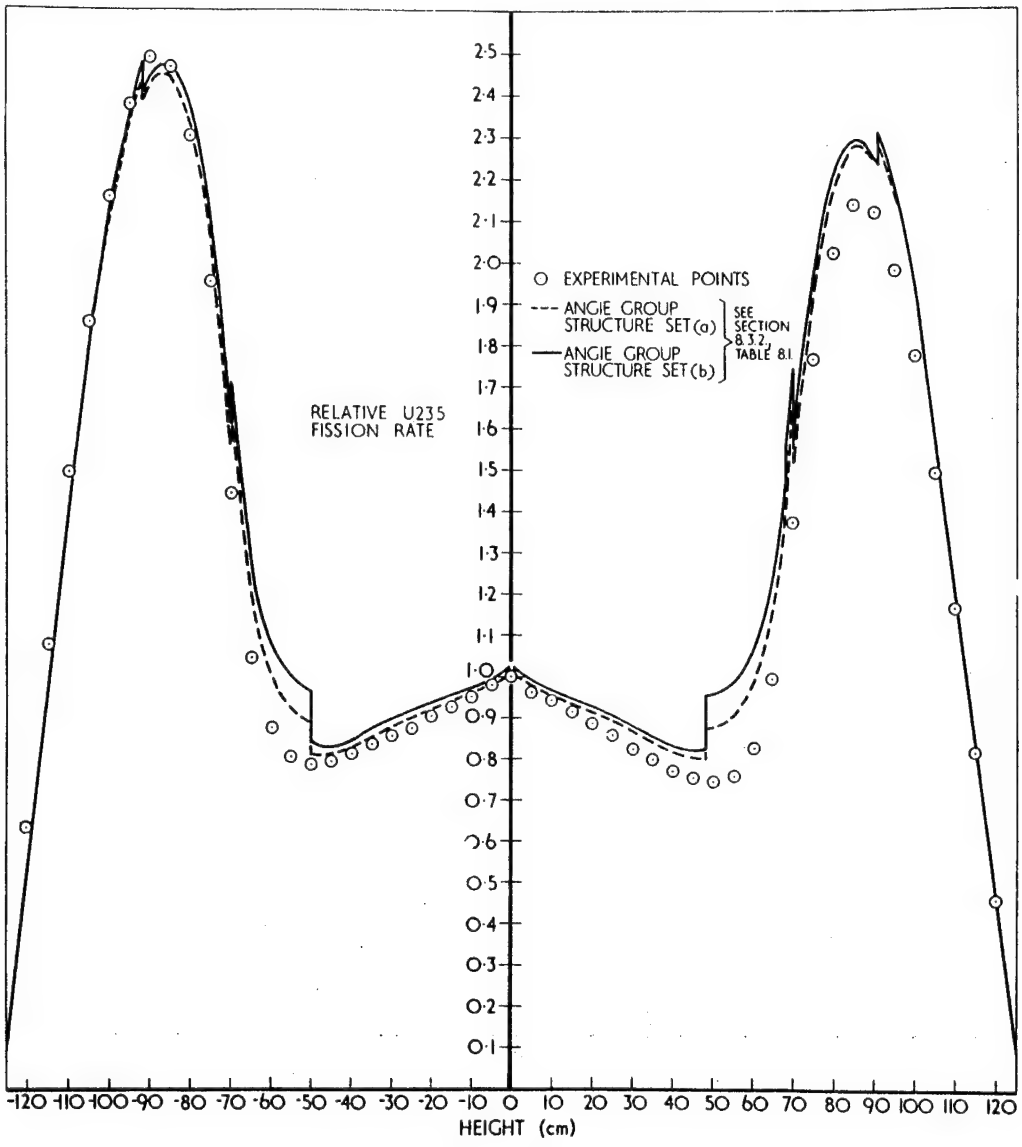


FIG. 7.3. AXIAL DISTRIBUTION OF U 235 FISSION RATE IN K 10 CHANNEL (FIRST CORE)

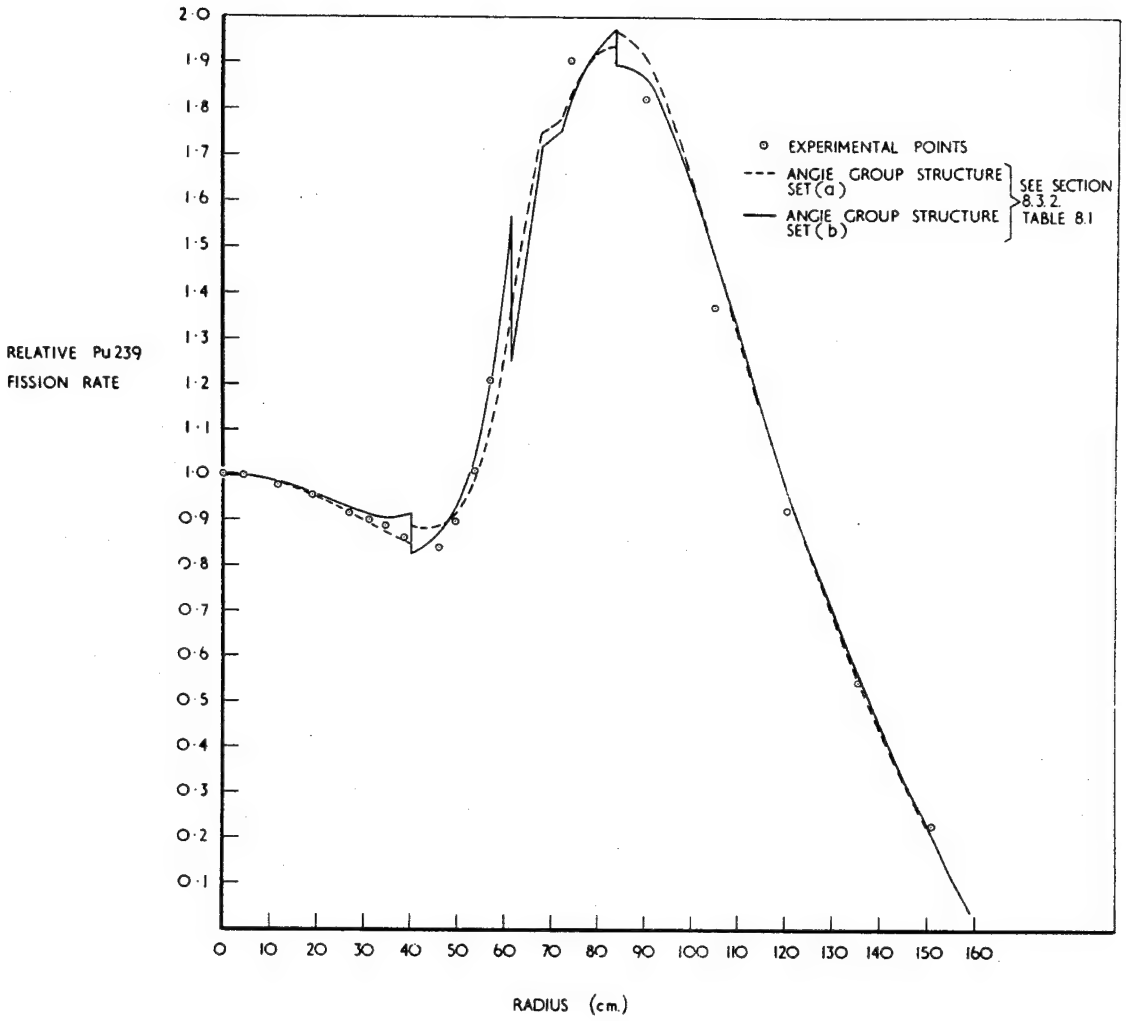


FIG. 7.4 RADIAL DISTRIBUTION OF Pu 239 FISSION RATE ON CORE CENTRE PLANE (FIRST CORE)

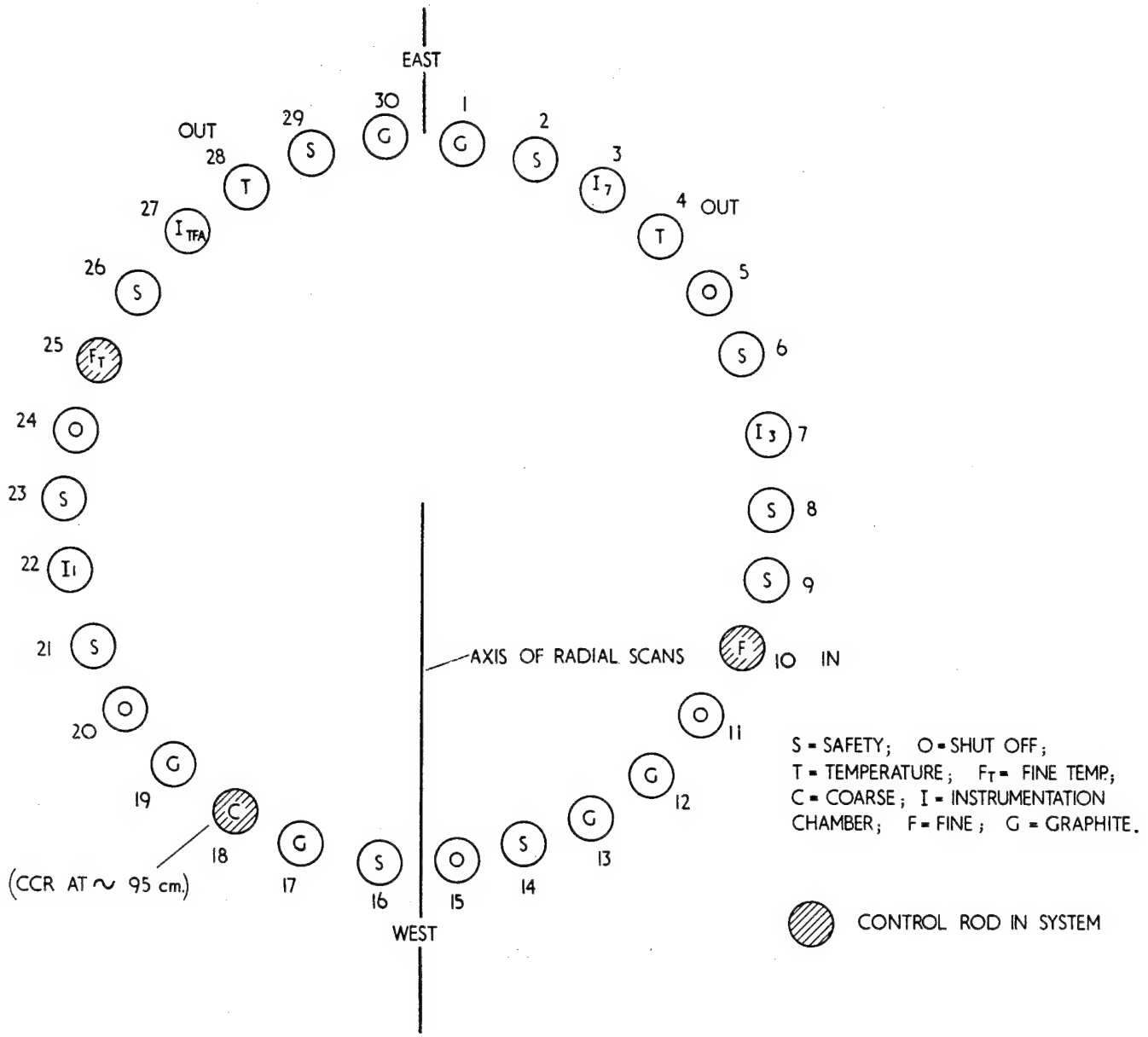


FIG. 7.5 CONTROL ROD CONFIGURATION FOR RADIAL SCANS (FIRST CORE)

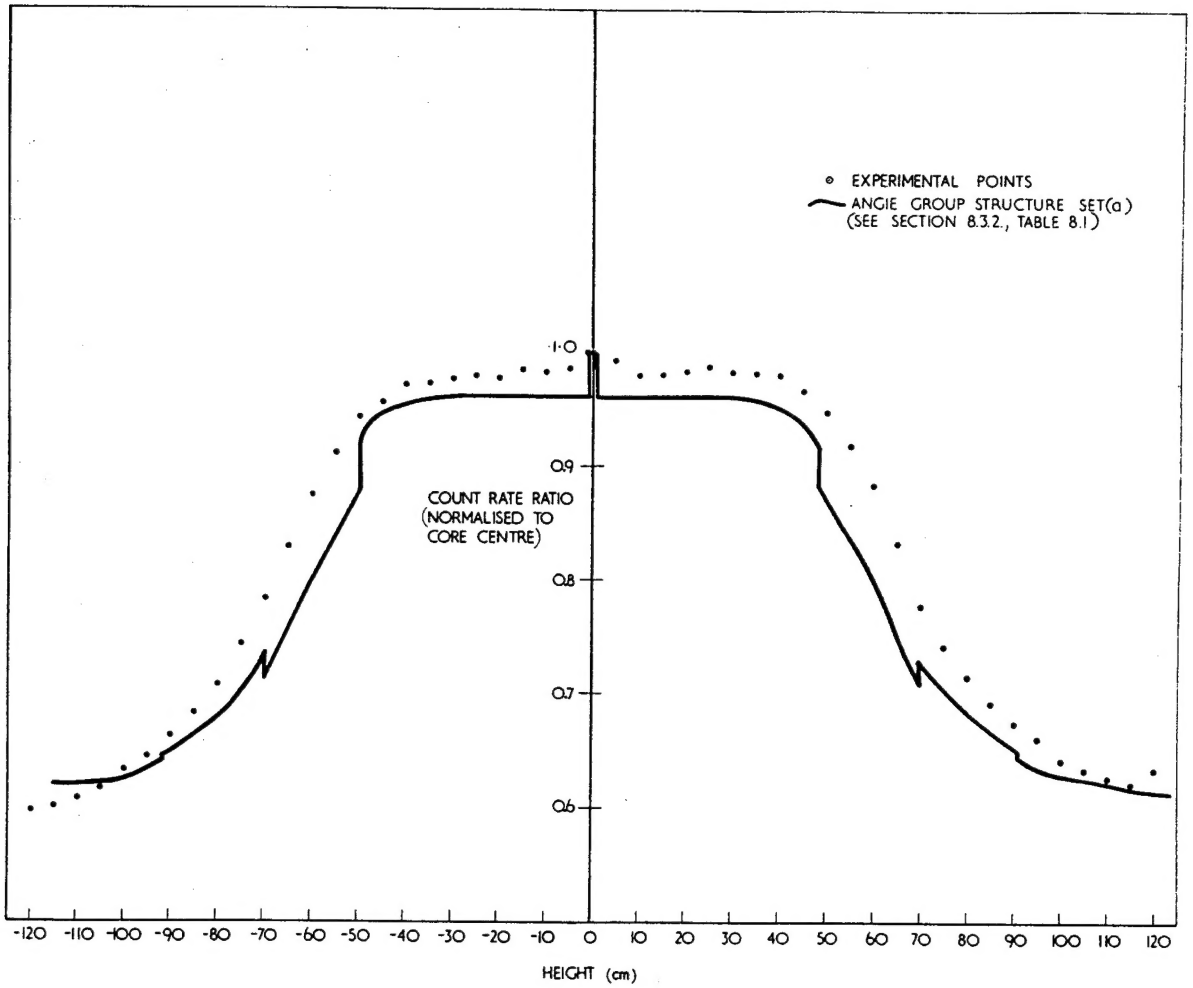


FIG.7.6 AXIAL DISTRIBUTION OF $Pu_{239}$ / $U_{235}$ RATIO IN K10 CHANNEL (FIRST CORE)

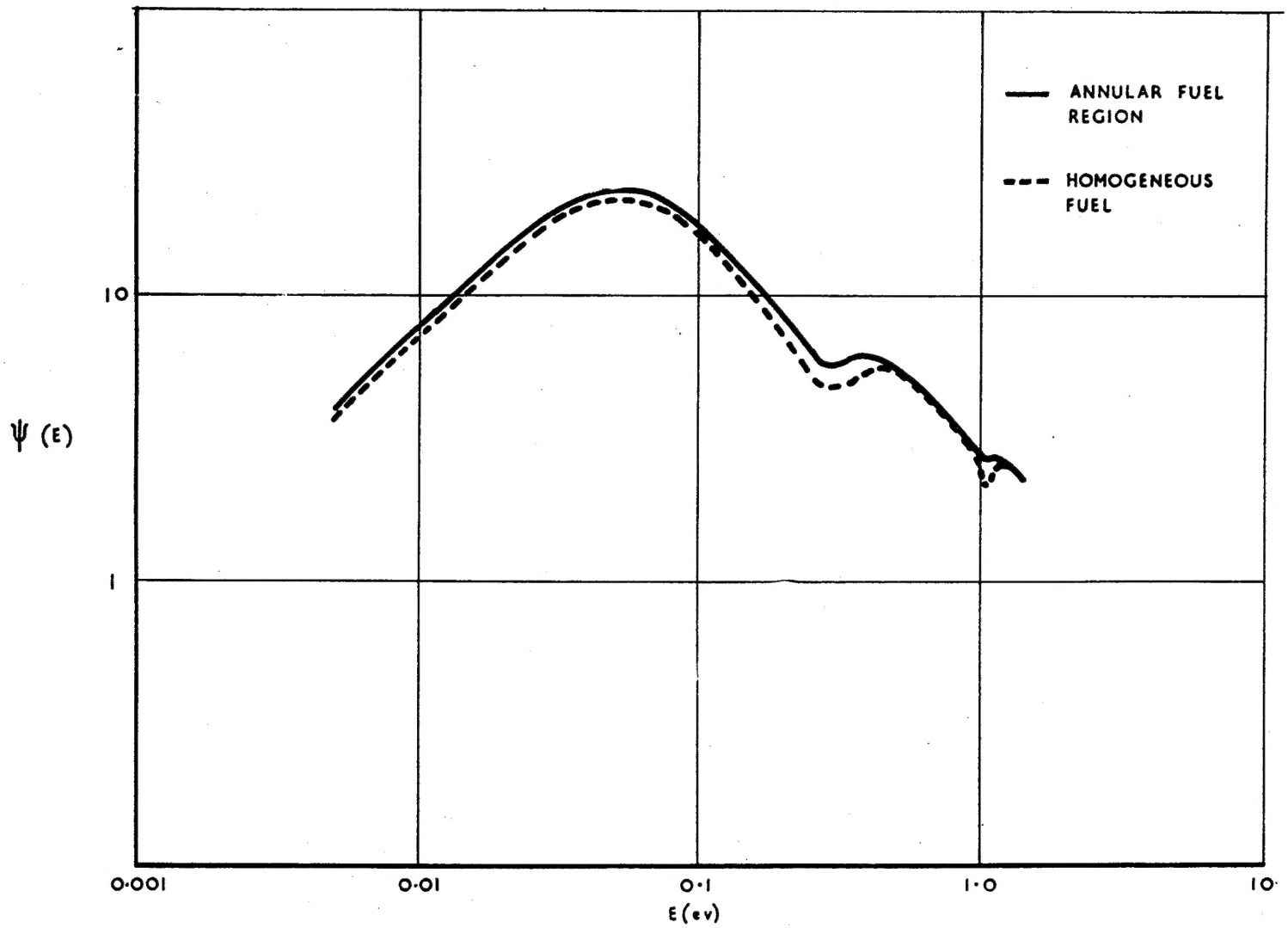


FIG. 8.1 COMPARISON OF DIRECTED SPECTRA WITH DIFFERING GEOMETRICAL MODELS

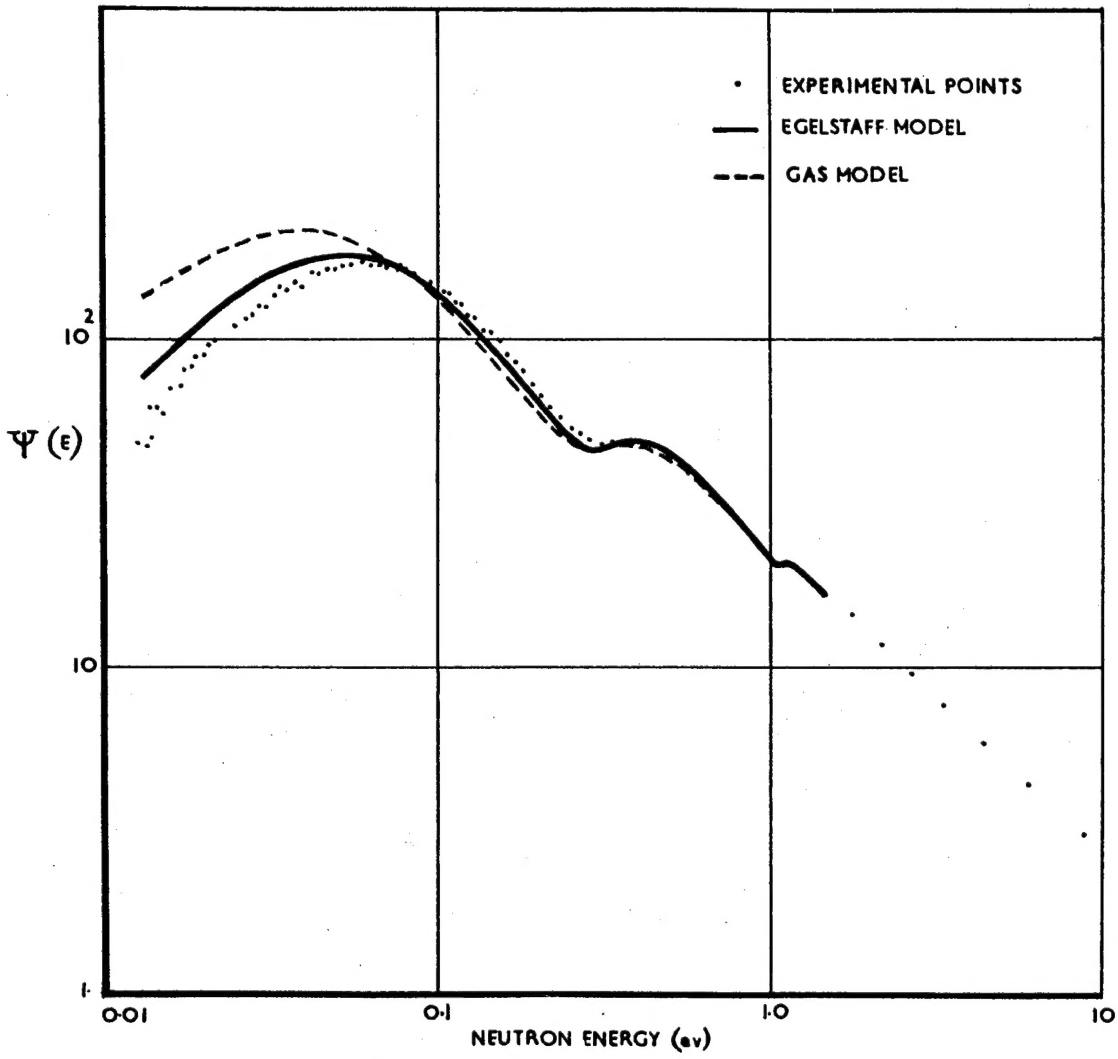


FIG. 8.2 THEORETICAL AND EXPERIMENTAL SPECTRA.

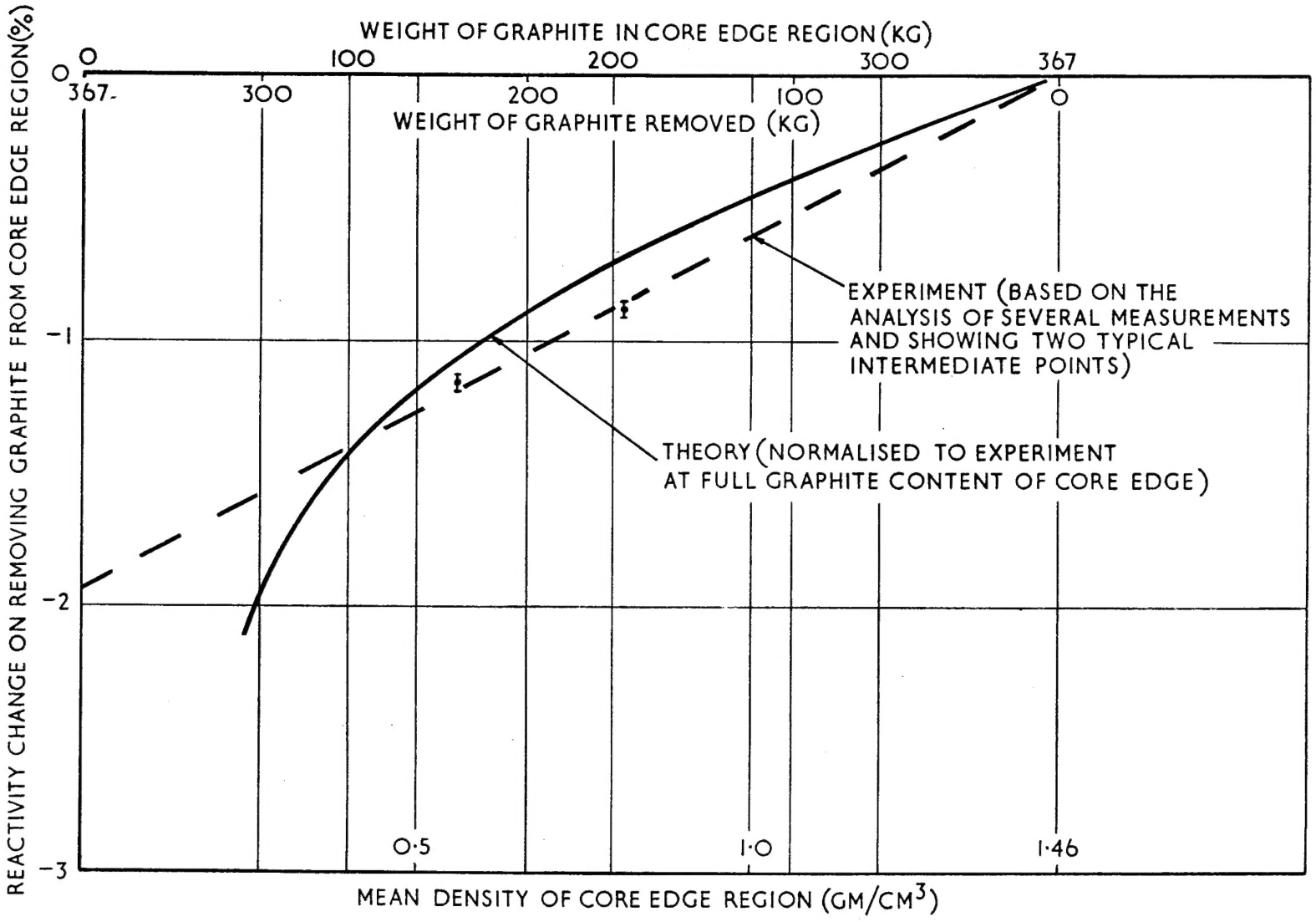


FIGURE 8.3 REACTIVITY CHANGE DUE TO GRAPHITE IN THE CORE EDGE REGION FOR THE FIRST CORE